BIOMECHANICS OF BLACK SOLDIER FLY LARVAE

A Thesis
Presented to
The Academic Faculty

by

Olga Shishkov

In Partial Fulfillment
of the Requirements for the Degree
Doctor of Philosophy in the
School of Mechanical Engineering

Georgia Institute of Technology
May 2020

BIOMECHANICS OF BLACK SOLDIER FLY LARVAE

Approved by:

Professor David L. Hu, Advisor
School of Mechanical Engineering
Georgia Institute of Technology

Professor Peter Yunker
School of Physics
Georgia Institute of Technology

Professor Cyrus Aidun
School of Mechanical Engineering
Georgia Institute of Technology

Professor John Brady
School of Chemical Engineering
California Institute of Technology

Professor Magnus Egerstedt
School of Mechanical Engineering
Georgia Institute of Technology

Date Approved: March 11th, 2020

To my parents,

Irina and Vladimir Shishkov,

and grandparents,

Taisia Polunovskaya and Mikhail Polunovskiy.

Preface

Joining the Hu Lab to work on collective dynamics was almost meant to be. Prior to my PhD, I was interested in experimentally studying fluid mechanics. I found probing a flow of air or water with techniques such as particle image velocimetry and figuring out its properties from the data to be deeply satisfying. I have also always been fascinated by insects, such as the ants crawling on the ground and collectively reaching decisions about how to gather food and fend off predators. When I realized I could combine these concepts, and measure the flows of animals using fluid mechanics techniques, I was hooked.

My research is arguably one of the more disgusting topics in the Hu Lab. The following thesis is all about maggots: how they eat, how they move, and how to raise them. Despite the perception of disgust around these insects, I have come to appreciate them for their amazing abilities to quickly decompose our waste and to make their way into any cracks and crevasses that they can find. While black solider fly larvae will always be my favorite type of fly larva, I have learned many things about different fly larvae species that I would like to share an in infographic that I made for ComSciCon Atlanta in March 2018.

WHO ARE MAGGOTS?

THE THOUSANDS OF MAGGOTS SQUIRMING IN THEIR STINKING, DECAYING FOOD SEEM MORE PART OF HORROR FILMS THAN SCIENCE PROJECTS AND BACK-YARD FARMS. HOWEVER, MAGGOTS - OR **FLY LARVAE** - ARE BOTH USEFUL AND FASCINATING, DESPITE OUR INITIAL DISGUST.

LIFE CYCLE OF A FLY:

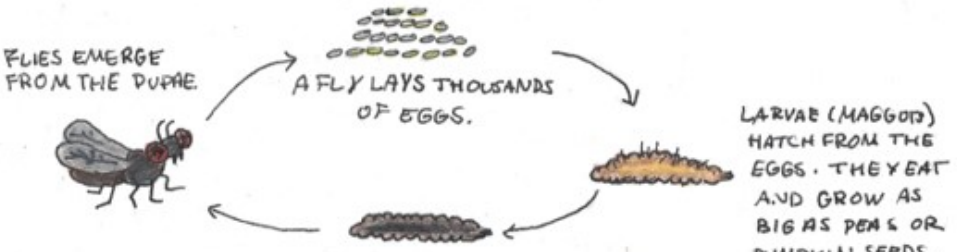

SOME LARVAE HAVE IMPORTANT JOBS:

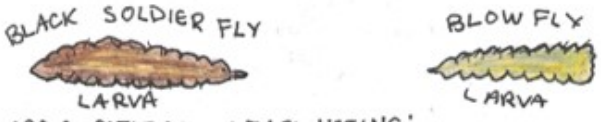

OTHERS ARE SCIENTIFICALLY FASCINATING:

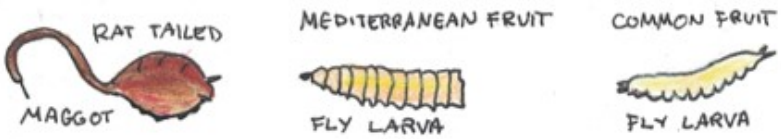

HERE'S A LOOK INSIDE THE WORLD OF FLIES AND THEIR LARVAE AND THE WEIRD THINGS THEY DO.

THE BLACK SOLDIER FLY'S LARVAE ARE GREAT AT RECYCLING:
THEY TURN FOOD WASTE INTO FRESH FOOD!

← BLACK SOLDIER FLY

A FULLY GROWN LARVA

A BLACK SOLDIER FLY LARVA EATS TWICE ITS BODY WEIGHT PER DAY.

ITS FAVORITE FOODS INCLUDE:

FOOD WASTE

FECES

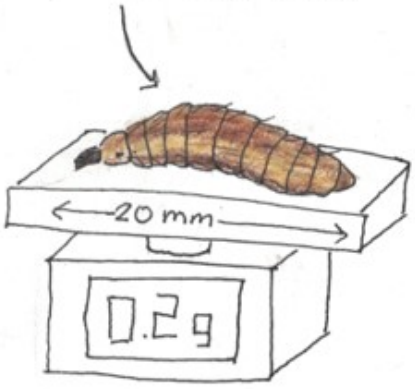

LARVAE THAT EAT FOOD WASTE ARE NUTRITIOUS:
42-45% PROTEIN; 31-35% FAT (BY DRY WEIGHT)

WE WASTE 1/3 OF THE FOOD WE GROW. IF WE FEED LARVAE OUR FOOD WASTE, WE CAN FEED LARVAE TO:

FISH

CHICKENS

... EVEN PEOPLE!

BLACK SOLDIER FLY LARVAE ARE NOT DISEASE VECTORS—THEY ALSO HAVE ANTIMICROBIAL PROPERTIES. THEY HAVE BEEN FOUND TO REDUCE CONCENTRATIONS OF SALMONELLA AND E. COLI IN FECES AND MANURE.

IMPROVING SANITATION ON FARMS AND IN LATRINES IS ANOTHER USE FOR THESE LARVAE.

(2)

BLOW FLY LARVAE HAVE JOBS IN MEDICINE AND FORENSICS.

A BLOW FLY LAYS EGGS ON CARCASSES →

ITS LARVAE EAT THE CARCASS AS THEY GROW →

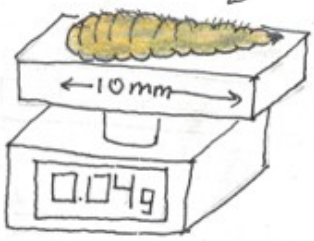

HOW LONG BLOW FLY LARVAE TAKE TO GROW DEPENDS ON THE TEMPERATURE (ABOUT 8 DAYS AT ROOM TEMPERATURE). ESTIMATING AGES OF FLY LARVAE ON CORPSES GIVES EVIDENCE FOR THE TIME OF DEATH.

BLOW FLY LARVAE LIVE IN HUGE AGGREGATIONS. THEY EAT SO FAST THAT THEIR METABOLISM GENERATES HEAT. ENOUGH LARVAE GENERATE TEMPERATURES TOO HOT FOR THEIR SURVIVAL.

A FEW LARVAE STAY COOL:

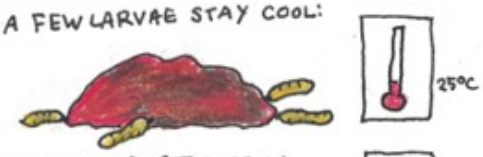

MORE LARVAE GET WARM:

THEY REGULATE THEIR TEMPERATURE BY CRAWLING AWAY IF IT GETS TOO HOT.

TOO MANY LARVAE GET HOT!

BLOW FLY LARVAE HAVE BEEN USED IN MEDICINE SINCE MEDIEVAL TIMES TO EAT DEAD FLESH FROM WOUNDS.

THEY ONLY EAT DECAYING FLESH, AND DO NOT TOUCH HEALTHY TISSUE.

BLOW FLY LARVAE ARE EFFECTIVE FOR TREATING DIABETIC ULCERS AND CHRONIC WOUNDS.

STERILE, SPECIALLY BRED LARVAE HAVE BEEN APPROVED FOR WOUND CLEANING BY THE FDA SINCE 2004.

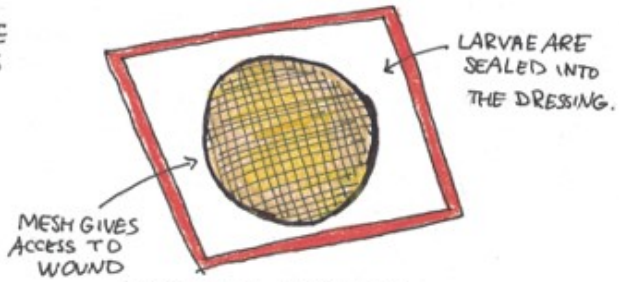

A "MAGGOT DRESSING"

③

A DRONE FLY (NOT A BEE!)

DRONE FLIES LAY THEIR EGGS IN DIRTY WATER, SUCH AS DRAINAGE DITCHES AND SEWERS.

THEIR LARVAE HAVE UNIQUE ADAPTATIONS ALLOWING THEM TO SURVIVE IN THESE POLLUTED, LOW-OXYGEN WATERS.

A DRONE FLY LARVA IS CALLED A

RAT-TAILED MAGGOT:

THE RAT-TAILED MAGGOT IS NAMED AFTER ITS TAIL.

THIS TAIL WORKS AS A SIPHON - THE LARVA IS SUBMERGED, BUT CAN BREATHE BY DRAWING IN AIR FROM THE SURFACE:

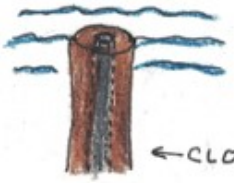

AIR ENTERS THE TAIL THROUGH A SPIRACLE, OR OPENING, ON THE TIP.

← CLOSE-UP OF TAIL

IF THE WATER IS TOO THICK, IT CAN SWIM UP TO BREATHE THROUGH PORES ON ITS HEAD.

TO SURVIVE IN WATER FILLED WITH BACTERIA AND FUNGI, THE LARVA IS COVERED IN *NANO* PILLARS.

← THE NANOPILLARS ON THE SKIN OF THE LARVA ARE TINY- 100 nm WIDE! 1000 NANOPILLARS COULD FIT AROUND ONE HUMAN HAIR.

THESE NANOPILLARS ARE SO CLOSE TOGETHER THAT BACTERIA DO NOT STICK TO THE LARVA.

THERE ARE NO NANOPILLARS ON THE LARVA'S TAIL TIP, WHERE IT REACHES FOR AIR.

THESE ADAPTATIONS ALLOW THESE LARVAE TO THRIVE IN DANGEROUS, BUT NUTRITIOUS WATER.

(4)

LARVAE OF THE MEDITERRANEAN FRUIT FLY (AND SOME OTHER FLY LARVAE) ARE THE ONLY SOFT, LIMBLESS ORGANISMS THAT CAN JUMP!

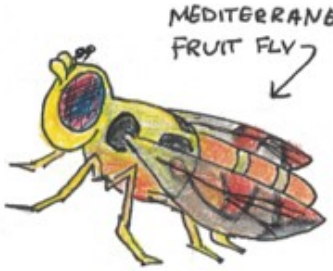

FIRST, THE LARVA ROLLS UP AND GRABS ITS TAIL WITH A PAIR OF MOUTH HOOKS:

THEN TIGHTENS ITS BODY USING STRONG MUSCLES!

FINALLY, IT RELEASES ITS MOUTH HOOKS AND LEAPS!

JUMPING GETS THE LARVA OUT OF THE FRUIT IT IS EATING AND TO A SAFE SPOT TO PUPATE. LARVAE MOTION IS INSPIRING ENGINEERS TO MAKE SOFT, UNDULATING ROBOTS.

FLY LARVAE ARE SO MUCH MORE THAN DIRTY DECOMPOSERS. BY STUDYING COMMON FRUIT FLY LARVAE, WE KNOW THEY HAVE PERSONALITIES:

THEY ARE SOCIAL, AND EAT TOGETHER:

THEY LOOK FOR FOOD AND HIDE FROM LIGHT:

SOME ARE "ROVERS", AND EXPLORE:

WHILE "SITTERS" ARE LAZIER:

COMMON FRUIT FLY (THE ONE USED IN SCIENCE)

ITS LARVA

SMELLY, WEIRD MAGGOTS MAY BE GROSS AND UNCANNY, BUT THEY ARE BOTH USEFUL AND FASCINATING. WHILE THEY EAT OUR WASTE AND LIVE IN OUR SEWERS, REMEMBER:

FLY LARVAE ARE JUST HUNGRY BABIES!

5

ACKNOWLEDGEMENTS

A PhD thesis is never a solitary endeavor and so I have many people to thank who have helped me over the years.

First, I would like to thank my advisor David Hu for inspiring me to study collective dynamics, for showing me the value of bold and creative research, and for confidence in my ability to do excellent work.

Next I would like to thank my committee: Peter Yunker, Cyrus Aidun, Magnus Egerstedt, and John Brady for providing experimental and theoretical advice.

I would like to give thanks to all of our collaborators: Scott Franklin for theoretical contributions to our experiments compressing fly larvae, Daniel Goldman for expertise on granular mechanics and invaluable experimental advice, Miguel Fuentes-Cabrera for insight on collective dynamics of feeding behavior, Saad Bhamla for use of his Dun Inc imaging system, Jonathan Goldman for all of his contributions to commercializing the aerating bed for larvae and assistance with funding, Ahmad Omar for help with modeling, Jonathan Michel and Shane Jacobeen for help with the universal testing machine, and Alison Onstine and Angie Lessard for advice on biology and for finding any equipment for my experiments. I would also like to acknowledge the Georgia Research Alliance for funding our work on the aerating bed for larvae.

This project could not have happened without fresh, active black soldier fly larvae to use in my experiments. Thus, I would like to thank Sean Warner and Patrick Pittaluga from Grubbly Farms for providing larvae and invaluable advice at the start of my PhD studies; and Jonathan Cammack and Jeffrey Tomberlin at EVO Conversion Systems for providing

larvae and encouragement during the later years of my PhD studies.

I would like to thank Patricia Yang, Alexis Noel, Thomas Spencer, Alexander Bo Lee, Marguerite Matherne, Hungtang Ko, and Andrew Schulz for being the best labmates I could hope for and for taking care of my axolotl when I have been out of town.

Also, many thanks to Glenda Johnson and Katherine Drake for helping me get through the PhD program as smoothly as possible.

I would also like to thank my most dedicated, thoughtful undergraduate students: Christopher Brown and Michael Hu for working on the study of fly larvae feeding behavior and for putting up with my inexperience in mentoring at the start of my PhD, Joshua Trebuchon for working on the study of larvae under compression, Anthony Chirumbole, Parth Patel, and Michael Yared for working on the aerating bed for fly larvae, Nicolette Prevost for working with the puppy videos and Robotarium, and Stephen Kalinksy for contributing to the work with Bristlebots.

I would never have made it this far without my family, and so I would like to thank my parents, Irina and Vladimir Shishkov, my brother, Denis Shishkov, and my grandparents, Mikhail Polunovskiy and Taisia Polunovskaya, for encouraging me to pursue graduate school and being my biggest fans.

And, finally, I would like to thank Temmie, the softest dog and the best writing companion.

TABLE OF CONTENTS

LIST OF FIGURES

LIST OF TABLES

SUMMARY

The black soldier fly is a non-pest insect that is raised by startup companies. The larvae of the black soldier fly are used as a sustainable animal feed. While much is known about the biology of these larvae, little is known about their behavior in large numbers such as their rates of eating or their ability to withstand piling on top of one another. In this thesis, we present experiments on the feeding, compression, and pile formation of swarms of black soldier fly larvae. The consumption of a food item is limited by the number of larvae that can surround the food and the breaks the larvae take while eating. We discover that larvae form fountains around food, replacing each other so that the food is distributed among the larvae that do not have access to food. During eating, the larvae heat themselves up, a problem we solve using an aerating bed. When vertical forces are applied to swarms of larvae, they actively rearrange to re-distribute the stress. The time scales of relaxation of dead larvae are in the form of stretched exponentials, models which have been used to describe the relaxation of balls of crumpled paper and other hierarchical materials. In confinement, larvae spontaneously form and disassemble piles of hundreds of individuals. We control the timing of the disassembly of these piles using vertically intruding objects. This research offers both practical suggestions for raising fly larvae as a sustainable feed for chickens and fish and new insight into the collective dynamics of animals while feeding and in confinement.

CHAPTER I

INTRODUCTION

1.1 Motivation

The motivation behind this thesis is to understand the behavior of black soldier fly larvae, *Hermetia Illucens*, a non-pest insect under consideration as a method of bio-converting food waste to sustainable protein. A black soldier fly larva, as shown in **Figure 1.1.1(a)**, weighs 0.1 to 0.2 grams, and is composed of approximately 42% protein and 35% fat by dry weight[1]. This makes them a candidate for sustainable feed for animals such as chickens and fish. Humans produce about 1.3 billion tons of food waste per year, approximately one third of the food grown for human consumption[2]. In addition to being a waste of resources, rotting food waste is an environmental hazard that can spread diseases and release excess methane and carbon dioxide[3]. Each black soldier fly larva eats up to twice its body weight per day in decomposing organic matter, and is particularly suited for eating fruit and vegetable waste. Black soldier fly larvae can be fed the food waste that would otherwise be left to rot in landfills (such as the pizza in **Figure 1.1.1(b)**), which makes feeding them cheap and environmentally friendly, and then the larvae themselves can be fed to livestock for human consumption. Additionally, black soldier fly larvae can be used to manage feces for sanitation in rural areas[4].

Startups all over the world, such as Grubbly Farms, Evo Conversion Systems, and others, raise black soldier fly larvae and sell them. This market has untapped potential in the animal feed industries. However, an understanding of how large groups of larvae behave remains missing. In this thesis, we investigate larvae from the individual larva to aggregations of tens of thousands to answer questions tying into how to efficiently raise them. When investigating the larvae in large numbers, we view them as an active material, as this allows us to draw upon the wide literature of active matter and collective dynamics for context to understand their behavior.

We begin the thesis with a study of the eating behavior of fly larvae, in which we discover that larvae form a "fountain" around a piece of food. We then investigate how larvae behave when subjected to external forces pushing upon them, as they might during

packaging and shipping. Third, we investigate how larvae behave when confined to plastic bins by measuring their motion between corners of 2D containers and driving this motion. We wrap up our experiments with black soldier fly larvae. by building an aerating bed to raise overheating larvae in. We briefly discuss how other animals feed in groups. Finally, we present dimensional analysis regarding larva motion, and close with a discussion of the implications of our work both for raising fly larvae and for the study of active matter.

Figure 1.1.1: a. The black soldier fly larva shown is 14 mm long and weighs 0.1 g. b. A group of larvae consume a 40-cm diameter pizza in two hours. The motion of the pizza crust and cheese away from the center indicates that the motion of larvae is correlated with their neighbors. These images are courtesy of Grubbly Farms.

1.2 Background

1.2.1 Bioconversion with black soldier fly larvae

Approximately one-third of the food made for human consumption – 1.3 billion tons per year – is wasted. 45% of this food is fruits and vegetables. Meanwhile, as of 2005, 854 million people are chronically malnourished[5], and it is projected that a 25% to 70% increase in food production will be necessary to feed the growing world population by 2050[6]. Food waste occurs for a variety of reasons, from poor storage (such as a lack of refrigeration and packaging in markets) to excess leftovers (such as restaurant portions that are too large and remain unfinished). This contributes to climate change both by wasting the resources

used to produce the food, polluting the land near the landfill, and generating methane and carbon dioxide through its decomposition[3,7].

While it would be ideal if all of this food waste went to the hungry rather than being wasted, some food wastage is inevitable. The black soldier fly larva is under consideration as a method of converting some of this waste into feed for chickens and fish, and thus recycling it back into the system. Larvae have been under consideration as a feed supplement for poultry and swine since the 1970s[8,9]. Scientific interest in these larvae picked up with Dr. Craig Sheppard's work in 1983, which noted the exceptional ability of the larvae to manage manure in chicken production and thus keep away pests, such as house flies, which could spread disease or otherwise be harmful to the chickens[10]. These larvae became more and more popular in the 1990s and 2000s, with work into using the larvae for manure management and sanitation[11,12], rearing methods[1,13,14], and nutritional potential in animal feed[15].

The black soldier fly lays up to 1000 eggs at a time, which hatch after 4 – 14 days[13]. After hatching, larvae grow over two weeks to several months, depending on the environmental conditions and available food. They go through six instars before pupating[16]. When a larva pupates, it stops eating, its mouth turns into a sucker attachment, and the larva climbs out of the rotting vegetation it was growing in to a safe, dry spot. This property is often used by larva growers to get larvae to self-harvest: larvae are grown in bins with sloped sides, and climb out of the bins when they are fully grown. Black soldier flies spend approximately two weeks as a pupa[17]. When the fly emerges, it lives for 8 - 9 days. It has no mouth to feed with, and only mates, lays eggs, and then dies[18]. Since the adult fly does not eat, it does not spread diseases.

In the United States, black soldier fly larvae have been approved for feed for carnivorous fish and for poultry since 2018. They are grown both by large companies, such as EVO Conversion Systems (www.evoconsys.com) and Enviroflight (www.enviroflight.net), by farmers seeking to reduce manure, and by at-home composters with backyard chickens. Although how to raise these larvae and their nutritional properties have been deeply investigated, many questions about their biology and how they are to be raised remain unanswered. In this thesis, we use biomechanics to answer some of these questions and make black soldier fly larvae a viable method for turning food waste into sustainable protein. Since larvae are generally found in large aggregations, it is valuable to understand larvae as a group in

addition to focusing on the individual. To accomplish this, we turn to studying larvae as active matter.

1.2.2 Collective dynamics of fly larvae

The success of animals that live in groups, such as black soldier fly larvae, arises from their collective motion. In this thesis, we investigate how these larvae collectively sense food patches and respond to forces. Collective sensing is known to exist in golden shiners, schooling fish that like to hide in shaded areas. The fish mimic the motion of their neighbors to collectively follow dark patches moving around the water[19]. Termites sense vibrations to communicate locations of food by drumming their heads on the ground[20]. Some animals are able to build structures out of their bodies. Army ants, which march over long distances in their search for food, build bridges across gaps to allow the colony to cross. These bridges change in size based on ants detecting traffic flow over the bridge and adjusting their position to keep the bridge stable. The ants balance the need for ants forming the bridge to ants foraging to create the optimal path[21]. In this thesis, we look at how larvae form piles around food to both sense it and to allow other larvae to reach it. On a smaller scale, cells in an expanding cell sheet (such as during the growth of tissues in embryonic development) are guided by the forces that they exert on each other. The stresses of cells pulling in the same direction expands the sheet outwards[22]. As part of this thesis, we investigate how larvae react to the forces they experience from each other and from their environment. Whether visual or tactile, it is the interaction of organisms with one another that makes these collectives succeed.

Understanding the behavior of black soldier fly larvae is important to both raising the larvae better and for inspiring collective robotics. Many swarm robotics platforms have been developed to make use of complexity and collective behavior. The connection between animal collectives and swarm robots is easy to make: individuals in both follow simple rules to achieve complex group behaviors, and there is a wide range of behaviors to choose from. A wide range of research exists on laboratory robot swarms[23]. The Robotarium at Georgia Tech, for example is an open-access robot swarm for modeling[24]. Another example is Harvard's Kilobots, 1024 robots that can self-organize in many shapes and transport objects[25–27].

The advantage of fly larvae-inspired robot swarms is that, like larvae, they would not

avoid collisions – they would make use of them to transfer information. Most robot swarm implementations only consider obstacles and robot-robot interactions in terms of avoiding collisions, but recent theories suggest that robots can gather information from how they collide[28]. A similar concept has been tested with light-avoiding robots built to mimic bees[29]. Robots sharing information by colliding with each other and objects in their environment eliminates the need for many other sensors on the robot as well as collision avoidance mechanisms. Thus, this thesis has applications both to raising fly larvae for animal feed and for the study of other animal behavior and swarm robotics.

1.2.3 Eating behavior of fly larvae

Figure 1.1.1(b) shows larvae consuming a 16-inch pizza in two hours. When farming larvae, maximizing eating rate is desired so that the larvae can grow as quickly as possible. While past studies of larva feeding give estimates for their eating rate[1], little detail is given on the number of individuals. The goal of this study is to determine the mechanism by which groups of larvae feed.

Although there has been much work done on collective animal movement[30], little is known about collective feeding. Such feeding behavior is universal because migratory animals often feed together. This is the case for swarms of locusts, which can destroy fields of crops, or piranha shoals, which can remove the flesh from animals in minutes. In fact, high feeding rates are used to accomplish tasks that would be difficult to do otherwise: dermestid beetles eat dead flesh so thoroughly that they are used by museums to clean bones, but how their feeding rate depends on the number of beetles remains unknown[31]. Comparatively more work has been done on the feeding of livestock, due to its importance to agriculture. However, it has been investigated for specific, not general cases – for example, the behavior of growing pigs in single-space feeders or the social consequences of moving cows between groups[32,33]. Moreover, experiments with cows and pigs necessarily involve fewer numbers of individuals than the group feeding of insects.

In order to understand how larvae feed so quickly, one of the methods we use in this thesis is the visualization of their collective movement. Tracking individuals in three-dimensional swarms has been done with hundreds of birds[34,35]. The larvae are challenging to visualize because the individuals are in closer proximity than birds in flocks or fish in schools. Rather than visualize the motion of larvae inside the opaque aggregation, we visualize it with 2D

imaging from the top and bottom, and use particle image velocimetry (PIV) to analyze their flows and infer motion inside the aggregation. Typical PIV analysis uses tracer particles in the fluid to be imaged. The positions of the tracer particles in frames of camera images are correlated to find velocity vectors between frames. In active matter research, the technique is adapted so that the organism being studied is used as the tracer particle. PIV has been successfully used with bacteria and with microtubule networks[36,37]. Bacteria swim in a fluid or atop a substrate and 2D layers have been previously visualized. We adopt similar methods, and film the top and bottom of the larva aggregation in our chapter on investigating how larvae eat.

1.2.4 Compression experiments as a measure of activity

Black soldier fly larvae have several properties that make suitable for understanding how organisms deal with compression. The larvae are 10 to 20 mm long, large enough to visualize without microscopy but small enough to compress with a typical universal testing machine. It is inexpensive to obtain thousands of black soldier fly larvae to investigate their collective dynamics, and they do not bite or transmit diseases to humans. Additionally, understanding the compression of black soldier fly larvae has potential applications to industry. Little is known about optimal conditions to raise the larvae, such as the size of the container they should be grown in or the depth of larvae in the container. Investigating the behavior of these larvae under compression can yield insights to how tightly they can be packed during shipping in order to reduce shipping costs or increase their safety.

In our chapter on compressing black soldier fly larvae, we consider the larvae as a granular viscoelastic material. They are granular because the interactions of larvae are associated with dissipation of energy through friction. They are viscoelastic because they act like both fluids and solids: if squeezed, they store energy like a spring, or flow to dissipate energy. In general, to determine the extent of the fluid and solid-like behavior of a material, a creep test is performed, in which the material is compressed under constant strain. In response, viscoelastic materials relax, or rearrange to dissipate energy and relieve stress, a phenomenon which is manifested as an exponentially decreasing stress[38]. For many materials such as Jello, the rate of this relaxation is characterized by a single parameter called the relaxation time, τ, where the stress scales as $e^{-\frac{t}{\tau}}$. However, there has has been a rising interest in hierarchical materials, such as crumpled balls of paper or aluminum

that consist of self-avoiding fractal structures due to the many length scales of crinkles[39]. Hierarchical materials are common in biology[40–42]. The relaxation of these materials is best described by a stretched exponential in which the exponent is raised to a power so that stress scales as $e^{-(\frac{t}{\tau})^{\beta}}$. The effect of the exponent is that the function is "stretched" and takes longer to come to a steady-state value than a normal exponential[43–45]. We compress black soldier fly larvae to various volume fractions. Then we use a stretched exponential fit for the measured pressure as a function of time, and extract properties such the speed at which these larvae are able to rearrange and relax the pressure on their bodies.

1.2.5 Synchronizing pile formation of black soldier fly larvae

Insects such as ants and bees are known for their ability to build vast assemblages of thousands of individuals. Fire ants survive flash floods by linking their bodies together to build waterproof rafts. When these rafts anchor to protruding vegetation, they can reform into large towers up to 30 body lengths in height[46]. Bees form large hanging swarms to protect the queen, showing similarity to stalactites[47]. The physical properties of these swarms are understood using techniques such as rheology. However, little is known about how these assemblages form in the first place, and how they disassemble. Understanding these questions will be useful to biologists and physicists who study swarms and the roboticists that design swarming robots.

In our chapter on synchronizing motion of larvae in corners, we study the behavior of larvae raised in rectangular bins, where they grow from newly hatched larva to pupa over a period of weeks. **Figure 1.2.1(a)** shows a photograph of a typical bin for larvae. These are an excellent model organism for studying aggregations because like the ants and bees, the larvae tend to aggregate. They aggregate around food, continuously bringing in new larvae to feed[48]. The ability of the larvae to withstand the weight of up to 53,000 larvae[49] enables them to tightly pack their bodies. They also aggregate in the corners of their bins, generating so much force on the walls that they can break the glue holding the walls together. The aggregations can even become tall enough that larvae use them to climb out of their bins. Understanding how such piles are made and broken can inspire ways to better contain these larvae for industrial applications where they will be raised at scale.

Piles of larvae show similarities to piles of inactive materials. Sand and other granular materials will form piles with a constant angle of repose[50]. Avalanches are known to be

Figure 1.2.1: a. Larvae in a bin pile up in corners. The bin is about 36 cm wide. b. The experimental setup in our study, larvae confined to a two dimensional bin formed using two vertical petri dishes. The container is 95 mm long.

initiated by the motion of the top layer. In an inactive granular pile, the grains on the surface of the slope are free to move while the grains underneath are static. An avalanche occurs when this top layer shears the material underneath to force it downwards [51,52]. Larvae are similar; however, the motion of free larvae at the top layer cannot drag larvae along with them, since the larvae are oriented with their heads downwards and can only crawl forward. Thus, something must penetrate the pile of larvae to get the larvae within it to move.

Black soldier larvae fly are active particles because they have their own energy source. Their ability to form piles is more similar to the behavior of shaken inactive particles than that of avalanches in which all the particles are static. In 1831, English physicist Michael Faraday, who is primarily known for his studies of electromagnetism, performed experiments with vibrated sand grains. At particular frequencies, he observed that the grains form piles, in a process now known as "Faraday tilting" [53]. When the grains are confined to a 2D container and shaken, they pile up in the corners of the container under a range of frequencies and amplitudes of shaking. Although this phenomenon has been repeated by granular physicists in both experiments and simulations, the physical mechanism driving it remains unknown. It is thought to be caused by the interaction of the particles with the

surrounding air, and the change in air pressure[54–56]. Our study of black soldier fly larvae forming piles may give insight into studies of inactive materials where piles can be made or broken up.

1.2.6 Cooling fly larvae with aeration

When black soldier fly larvae are grown in large numbers, they need to be cooled from the heat generated by their metabolism to prevent all of them dying from overheating. This is based on observations in the black soldier fly industry that the larvae cannot be raised in external temperatures above 36°C, above which only 0.1% of 4 – 6 day old larvae survive to become adults. The optimal temperature for raising larvae is 27 – 30°C[57,58]. However, black soldier flies have been observed to mate and lay eggs in external temperatures up to 47°C, suggesting that the larvae should be able to survive at those temperatures as well[59]. Additionally, black soldier flies are native to Georgia where heat waves often reach 44°C.

Raising larvae at temperatures above 36°C has been impossible because these larvae generate heat through their fast metabolism. When larvae grow up free to crawl around on a compost pile, they can easily crawl away from areas that are too hot. Currently in the black soldier fly industry these larvae are raised in plastic bins, where they cannot easily escape excess heat.

While there is no existing literature on temperature generation by black soldier fly larvae, temperature generation by blow fly larvae species (Diptera: Calliphoridae) is well documented. Unlike black soldier flies, which prefer to eat fruit and vegetable compost, blow fly larvae are know to be voracious eaters of animal flesh – they are the piranha of the maggot world. The presence of these flies and the age of their larvae on corpses can be used to measure the post-mortem interval, or the time of death. This information can then be used in forensic investigations in which knowing the time at which a person was killed can narrow down the list of murder suspects. Blow fly larvae, like black soldier fly larvae, are known to be temperature dependent in their development. Different blow fly larva species are known to tolerate different temperatures, and larvae that are able to tolerate higher temperatures out-compete larvae that cannot tolerate those temperatures by metabolically raising the heat on the carcass they feed on[60].

Since larval development is affected by temperature, it is important to characterize how heat generated by aggregated larvae affects their environment. Temperatures in large

aggregations of larvae can be anywhere from 12 to 32°C above the ambient. This heat can speed up the development of larvae if the surround temperatures are cold enough to inhibit their growth. At least 100 larvae need to be present for this effect to be relevant. Larvae have not been found to reduce their heat generation to prevent overheating, but piles of larvae do split in an attempt to thermoregulate. Upper lethal temperatures for blow fly larvae are found to be around 45°C[61–63].

While this has only been investigated in blow fly larvae and not black soldier fly larvae, we present experiments in our chapter on cooling larvae suggesting that black soldier fly larvae have similar thermodynamic behaviors. Since only 100 blow fly larvae have been observed to generate heat, it is no surprise that thousands of black soldier fly larvae within a plastic bin overheat and die when they are fed. This limits the number of larvae that can be produced within a space. The current recommendation is to grow larvae in layers 2-3 inches deep[64]. Ideal conditions for raising larvae are 1.2 larvae per square centimeter. If larval eating rates are limited, they can be raised in depths as 5 larvae per square centimeter (2 lb per square foot), but this decreases the amount of food waste that can be processed and the rate of larva growth[13,65]. A common recommendation is to raise no more than 3 lb of fully grown larvae per square foot, or 7 larvae per square centimeter.

1.3 Thesis outline

In this thesis, we investigate the mechanics of their motion and apply this to new ways to raise larvae. We begin by describing our experimental methods in Chapter 2, from the general details of how larvae were cared for to the specific details of each experiment.

In Chapter 2, we describe the experimental methods that we use to study fly larvae. In Chapter 3, we describe our theoretical methods. In Chapter 4, we elucidate the mechanism by which groups of black soldier fly larvae can eat so quickly. We use time-lapse videography and particle image velocimetry to investigate feeding by black soldier fly larvae. Individually, larvae eat in 5 minute bursts, for 44% of the time they are near food. This results in their forming roadblocks around the food, reducing the rate that food is consumed. To overcome these limitations, larvae push each other away from the food source, resulting in the formation of a fountain of larvae. Larvae crawl towards the food from below, feed, and then are expelled on the top layer. This self-propagating flow pushes away potential roadblocks, thereby increasing eating rate. We present mathematical models for the rate of

eating, incorporating flow rates measured from our experiments.

In Chapter 5, we describe how larvae rearrange to reduce the forces upon them when compressed. We use a universal testing machine to conduct creep tests on larvae, squeezing them to set volume fractions and measuring the time course of their reaction force. Live larvae come to pressure equilibrium ten times faster than dead larvae, indicating that their small movements can rearrange them faster than just settling. The relaxation of dead larvae is well described by stretched exponentials, which also characterize hierarchical self-avoiding materials such as polymers or balls of crumpled aluminum foil. The equilibrium pressures of live larvae are comparable to those of dead larvae, suggesting that such pressures are dictated by the physics of their bodies rather than their behavior. Live larvae perform fluctuations to actively maintain this equilibrium pressure. This ability to survive large pressures might have applications in the larvae-rearing industry, where both live and dead larvae are packed in containers for shipping.

In Chapter 6, we study how larvae pile up in corners of plastic bins. This can allow them to break the bin or escape over its edge. In this combined experimental and numerical study, we confine 300 larvae in flat vertical containers and measure the motion of larvae. The larvae oscillate between corners once per hour. Using particle image velocimetry, we observe oscillations in the velocity and the position of the center of mass of the swarm. The oscillations of velocity lag behind position by 13 minutes. Active matter simulations using elongated swimmers confirm that the oscillation of the larvae in containers can result solely from the physics of their interactions and their activity. We drive the motion of larvae from corner to corner by pushing down on the peak of the pile, and breaking through the jammed larvae. This is a new active matter phenomenon that has implications both for the physics of animal motion and new ways to raise fly larvae in industry.

In Chapter 7, we build an aerating bed to raise larvae in. It is known from forensics studies that fly larvae generate heat through their metabolism. When larvae are found on compost piles, they can crawl away when they get too hot. However, when the larvae are raised in plastic bins they can easily overheat and die because of this excess heat. Aeration cools larvae more effectively than only air conditioning the space they are raised in.

Chapter 8 discusses an aside from the study of fly larvae, and a potential application to swarm robotics. We investigate the phenomenon of "puppy pinwheeling" in which a litter of puppies gathered around a food bowl spontaneously begins spinning as the puppies eat. We

present measurements of how quickly puppies spin as they eat. We then make two robotic models of this behavior: first, we use the Georgia Tech Robotarium as an agent-based model. We then use Bristlebots, simple vibrating robots, placed in bowls to simulate feeding. We find that both agent-based robots and Bristlebots rotate around circular objects.

Chapter 9 summarizes the scales of experiments with fly larvae, and draws connections between these scales to understand motion of larvae in different scenarios. In this chapter we present dimensionless parameters for larvae showing that their inertial forces are low, and viscous and gravitational forces dominate their motion.

We conclude this thesis in Chapter 10 with implications of our work and future directions.

CHAPTER II

EXPERIMENTAL METHODS

In this chapter, we discuss the experimental methods that we use to study fly larvae from how we cared for larvae to filming, particle image velocimetry, and aeration.

2.0.1 Larva care

Black soldier fly larvae are obtained at 8–12 days old. Masses of larvae are determined as an average mass of 100 larvae, and were generally between 0.8 and 0.1 g in our experiments on feeding, compression, and piling. Larvae are obtained from Grubbly Farms prior to January 2019 and from Evo Conversion Systems from January 2019 onward. Unless otherwise stated, larvae are kept at room temperature and are starved between trials to prevent them from pupating.

For experiments measuring larva eating rate, black soldier fly larvae are obtained from Grubbly Farms at 8–12 days old, and weighing about 0.1 g. They are starved for 24 hours before any experiments. On the remaining days, larvae in the individual eating rate experiments and PIV experiments are fed chicken feed; larvae in group feeding rate experiments are fed leftover fruit pulp from smoothies. Larvae obtained from Grubbly Farms for the particle image velocimetry portion of the study had an average mass of 0.09 g.

For experiments compressing individual larvae, larvae are obtained from Grubbly Farms at an average mass of 0.1 g in August 2018. For all other compression experiments, batches of 10,000 larvae are obtained from EVO Conversion Systems at an average mass of 0.07 to 0.08 g during the period January to March 2019.

For experiments on the piling behavior of larvae in corners, black soldier fly larvae are obtained on two separate occasions: first, in January 2018 from Grubbly Farms and then in September 2019 - January 2020 from Evo Conversion Systems. The larvae obtained in September 2019 had an average mass of 0.09 g/larva, the larvae obtained in January 2020 had an average mass of 0.1 g/larva, whereas the mass in 2018 was not recorded but was likely comparable.

2.1 Eating behavior of fly larvae

2.1.1 Larva measurements

Larvae in PIV trials are counted by weighing 100 larvae on an analytical balance, finding an average larva mass of 0.09 g. We use this mass to measure out 1,000 larvae, again on an analytical balance. The larvae are placed in a 250 mL beaker, where we immediately measure their volume so they do not have time to actively settle. We find that 1000 larvae have a volume of $V_{total} = 175$ mL. If every larva has an average length $L = 13.7$ mm, width $w = 4.3$ mm, and height $h = 3.2$ mm, then its volume, that of an ellipsoid, is $V_{larva} = \frac{\pi}{6}whL \sim 0.1$ cm^3. The average packing fraction of larvae is therefore $1000V_{larva}/V_{total} = 0.56$. The maximum packing of ellipsoids is 0.735, so larvae are much less densely packed than they could be if they were allowed to settle.[66] Using this packing fraction, we proceed by using volume to measure out 3000, 5000 and 10,000 larvae in increments of 175 mL of larvae.

In group feeding trials, the number of larvae in an aggregation is estimated by weighing the aggregation with an analytical balance (for 1000 or fewer larvae) or a Smart Weigh ACE110 Digital Scale (for more than 1000 larvae).

2.1.2 Feeding by a single larva

The mouth of a dead larva is photographed with a BK PLUS lab system by Dun, Inc. We determine the chemical composition of the mouth and head by examining a dead larva in a scanning electron microscope (LEO 1530 by Carl Zeiss, AG, Oberkochen, Germany) with an attached energy dispersive x-ray spectrometer (Oxford Instruments, Abingdon, UK).

High speed videos are taken with a Phantom Miro M110 high speed camera at 500 frames per second. The larva's mouth is pushed through a hole in a piece of tape to hold it in place during filming. We track the positions of the maxillae in the high speed video using the free software Tracker from physlets.org. The length of the mandibular brush, $L_{brush} = 0.38$ mm, is used for scale. There is error due to the head movement of the larva, but this displacement is small compared to the movement of the maxillae. To measure how often larvae feed, we perform experiments with single larvae. We place each of 10 larvae into 10 separate 100-cm diameter petri dishes, and fed them with a 0.2-g lump of food in the center of the dish. The food is a mixture of 50% chicken feed (Southern States Layer and Breeder) and 50% water by volume. This food stays in a single lump without leaking

unless a larva breaks it, facilitating our tracking if a larva makes contact and is eating. We film a top view of the larvae with a Sony handycam (Model HDR-XR200V) for over an hour, and watch the videos afterward to mark the durations that the larvae remains in contact with the food, which we assume are the durations that the larvae feed. Fluorescent ceiling lamps are used to light the half of the laboratory that trials are not occurring in, indirectly lighting the larvae and not disturbing their feeding.

Throughout this study, we continue to use Sony handycams for all filming except high speed, but we will vary the food and lighting.

2.1.3 Particle image velocimetry (PIV) of a group of larvae

A specially constructed apparatus is used to perform PIV on groups of larvae (**Figure 2.1.1(a)**). A 10-gallon fish tank is set up on a metal cart with cameras mounted both above and underneath the tank. Fluorescent ceiling lamps illuminate the top view. To illuminate the bottom view, we point two LED lamps (Visual Instrumentation Corporation, Model 900420 W) from the side. The lamps are covered in thin packaging foam and red cellophane because lighting in this spectrum is less disruptive to insects.[67] To commence experiments, half of an orange slice (weighing 12 g) is pushed through a toothpick glued upright in the center of the tank. The orange slice is not peeled so that larvae do not tear it from the stick.

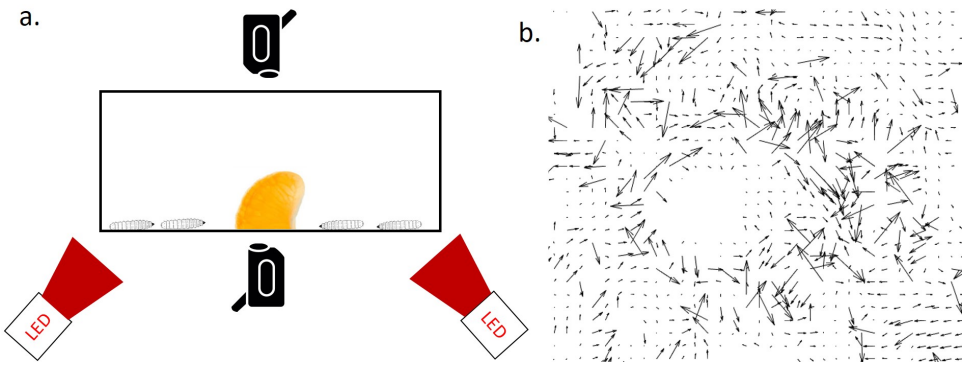

Figure 2.1.1: a. Setup of particle image velocimetry experiment. Larvae are placed in a 10 gallon aquarium with cameras filming the top and bottom. b. Sample instantaneous vectors from a top view of larvae around food. The vectors do not point to any mean flows, showing the need for averaging.

Larvae aggregate around the orange as they eat it. We use PIV to determine the flow

properties of the larva aggregation. Within the aggregation of larvae around food, we can define a "mixing region" as the area around the orange where the average velocity of larvae is greater than a threshold of 0.125 mm/s, or 1/16th the speed of a free larva. The mixing region is characterized by an inflow of larvae on the bottom layer and an outflow of larvae on the top layer, indicating that larvae form a coherent flow around food. Many of our calculations will refer to the velocity and size of this mixing region.

We do two types of experiments: an experiment with both a top and bottom view, and then experiments with varying numbers of larvae with a top view only. Performing analysis on both top and bottom view is time-consuming, so the bottom view is performed sparingly. In the top and bottom views, 600 mL of larvae (approximately 3500 larvae) are placed in the tank and eat an orange slice as they are filmed. For each video, one hour of footage is filmed. One frame per second of the resulting video is extracted from top view, and one frame per five seconds of the video is extracted from the bottom view. Larvae on the bottom are jammed by the surrounding larvae and move slower than the ones on top. Larvae on the top view move faster, but less frequently, than larvae on the bottom view. Consequently, a longer time between frames is needed on the bottom view. Frames are extracted using the free software, Video to JPG Converter (www.dvdvideosoft.com).

Digitization and data extraction from the images is accomplished with MATLAB. We write a script to crop raw images and convert them to white larvae on a black background. PIVLab[68,69] is used to measure the velocity fields between each pair of consecutive frames. A mask is drawn on top of the orange slice to avoid analyzing that area. The interrogation windows, in which particle positions are correlated, decrease in size from 64 pixels to 32 pixels in two passes of analysis. Sample instantaneous vectors are shown in (**Figure 2.1.1(b)**). For the experiment with a top and bottom view, results are averaged over 2000 seconds, starting at 500 seconds, which we see as steady state. We validate our PIV analysis by randomly reshuffling frames from 500 to 2500 seconds in the top view of this experiment: the resulting vector field after averaging, shown in **Figure 2.1.2**, shows the absence of a mixing region, as expected. This confirms that the resulting mixing region is not an artifact of our analysis.

For this single trial with a top and bottom view, the mixing region is not clearly above a particular threshold. This is likely caused by the bottom lighting disturbing the behavior of the larvae. Instead, we estimate the mixing region by measuring it within PIVlab to be

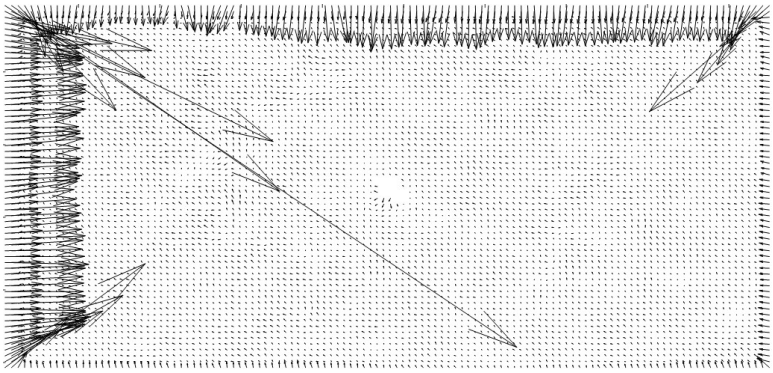

Figure 2.1.2: When vector fields used for averaging in the top view in the top and bottom view PIV experiment are reshuffled in time, their average no longer shows a mixing region. This indicates that the mixing region found through PIV analysis is valid.

about 80 cm^2 for the top view and 60 cm^2 for the bottom view (including the orange). We then draw this mask around the mixing region in the top and bottom views to determine the average velocity magnitude, divergence, and vorticity.

In our trials with multiple group sizes, we perform top-view PIV experiments with 500, 1000, 3000, 5000, and 10,000 larvae. Since larvae can only enter the mixing region from the top or bottom layer, the number of larvae leaving the food on the top view must be equal to the number of larvae coming in to eat on the bottom view. Thus, the top view is sufficient to calculate both the flow rate of larvae away from and towards food. The top view yields more consistent results because the bottom view lighting disturbs larva feeding. With fewer than 500 larvae in the container, the mixing region is too small for PIV analysis, so the analysis starts with 500 larvae. Only fluorescent ceiling lamps are used in these experiments, and the bottom view is not filmed. Only 35 minutes of footage is filmed in these cases. 1500 seconds of motion are averaged, and a velocity limit of 10 mm/s, 5 times the speed of a free larva, is selected in the 1000 and 5000 larva trials as there was some noise in a corner of the container that yielded velocities over 10 times the speed of a free larva. We then select the mixing region with our threshold velocity of 0.125 mm/s. The average vector fields are saved for further analysis as described in §2.4.

2.1.4 Measuring flow rate from PIV

We define the rate of outflow of larvae as the number of larvae leaving the food per minute on the top layer of the mixing region. By conservation of mass at steady-state, this flow

rate is necessarily equal to the larvae entering the food below. To estimate the flow rate of larvae for mixing regions with 500 to 10,000 larvae, we calculate the flux from the boundary as determined by MATLAB. We use the equation Q for number of larvae leaving per minute as,

$$Q = \frac{1}{V_{larva}} \sum_{boundary} (\mathbf{v} \cdot \mathbf{n}) dA, \tag{1}$$

where $\mathbf{v}$ is the velocity vector at each point, $\mathbf{n}$ is the normal to the boundary segment at that point, dA is the length of the segment multiplied by the layer depth (the height h of a larva, 3.2 mm), and $V_{larva} \sim 0.1$ mL is the volume of a larva. The segments are measured by connecting the midpoints of the two boundary sections surrounding the point, and their length is 5 ± 1 mm. The relationship between the number of larvae and flow rate is shown in **Figure 4.2.2(f)**. We model this trend using a linear best fit for 1000 to 10,000 larvae:

$$Q = aN + b \tag{2}$$

where a and b are coefficients and N is the number of larvae. To validate calculating average vector fields over 1500 seconds for outflow calculations, we additionally recalculate Q with velocity fields calculated with 1000 seconds of averaging starting at 1000 seconds, and 500 seconds of averaging starting at 1500 seconds. We compare these average velocity fields for the 1000 to 10,000 larva trials. We find that the flow rate of larvae changes by a maximum 8 larvae per minute with averaging over 1000 seconds and maximum 11 larvae per minute with averaging over 500 seconds. Since Q is on the order of 50 larvae per minute for 1,000 larvae and 100 larvae per minute for 3,000 to 10,000 larvae, we are re-assured that the flow rates are repeatable measurements.

2.1.5 Measuring group eating rates

We measure larva eating rates by feeding orange slices weighing 6 – 18 g to larvae in bins. Filming is done under red light to avoid disturbing the larvae. Groups of larvae numbering 500 and fewer are placed into plastic drink cups as shown in **Figure 4.3.1(a)**.Groups of 10003000 larvae are placed into 1 l beakers. Groups of 5000 - 10,000 larvae are placed into containers (34.6 cm x 21 cm x 12.4 cm plastic Sterilite) while groups of 15,000 - 30,000 are placed in larger containers (42.9 cm x 29.2 cm x 23.5 cm plastic Sterilite). The test with 58,000 larvae is done in a concrete mixing tub (86.4 cm x 58.4 cm x 17.8 cm).

Experiments are performed throughout the summer and fall of 2016, in both an indoor laboratory and in an open-air warehouse. All experiments involve feeding an orange slice to larvae of various group sizes, and then weighing it (Mettler Toledo Classic Plus analytical balance) to determine the amount eaten. The duration of eating is varied from 5 minutes to 30 minutes, depending on the size of the group. Larger numbers of larvae eat faster, so necessitate a shorter experimental duration; smaller numbers of larvae required longer times in order to obtain an accurate estimate of the mass eaten. The slice was weighed after 30 minutes for aggregations of 200 or fewer larvae and three of the 500 larva trials, and after 5 minutes for aggregations of 1000 or more larvae and the other three 500 larva trials. Eating rates are adjusted for evaporation of the food piece, measured to be 0.2% of initial weight every 30 minutes.

The surface area of a 12 g half of an orange slice is measured by taking pictures of its faces with a ruler for scale, and measuring the areas of the sides by selecting them as a polygon in ImageJ. The area of the curved surface is estimated by measuring it in ImageJ and then multiplying that area by the ratio of its actual length (from the crescent side image) to its projected length (from the curved side image). The total area of the orange is given by $A = 2A_1 + A_2 + A_3$, where $A_1 = 1143$ mm is the area of the crescent-shaped face, $A_2 = 1191$ mm is the area of the curved face, and $A_3 = 590$ mm is the area of the bottom surface. The surface area is then about $S = 4067$ mm^2. Large numbers of larvae coat the entire piece of food after about 10 minutes of eating, although there is a location on the orange slice where larvae do not eat for some of the experiment.

2.2 Compressing fly larvae

2.2.1 Compression tests with varying volume fraction

We measured larval activity by compressing aggregations of larvae with a Zwick Roell Universal Testing Machine (UTM). **Figure 5.1.1(a)** demonstrates the experiment for the volume fraction $\phi = 0.80$. When the larvae were compressed by the UTM, they changed orientation, as shown by the schematics of their positions before and after compression (**Figure 5.1.1(b-c)**). The loading cell is a compression plate with a diameter of $D_{plate} = 90$ mm and 1 kN maximum force. The container for larvae was composed of a clear acrylic tube with wall thickness 3.1 mm and inner diameter $D_{chamber} = 95$ mm, which forms a tight enough fit with the compression plate to prevent larvae from escaping. The tube was

glued to a 5.2-mm thick acrylic plate.

Experiments were performed with 2000 randomly selected larvae, whose number, N, was estimated by the ratio of total weight (158 g) and mass of a single larva of $m_L = 0.08 \pm 0.02$ g. We estimated the volume of a larva, $V_L = m_L/\rho_L$ as its average mass, $m_L = 0.08$ g, divided by the density of water, $\rho_L = 1$ g/mL. Several days after the tests with live larvae were finished, the larvae were sacrificed in a household freezer for 24 hours during which each larva reduced in mass to 0.06 g. Tests were then repeated using 158 g of thawed dead larvae. Since the dead larvae were lighter than live ones, we froze adequate numbers of larvae to offset their reduction in mass.

We report all data in terms of volume fraction ϕ, which is derived from the height H of the larvae measured by the UTM. Consider a cylinder of height H, bottom plate height H_{offset}, and diameter $D_{chamber}$. The volume fraction of larvae ϕ may be written as the ratio of the total volume of larvae, NV_L, to the inner volume of the cylinder $\frac{1}{4}\pi D^2_{chamber}(H - H_{offset})$:

$$\phi = \frac{4NV_L}{\pi D^2_{chamber}(H - H_{offset})}. \tag{3}$$

Note that the height of the endcap, $H_{offset} = 5.2$ mm, was used in order to accurately measure larvae height using the UTM. Larvae in the tube are lightly shaken by hand before the test begins to randomize their arrangement and negate the effects of their own settling.

Once larvae are in the tube under the UTM, we performed creep tests to measure the time course of applied forces. A creep test applies forces to maintain the larvae at set volume fractions ϕ. We tested volume fractions between 0.56 and 0.80 by lowering the plate to heights between 33 mm and 45 mm, with 1 mm increments between tests. The lowest volume fraction was set by the larvae's tendency to clump together. Giving them a larger volume than their preferred spacing resulted in incomplete contact between the larvae and the top plate. The test began with the plate being lowered onto the aggregation at 100 mm/min, with an initial force of 0.1 N, until it reached the specified separation between the plate and the floor of the UTM. The plate then stopped and the UTM recorded the force F for 1000 seconds, after which the plate was lifted. Each compression test was also recorded with a Sony Handycam (Model HDR-XR200V).

We calculated the pressure as the force divided by the area of the compression plate

$\frac{1}{4}\pi D_{plate}^2$:

$$P = \frac{4F}{\pi D_{plate}^2}. \tag{4}$$

As a visualization of larvae settling, 2000 larvae with an average mass of 0.07 g/larva were placed in a 400 mL beaker and are allowed to settle for an hour, as shown in **Figure 5.1.1(d - e)**.

2.2.2 Experiments compressing individual larvae

To measure the maximum force that a single larva can tolerate, we compressed five larvae in five individual tests to a force of 40N at a speed of 5 mm/min with an initial force of 0.2 N so that the top plate can contact the larva.

In experiments with a single larva, the pressure is estimated using the larva's initial top area. The top area is obtained by taking an image of a larva and measuring its area within ImageJ[70]. The pressure can then be written $P = \frac{F}{A}$. We take the peak in pressure as the stress at which the larva exploded. Pictures of the larvae from the top and side are taken with an Andonstar Digital Microscope. The strain ϵ for a single larva may be written $\epsilon = \frac{h_0 - h}{h_0}$, where h is the height of the compressed larva as measured by the UTM and h_0 is the initial height of the larva. Since the UTM compresses the larva to get a measurement of its height, we measure the side of the larva in ImageJ to obtain an initial height for these strain calculations.

2.3 Synchronizing piling of larvae

2.3.1 Measuring centroid of larva swarm

Setups are made from the lids of square petri dishes taped together with duct tape, with a hole cut in the top for loading and unloading larvae. The resulting container is 95 mm tall, 95 mm wide, and 18 mm deep, which we refer to henceforth as the "bin". We perform experiments in January 2018 and September 2019. In the experiments, we place 280-300 larvae into each of 4 bins. The larvae numbers are estimated either by counting them individually or by weighing sets of 27 g of larvae, which is equivalent to 300 larvae using the mass of a single larva. We perform 3 sets of experiments with at least one day of break in between, filming for 5 - 13 hours with a Sony Handycam model HDR-XR200V. We record four containers simultaneously, generating a total of 100 hours of filmed larva motion.

Digital processing is performed in MATLAB. Frames from the videos are extracted at a rate of 1 frame per second using the command ffmpeg (https://www.ffmpeg.org/about.html). A MATLAB script crops out individual containers, detects the mass of larvae through a color threshold, and records the position of the centroid of the larvae for each frame of the video. The centroid is reported as a proportion of the width of the container, measured from the left. A moving average of 100 seconds is used to smooth out any noise. Visually, we find that smallest and greatest centroid positions correspond to the larvae being the most aggregated to the left and right side of the container, respectively. We plot on a histogram the 80 measurements of the period of centroid motion and fit it to a gamma probability distribution function in MATLAB.

2.3.2 Particle image velocimetry

For particle image velocimetry analysis, we paint by hand the rear 2 or 3 segments of 300 larvae, which weigh 27 grams total. A number of paints were tested, but Testors Glossy Red (# 2503) paint marker works best. Their motion is filmed in a bin for 3 hours. Frames are extracted for every second of video, and the images are converted into black and white with a MATLAB script, with white patches corresponding to the red ends of the larvae. The black and white images are analyzed with PIVlab[71]. The instantaneous vector fields are saved and analyzed using a 180-second rolling average and a 1 mm/s maximum for the velocity magnitude limit. The average horizontal velocity throughout the container is saved at each time. A rolling average of 1000 seconds is taken to dampen out any remaining noise. The center of mass analysis from the previous section is also performed on the videos here with a 1000 second moving average to ensure that the larvae behaved similarly to the longer trials.

2.3.3 Synchronizing motion with intruders

We attach two stepper motors with lead screws (https://www.pololu.com/product/2689) to each side of the vertical bin. A laser-cut acrylic extension is attached to each motor's traveling nut to enable the extension to reach very close to the bin of larvae. A magnet is attached to the end of each extension, and an M3 x 10 mm screw is held by the magnet to the other side of the container. When the motor is turned on, the lead screw rotates, causing the extension with magnet to travel vertically, dragging the screw along with it.

This setup is shown in **Figure 6.1.3(a)**. The screws are initially positioned at the top of the container, far from the larvae.

The bin is filled with 300 larvae and filmed for five hours. After 2.5 hours, the larvae begin to switch between corners of the bin. This is a long preparation time for switching of the pile from corner to corner, and we have no explanation for it. It may be related to the room temperature and lighting at the start of the experiment, as the temperature in the room was increased slightly two hours into the experiment. Once the larvae form a pile in the left corner of the container, we begin forcing their motion with the stepper motor. The motor is turned on to move the left side screw down through the larvae at a speed of 0.5 mm/sec. Five minutes later, the screw is raised at a speed of 2 mm/sec. Fifteen minutes after that, the procedure is repeated with the right side screw. This is then repeated for 2.5 hours. The centroids of the larvae are then determined, and a sinusoid fitted to the centroid data. The video is saved at 64x speed using Windows Movie Maker and each magnet was tracked in this video with the free software Tracker (https://physlets.org/tracker/).

We also attempt moving either an M3 x 12 mm screw or a magnet measuring 20 mm x 13 mm x 5 mm across the bottom of the container through the larvae by attaching a magnet to a New Era Pump Systems syringe pump set to move linearly at 5 mm/min, but larva corner switching is not consistently synchronized to this motion.

2.4 Cooling larvae with aeration

2.4.1 Investigating heat generation by larvae

We visualize heat generation by black soldier fly larvae by mixing approximately 2000 0.1 g larvae with food (chicken feed mixed with 50% water by volume). The mass of the food is not recorded but is enough that larvae are dispersed within the food, and the larvae are not limited in how much they can eat. We take a time lapse of the larvae mixed with food with a FLIR T450sc thermal camera at one image per minute.

To estimate the metabolism of fly larvae, we measure the oxygen consumption and CO_2 production of 50 larvae with and without food in a respirometer, shown in **Figure 7.1.1(c)**. 50 larvae are placed in the respirometer without food and measure first their oxygen consumption and then their CO_2 production for 300 seconds. We then add chicken feed mixed with water to the container, and repeat the measurements.

2.4.2 Aeration prototypes

Larvae are aerated with a fan from underneath. Our first prototype is made out of a 4 inch outer diameter acrylic tube with 1/8 inch thick walls with a mesh glued to one end. This bed is glued to a welded cone with a 12 inch diameter inlet and 4 inch diameter outlet. The cone is then glued to a 12 inch diameter portable ventilation fan (Strongway 2905 CFM maximum flow, Item 49945), oriented vertically. We test aerating larvae for cooling with this prototype by placing 500 mL of larvae mixed with sand substrate at 34°C in the bed and an equal volume in another section of the same 4 inch diameter tube with no aeration. These containers of larvae are placed in a room at 22°C, and the fan is turned on and both are filmed with the FLIR T450sc thermal camera. This setup is shown in **Figure 7.2.1(a)** with the aerated larvae on the right. We record the temperature over time in the frames from the video.

Once we have confirmed that aeration can cool larvae with this small prototype, we move on to raising larvae in a 12 inch diameter fan to investigate how aeration affects their growth. The same fan is used. This time a right angle fitting is attached to it to reorient the airflow. A barbecue grate is placed inside the top of the right angle fitting, a mesh is glued on top of the grate, and a twelve-inch diameter tube is placed on top of the grate. Hot glue around the connection of the tube to the mesh seals up holes and cracks in the connection and prevents larvae from escaping.

We test this bed by growing out larvae in it. At Grubbly Farms, we place 20,600 (measured by weight) nine day old larvae with an average mass of 0.12 g/larva in the bed, turn on the air, and leave the fan on as the larvae grow until the larvae are 14 days old and ready to harvest. The larvae are fed the same diet per larva per day as the rest of the larvae being grown at the facility at lower densities and without aeration.

Our final prototype can fit hundreds of thousands of larvae. The fan (Vortex V-16XL) has a maximum airflow of 4515 CFM and maximum static pressure of 2.55 in H2O. The speed can be controlled from barely aerating the larvae to fully fluidizing them. The fan is inserted into a round hole cut into a wooden air box that four bus boy bins (20 inches long by 15 inches wide by 7 inches tall) can fit into. The bins have circular holes cut out in them with mesh lining the holes. A schematic of this design, which can be scaled up by adding more bins, is shown in **Figure 7.2.3(a)**; a photograph of the setup is shown in **Figure**

7.2.3(b). When filled with larvae, the bed is surrounded by a mesh tent to prevent larvae from escaping. This bed is set up at the Techway building in the North Avenue Research Area. We get 200,000 larvae from Evo Conversion Systems. After growing out the larvae, we place them in this bed at an initial weight of 0.02 g/larva. The fan is turned on to the lowest setting and allowed to run as the larvae are grown in the bed for 21 days. Three bins are filled with larvae and each bin of larvae gets 1 liter of chicken feed mixed with water per day.

2.5 Spinning during feeding

To investigate how puppies pinwheel during feeding, we first look at the numerous Youtube videos of the phenomenon on Youtube. The list of 24 videos used is given in Appendix 2. We measure the frequency of revolution in revolutions per minute by watching a puppy in each video frame by frame and noting the time it takes for the puppy to complete a revolution around the food bowl, and then converting to degrees per second. The number of puppies around the bowl in each video is recorded.

The Robotarium model consists of twelve robots that are all programmed to go to the center of the arena at a constant speed. A circular boundary around the center of the arena is used to represent the edge of the food bowl. When the robots reach this boundary, they update their target so as to keep moving forward and rotate to avoid collisions with the boundary. This, combined with the built-in collision avoidance mechanism, causes the robots to rotate around the center.

The Bristlebot model uses HEXBUG Nano robots (www.hexbug.com). We 3D print three bowls for the robots to spin around, with three different angles. The bowls are shown in **Figure 2.5.1** with dimensions.

In experiments with Bristlebots, from 1 to 19 bots are turned on, placed in the bowl, and recorded with a Sony Handycam for one minute. In the resulting videos, one robot is tracked in polar coordinates with the free software Tracker from Physlets.org for one revolution. Its rotational speed ω is calculated with a best fit line as a representation of the average speed in the container. This is done in each bowl three times, resulting in three plots of angular velocity vs. time for each angle. Then, the MATLAB curve fitting tool is used to fit a logistic function to each of the trials. As the robot speeds could have changed due to their battery levels depleting, the three sets of trials in each bowl are analyzed separately.

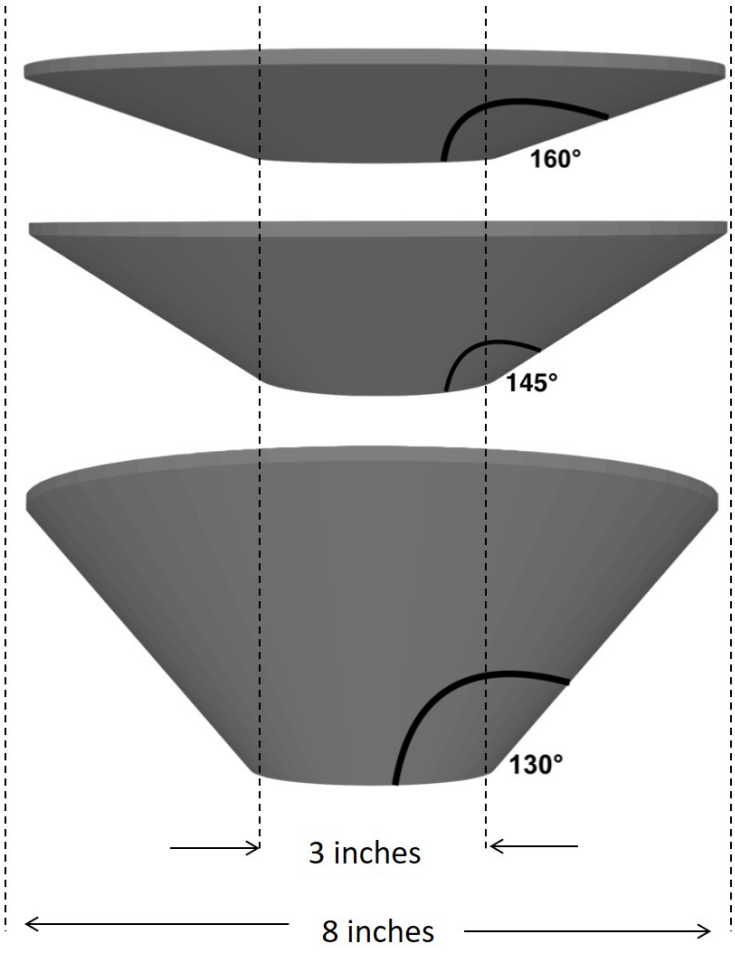

Figure 2.5.1: Bowls used for Bristlebot experiments.

Now we turn to the theoretical methods that we used for modeling how much larvae eat, how they move, and how to cool them off.

CHAPTER III

THEORETICAL METHODS

In this chapter, we describe the theoretical models used to study fly larvae: our model for eating rate, methods for simulating larvae piling in corners of containers, and simplified model of cooling with aeration.

3.0.1 Mathematical model of eating rate

In this section, we present a mathematical model for eating rate of groups of larvae. The mass M of food eaten is measured following a feeding time t. While experiments make instantaneous eating rates $\frac{dM}{dt}$ challenging to measure, we can make a single measurement of M, thus we report the average rate of eating during this duration as $\overline{\frac{dM}{dt}}$, which for simplicity we will refer to as $\frac{dM}{dt}$.

Experiments of single larva indicate that it only eats for a fraction of the time R where

$$R = \frac{\text{eating time}}{\text{total time}}. \tag{5}$$

As a consequence, the average eating rate of a larva will depend on the duration given. If the instantaneous eating rate is η_{inst}, then across long times, a larva will eat at a lower average eating rate η:

$$\eta = R\eta_{inst}, \tag{6}$$

due to the breaks it takes between meals.

When considering a group of N larvae, the average rate of eating depends on the number in the group. We divide group sizes into three regimes. First, we consider the regime where there are few larvae eating. Here, $N < N_{max}$ where

$$N_{max} \sim \frac{S\phi}{\pi(h/2)(w/2)}, \tag{7}$$

is defined as the number of larvae that can fit themselves around the food item of surface area S according to a random close packing. We assume that a larva's face has an elliptical cross-section, $w = 4.3$ mm wide by $h = 3.2$ mm tall, and that larvae are packed at $\phi = 0.895$, the maximum packing fraction of ellipses.[72]

In this regime, the eating rate increases in proportion to the number of larvae:

$$\frac{dM}{dt} = \eta N \text{ if } N < N_{max}, \tag{8}$$

since each larvae has access to the food. This regime ends when the larvae exceed the number of spaces N_{max} around the food. In the limit of many larvae ($N \gg N_{max}$), hungry larvae push away any larvae that are not eating. Thus, the slots around the food are always filled, and food is being eaten continuously on all sides. In this case, the rate at which food is eaten per larva increases to $\eta_{inst} = \frac{\eta}{R}$. The eating rate of the group in this regime is:

$$\frac{dM}{dt}_{max} = \eta_{inst} N_{max} \text{ if } N \gg N_{max} \tag{9}$$

where the condition for this regime will be clarified after consideration of the following intermediary regime.

Between the regimes with few and large numbers of larvae is an intermediate regime. Here, the larvae collectively generate a flow of Q larvae per minute towards the food. For simplicity, we neglect larvae leaving the eating region and assume that the inflow increases the eating rate according to a linear sum:

$$\frac{dM}{dt} = \eta(N_{max} + Q\tau) \text{ if } N_{max} \leq N \leq N', \tag{10}$$

where $\tau = 5$ minutes is the duration of the feeding for this number of larvae ($N > 500$ larvae). This increased in eating rate is bounded from above by the maximum possible eating rate $\eta_{inst} N_{max}$ given in Eq. (9). Using Eq. (10), the number of larvae N' at which eating rate is maximized is:

$$N' = \frac{N_{max}(1-R)}{aR\tau} - \frac{b}{a}, \tag{11}$$

a value that can be calculated from our experiments.

Altogether, we have the following three regimes

$$\frac{dM}{dt} = \begin{cases} \eta N & \text{if } N < N_{max} \\ \eta(N_{max} + Q\tau) & \text{if } N_{max} \leq N \leq N' \\ \frac{1}{R}\eta N_{max} & \text{if } N > N', \end{cases} \tag{12}$$

where we report dM/dt and η in the units of grams per hour.

3.0.2 Simulations of larvae aggregation in corners

Modeling fly larvae aggregation was done with the help of Ahmad Omar and John Brady, and this section was written by Ahmad Omar. We apply a *minimal micromechanical model* for larva dynamics that can qualitatively reproduce our experimental observations. To this end, we turn to a model for active dynamics that has been used throughout the literature [73,74] which we briefly describe here. Within this model, each active particle exerts a constant self-propulsive force $\mathbf{F}^{\text{active}} = \zeta U_0 \mathbf{q}$ in a direction $\mathbf{q}$ in order to move at a speed U_0 in a medium of resistance ζ. The particle orientation $\mathbf{q}$ undergoes *random* reorientation events that result in a characteristic reorientation time τ_R and run length (the distance an isolated particle travels before reorienting) of $U_0\tau_R$. We use a hard-disk interparticle force $\mathbf{F_i^{HD}}$ to keep the particles (2D disks of radius a) from overlapping in our simulations [75,76].

To model the geometry of the larvae, we linearly bond "passive" (no activity) beads to the active particle such that the active particle serves as one of the ends of a single oligomeric unit (see inset of **Figure 6.1.4(b)**). We link 4 discs together to form a single larva because the biological larvae have an aspect ratio of $L/w \sim 4$. The disks are connected with simple harmonic bonds with a spring constant $K = 82.5F^{active}/a$ and rest length of $r_0 = 1.1$ particle diameters such that bonded particles i and j separated by a distance $\mathbf{r_{ij}}$ experience a force $\mathbf{F_{ij}^{bond}} = -\mathbf{K}(\mathbf{r_{ij}} - \mathbf{r_0})$. We fix the total number of larvae to be 50, which are fewer than those in our experiments, but the largest number we could compute with our computer performance. Finally, we include a gravitational force $\mathbf{F^G}$ acting in the negative y-direction with a magnitude of g: $\mathbf{F^G} = 18\mathbf{F_{active}}$) (see **Figure 6.1.4(a)** for the definition of coordinate axes). The strength of gravitational force is much greater than the magnitude of the active force (e.g., $g \gg \zeta U_0$). Hard-wall boundary conditions are enforced in all directions and the box dimensions are set to 62 particle radii (or 7.75 larva lengths) in the x-coordinate and 80 particle radii (8 larva lengths) in the y-coordinate. In comparison, our experimental setup has dimensions of 7 by 7 larvae lengths.

With the forces now defined, we turn to the equations-of-motion for our particles. The motion of particle i is governed by the overdamped Langevin equation $\mathbf{F_i^{active}} + \mathbf{F_i^{bond}} + \mathbf{F_i^G} + \mathbf{F_i^{HD}} + \mathbf{F^{wall}} - \zeta\mathbf{U_i} = \mathbf{0}$ where $\mathbf{F_{ij}^{HD}}$ is interparticle force from particle j, $\mathbf{F^{wall}}$ is the force exerted by the boundary on the particle, and $\mathbf{U_i}$ is the instantaneous particle velocity. The active force $\mathbf{F_i^{active}}$ is identically $\mathbf{0}$ for all particles excluding the "head"

particles. The orientation dynamics of the active (or head) particles similarly follow an overdamped Langevin equation $\mathbf{L_i^R} - \zeta_\mathbf{R}\mathbf{\Omega_i} = \mathbf{0}$ where $\mathbf{\Omega_i}$ is the angular velocity of $\mathbf{q_i}$, $\mathbf{L_i^R}$ is the random reorientation torque and ζ_R is the rotational drag. Note that the orientation of the head particle $\mathbf{q}$ is entirely controlled by rotary diffusion and does not depend on, for example, the bond vectors, interparticle forces, etc. Further note that the rotational drag has no dynamical consequences as we can rewrite the angular equation-of-motion as $\tilde{\mathbf{L}}_\mathbf{i}^\mathbf{R} - \mathbf{\Omega_i} = \mathbf{0}$ with a redefined torque $\tilde{\mathbf{L}}_\mathbf{i}^\mathbf{R}$ which has white noise statistics $\overline{\tilde{\mathbf{L}}_\mathbf{i}^\mathbf{R}} = \mathbf{0}$ and $\overline{\tilde{\mathbf{L}}_\mathbf{i}^\mathbf{R}(\mathbf{t})\tilde{\mathbf{L}}_\mathbf{j}^\mathbf{R}(\mathbf{0})} = 2\delta(t)\delta_{ij}\mathbf{I}/\tau_\mathbf{R}$ where $\delta(t)$ and δ_{ij} are Dirac and Kroneker deltas, respectively. These orientation dynamics give rise to a rotational diffusivity τ_R^{-1} that need not be thermal in origin. The run length of the larvae in free space, $U_0\tau_R/a$, is set to 100. We emphasize that these equations of motion are *entirely athermal* as we do not include (thermal) Brownian motion as in traditional active Brownian particle models.

3.0.3 Model for larva cooling

We calculate the rate at which larvae are cooled by aeration using a lumped capacitance model. The lumped capacitance model assumes that the temperature of the solid (or larva) is uniform as the larva being cooled is small enough that conduction through the larva is far faster than convection. Convection is assumed to be the primary mode of heat transfer between the larva and air. The temperature is therefore only a function of the time t. A model of a larva surrounded by airflow is shown in **Figure 7.2.1(c)**. In this model, we assume that an individual larva at temperature T_i is surrounded by airflow at temperature T_∞ and a velocity that is to be calculated with the Ergun equation. The larva has a mass M, heat capacitance c, and heat conductance k_L, estimated for typical values for tissue[77–79]. An energy balance on a larva shows that the energy being transferred from the larva to its surroundings is equal to the energy change in the larva:

$$-\dot{E}_{out} = \dot{E}_{larva}. \tag{13}$$

We then find the rate of change of energy in terms of heat transfer properties. The rate of change of energy due to convection is controlled by the heat transfer coefficient, h, the area of the larva exposed to the air flow A (the surface area of an ellipsoid), and the temperature difference between the larva and the surrounding air. That balances the rate of change of energy in the larva:

$$-hA(T_i - T_\infty) = Mc\frac{dT}{dt}. \tag{14}$$

We can then solve for the temperature of a larva at any time t:

$$\frac{T - T_\infty}{T_i - T_\infty} = \exp\left(-\frac{hA}{\rho V c}t\right). \tag{15}$$

The area of a larva A is the surface area of an ellipsoid with length L, width W and height H[80]

$$A = 4\pi\left(\frac{(0.25LW)^{1.6} + (0.25WH)^{1.6} + (0.25LH)^{1.6}}{3}\right)^{\frac{1}{1.6}}. \tag{16}$$

To find the convective heat transfer coefficient h we use the Churchill and Bernstein correlation with a low Reynolds number approximation[81] for slow flow around a small larva in the aerating bed:

$$\mathrm{Nu} = 0.3 + \left(\frac{0.62 * \mathrm{Re}^{(1/2)}\mathrm{Pr}^{(1/3)}}{(1 + (0.4\mathrm{Pr})^{(2/3)}}\right)^{0.25}, \tag{17}$$

where the Reynolds number is calculated based on the air density ρ, air speed around the larva V, width of the larva w and air viscosity μ:

$$\mathrm{Re} = \frac{\rho V W}{\mu}, \tag{18}$$

and the Prandtl number is calculated based on the air heat capacitance $c_{p,air}$, viscosity, and heat conductance k_{air}

$$\mathrm{Pr} = \frac{c_{p,air}\mu}{k_{air}}. \tag{19}$$

The heat transfer coefficient is then

$$h = \frac{\mathrm{Nu}k_{air}}{W}, \tag{20}$$

and we can solve for the temperature at any time with Equation 15. This expression will only be valid if the Biot number is low:

$$\mathrm{Bi} = \frac{hL_c}{k_L} \leq 0.1, \tag{21}$$

where L_c is the distance to a larva's center (half its width).

The only thing left is to estimate the airflow speed, V. We know that this speed is low, since we keep the fan on a low setting so as to not fluidize the larvae. We can estimate it using the Ergun equation[82], which calculates the pressure drop of a fluid through a packed

bed based on the volumetric flow rate of an empty bed, the fluid properties, and particle properties. This equation states that the pressure drop, Δp in a bed packed with particles to a height L_{bed} is:

$$\frac{\Delta p}{L_{bed}} = \frac{150\mu(1-\epsilon)^2 U_0}{\epsilon^3 d_{part}^2} + \frac{1.75(1-\epsilon)\rho U_0^2}{\epsilon^3 d_{part}}. \tag{22}$$

where ϵ is the void space in the bed (volume fraction not taken up by larvae or substrate), ρ is the air density, U_0 is the air speed if the bed was empty, and d_{part} is the diameter of the particles in the bed. We estimate the void space to be $\epsilon = 0.4$, and the particle diameter d_{part} to be the diameter of a sand particle, as more of the bed is filled with substrate than with larvae in most of our trials. However if the bed is to be mostly filled with larvae so as to not waste space, this number can be adjusted.

To estimate the air flow through the bed, we use the power provided by the fan's specifications. The power of a flow is[83]:

$$P = VA\Delta p. \tag{23}$$

We calculate the pressure loss due to fittings in an empty bed by calculating the pressure loss due to the fittings on the bed (a cone reducing the 12 inch diameter fan to a 3.75 inch diameter tube with minor loss factor K and friction factor f in the smooth acrylic tube[83].

$$p_{loss} = 0.5\rho U^2(K + f\frac{L}{d_{bed}}); \tag{24}$$

Where the friction factor f is estimated for a smooth pipe and the Then, knowing the inlet power and flow rate of the fan without any fittings, we use equation 23 to estimate the airflow through an empty bed, U_0:

$$U_0 = \frac{P}{Ap_{loss}}. \tag{25}$$

To calculate the velocity of the fluid surrounding a larva, we take the area of airflow to be $A_{void} = A_{bed}\epsilon^{3/2}$ to convert the volume fraction ϵ to an area fraction. The air speed through the bed is therefore

$$V = \frac{P}{(0.25\pi D^2\epsilon^{3/2})(\Delta p + p_{loss})} \tag{26}$$

However, in practice, it is much more useful to control the air speed into the bed with a voltage regulator on the motor rather than attempting to calculate the precise speed necessary for cooling. This model is a simple estimate of cooling. We use distribution of the

sizes of larvae and sand particles in the bed, the packing fraction, and any other losses, as fitting parameters and adjust them so that the model fits the actual pressure in the bed. To get a better estimate of air flow through larvae and the cooling resulting from it, a detailed 3D CFD model can be done. Parameters such as the heat conductance and capacitance of a larva, he void space, and the distribution of particles in the bed should be measured. The aerating properties used in this calculation are given in **Appendix 1, Table 3 and 4**.

In the next chapter, we will present our results on how black soldier fly larvae eat in large groups and make use of the available space around a piece of food.

CHAPTER IV

BLACK SOLDIER FLY LARVAE FEED BY FORMING A FOUNTAIN AROUND FOOD

In this study, we investigate how larvae consume food so quickly in large groups. We present our experimental results, including observations of single larva feeding, PIV tracking of larva groups, and measurements of eating rate, and then discuss some implications of our work.

4.1 Individual larva behavior

We begin by studying a single larva, shown in **Figure 1.1.1(a)**. A larva's body is wedge-shaped, ending in a darkened triangular "beak" that is 0.4 mm long. The beak contains maxillae, spiracles, and a mandibular brush, shown in **Figure 4.1.1(a)**. In our assays of single larvae exposed to food, we find that 30% of larvae abstain from eating: these larvae do not touch the food but instead walk around the perimeter of their container. This may be due to their life stage or some other property we could not discern visually.

A single larva eats sporadically, as shown in the time course of eating in **Figure 4.1.1(b)**. During an hour duration, larvae eat in bursts of 5 $\pm$ 8 minutes (N=7), and then take 5 $\pm$ 10 minute breaks. The standard deviation shows that eating behavior is highly variable. We calculate the resting time, defined as the ratio of eating time to total time, as in Equation (5), to be $R = 0.44 \pm 0.27$.

A larva mouth consists of a pair of moving parts called maxillae, as shown in **Figure 4.1.1(c)**. They are driven in a dorsal-ventral motion, with the time-course of their position given in **Figure 4.1.1(d)**. We plot sinusoidal best fits to the positions y of the maxillae over time t for four cycles of raising and lowering:

$$y = A\sin(\omega t + \varphi). \tag{27}$$

The average amplitude of the motion is $A = 0.11$ mm and the average frequency is $\omega = 27$ rad/s. The phase difference between the maxillae is 0.63 rad, or 36°.

The maximum speed of the maxilla is then the maximum of the derivative of the best fit in Eq. (27) at $v = A\omega$. The shear rate of a maxilla, $\dot{\gamma}$, may be written as the velocity v

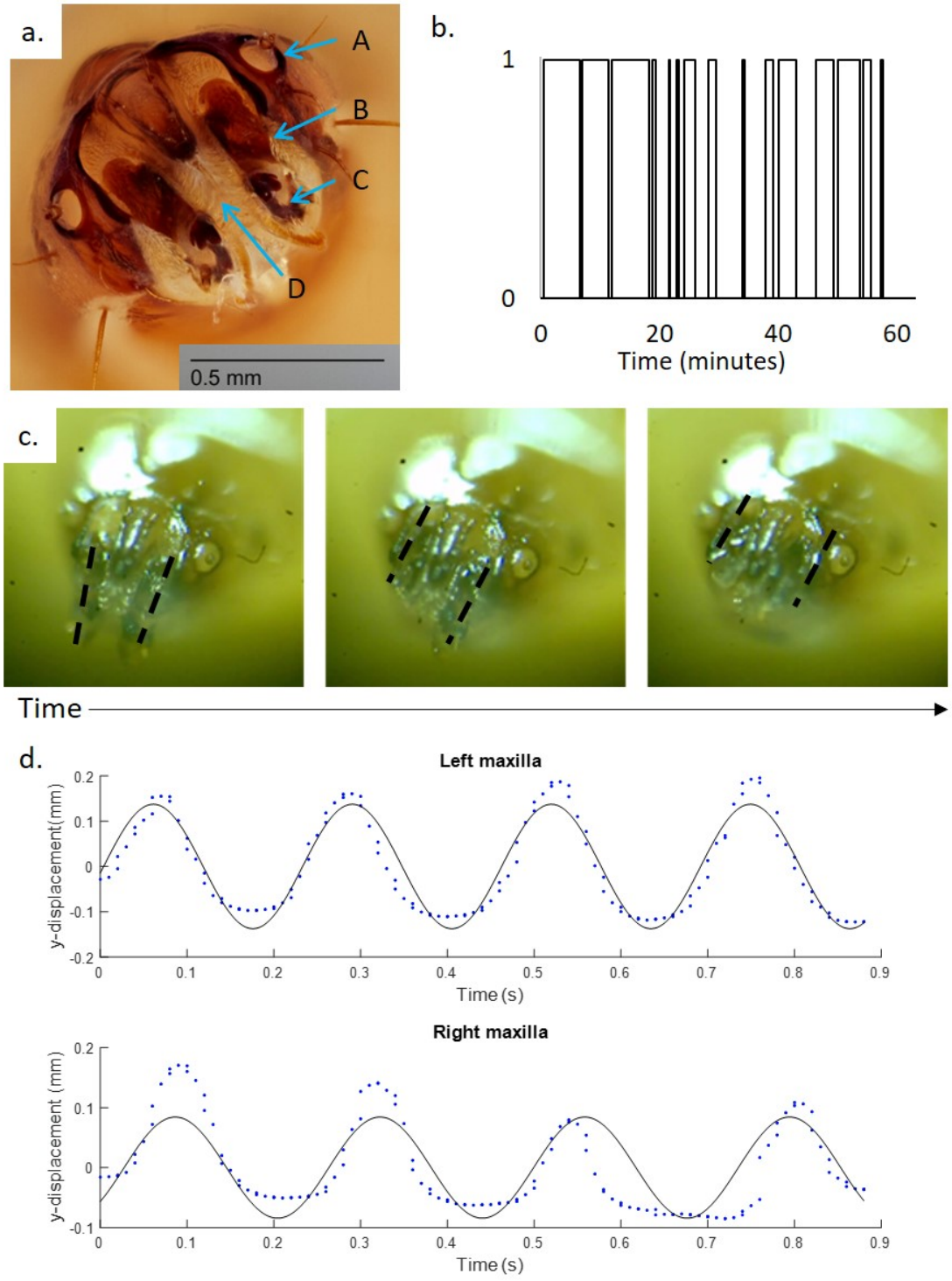

Figure 4.1.1: a. The mouth of a black soldier fly larva. The mouthparts are: A – spiracle; B – maxilla; C – maxillary palp; and D – Mandibular brush. b. A time course of larvae feeding behavior for 60 minutes. 1 – eating; 0 – not eating. c. Motion of the larva's mouth in high speed showing asynchronous raising and lowering of its maxillae. Maxillae are traced with dashed lines to highlight their position. d. Tracks of four periods of maxillae motion showing a periodic raising and lowering, with solid lines as sinusoidal best fits.

of a maxilla divided by the distance traveled in that time, $d = 2A$:

$$\dot{\gamma} = \frac{v}{d}. \tag{28}$$

The average shear rate of the maxillae is $\gamma = 14$ 1/s. We surmise that this high speed motion helps the larva to slice off pieces of food before the larva is pushed away by the other larvae crowding around a piece of food.

Using a scanning electron microscope with an attached energy dispersive x-ray spectrometer, we find small amounts of calcium, 0.49% by weight, in the mouth part, which is not present in the rest of the head of the larva. The composition of the larva's mouth and head are given in Table 1. The calcium in the mouth part can increase its hardness so it can bite through tough foods.

Table 1: Larva composition determined by EDS

Element	Mouth concentration (Weight %)	Head concentration (Weight %)
C	69.42	56.59
N	3.87	14.93
O	25.19	27.7
Mg	Not detected	0.09
P	0.1	0.31
S	0.27	0.11
K	0.61	0.22
Ca	0.49	Not detected
Zn	0.04	0.05

4.2 Particle image velocimetry (PIV)

Larvae are initially spread in an even layer surrounding the orange slice and proceed to gather around the slice over the first 5 minutes of the experiment. We start our PIV averaging at 8.3 minutes to be certain that the region is close to steady-state. A photograph of 3500 larvae forming a pile to feed on an orange slice near the end of an experiment is shown in **Figure 4.2.1(a)**. The pile is roughly conical, eight larva heights tall at the tip and 40 larva heights wide.

Filming from the top and bottom yields the views in **Figure 4.2.1(c)**. The naked eye sees that larvae move randomly, especially in the top view, but PIV can detect a coherent flow direction. In the top view in **Figure 4.2.1(d)**, larvae form a radial outflow.

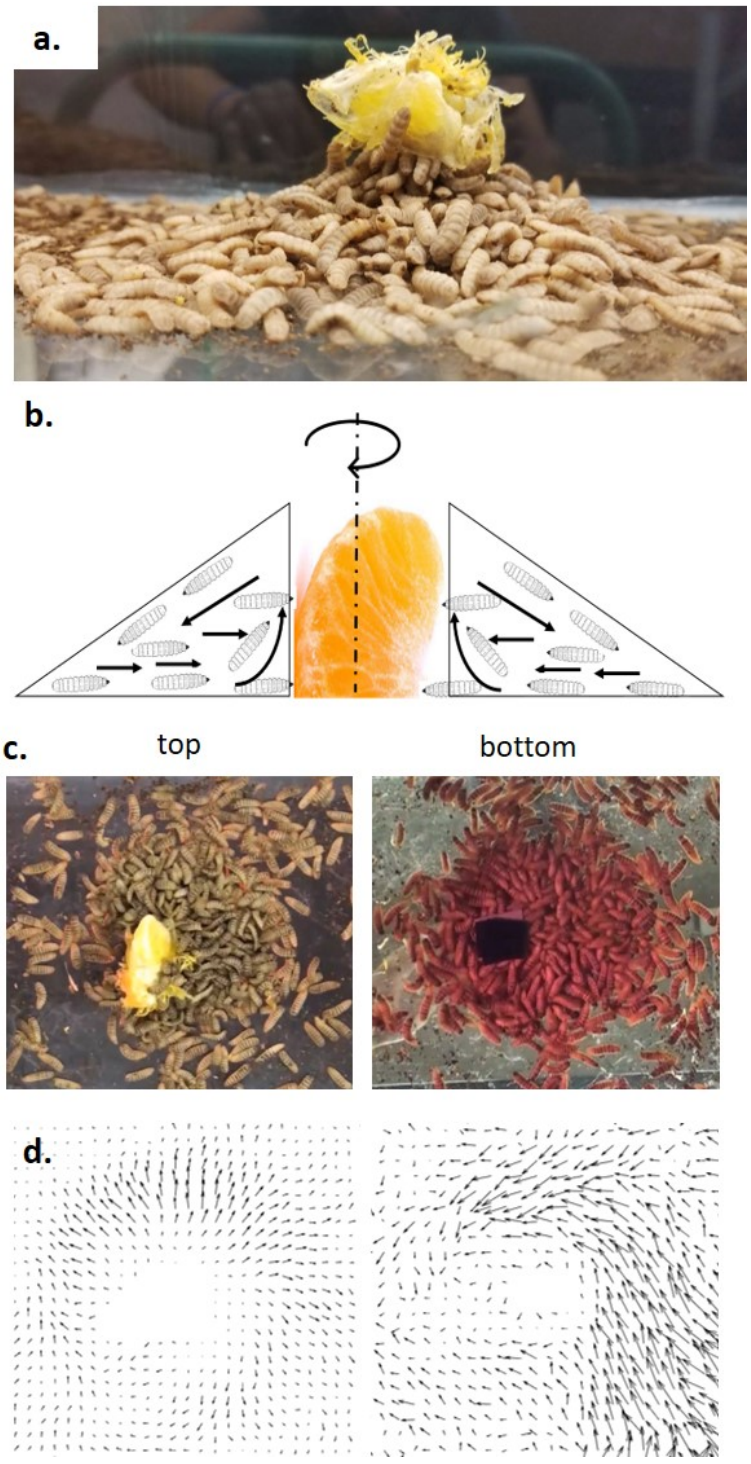

Figure 4.2.1: a. Side view of larvae eating an orange slice by building a flowing fountain of larvae around the food.b. Schematic of larva motion around an orange slice. c. The region of flowing larvae, seen from above and below, respectively. d. Velocity fields associated with the views in part c. They are calculated using PIV and averaged over 2,000 seconds. The center is not analyzed as it contains the orange slice.

In the bottom view in **Figure 4.2.1(d)**, the larvae form a combination of a vortex and an inflow. The vectors are averaged over 2000 seconds, and their length indicates their relative magnitudes. The average velocities on the top and bottom layers are comparable in magnitude, on the order of 0.1 mm/s or 0.007 body lengths per second, but much of this is part of the vorticity around the orange slice. Moreover, this speed is 20 times slower than the unimpeded speed of a single larva in a petri dish, 2 mm/s. The divergence and vorticity on the top and bottom layer are comparable in magnitude as well. The vorticity of the larvae on the bottom layer is negative of that from the top, as it is filmed from below and the axis is reversed; the entire aggregation of larvae therefore spins in the same direction.

Based on the top and bottom views, we surmise that physical picture is a fountain of larvae that are pumped inward and upward, as shown in the schematic in **Figure 4.2.1(b)**. Larvae flow in from the bottom and flow out only on the top layer while the entire mixing region spins. In other words, net motion only occurs on the boundaries, the free surface and the substrate beneath the larvae. The details of the calculated velocity and other parameters for the top and bottom layers are shown in Table 2.

Table 2: Larva flow properties derived from PIV

Property	Top	Bottom
$\overline{\mathbf{u}}$, Average speed (mm/s)	0.09	0.07
$\nabla \times \mathbf{u}$, Vorticity (1/s $\times 10^{-3}$)	0.9	-0.6
$\nabla \cdot \mathbf{u}$, Divergence (1/s $\times 10^{-3}$)	1.4	-1.7
Area (cm^2)	80	60

Snapshots from experiments using 500 to 10,000 larvae are shown in **Figure 4.2.2(a-e)** on the left. Larvae primarily gather around the orange and in the corners of the container. Watching the videos with a naked eye shows that a well-defined mixing region is present. The average speed of larvae outside the mixing region and away from the corners is 0.05 ± 0.006 mm/s, calculated for the 10,000 larvae experiment. Using the minimum velocity threshold of 0.125 mm/s, we define the mixing regimes precisely using PIV, shown by the regions highlighted in red surrounded by a dashed border in the right column of **Figure 4.2.2(a-e)**. The mixing region is not perfectly round and can be off center, as shown for 1000 larvae in **Figure 4.2.2(b)**. Higher numbers of larvae result in larger mixing regions. There is a very small region with 500 larvae in **Figure 4.2.2(a)**, while 10,000 larvae cover

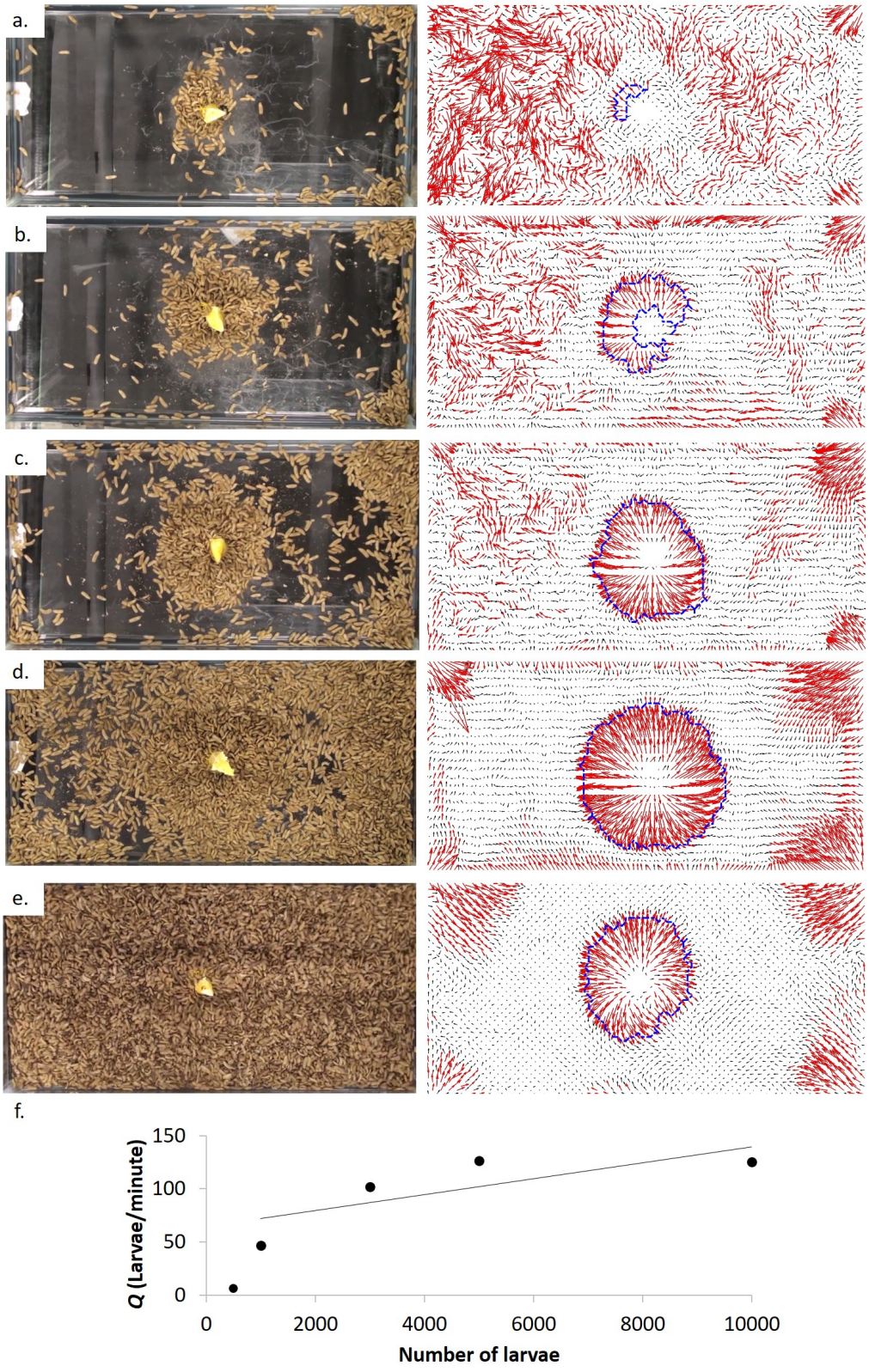

Figure 4.2.2: Images of the larvae and food after 33 minutes next to the corresponding time-averaged velocity fields, with the mixing region selected. a. 500 larvae b. 1000 larvae c. 3000 larvae d. 5000 larvae e. 10,000 larvae. f. The relationship between number of larvae and their flow rate.

the entire container floor in **Figure 4.2.2(e)**. Larvae also form outflows in the corners of the container similar to the outflow from the orange.

The relationship between the flow rate and group size is shown in **Figure 4.2.2(f)**. We estimate the flow rate by assuming that the inflow or outflow occurs over a layer depth of one larva height (3.2 mm), as in Eq. (1). The flow rate increases linearly with number of larvae for 1000 and more larvae, as in Eq. (2): $Q = 0.0075N + 64.337$, $R^2 = 0.6013$. This relationship will be used in our mathematical model where we estimate feeding rate.

4.3 Eating rate as a function of group size

We feed orange slices to larvae groups across four magnitudes in numbers, from 10 to 58,000. **Figure 4.3.1(a)** shows an experiment with a simultaneous test of 1, 10, 100, 200 and 500 individuals. In the containers with 500 larvae, the orange slice is not visible because it is buried by larvae after 10 minutes of the experiment. In the containers with a single larva, the larva lays hidden under the orange slice, and so that data point is not used.

Larvae rotate the orange slice as they consume it, but this rotation is bounded by the walls of the container. **Figure 4.3.1(b)** shows the relation between number of larvae N and their eating rate dM/dt. By plotting linear best fits to the small ($N \leq 500$) and large ($N \geq 1000$) numbers of larvae, we find they intersect at $N_0 = 1300$ larvae.

We use the properties of the orange slice, individual larvae, and larva flow rates to model the eating rates of these larvae in three regimes, as in Equation (12). Based on the surface area limit in Equation (7), if a larva's head is $w = 4.3$ mm wide by $h = 3.2$ mm tall, then the maximum number of larvae that can eat an orange with a surface area $S = 4067$ mm^2 at one time is $N_{max} \sim 337$ larvae. This prediction for N_{max} is 1000 larvae below the experimentally found N_0. This is in part due to the calculation for N_0 not accounting for mixing of larvae, which allows more larvae to access food. Additionally, the experiments at higher numbers of larvae were done at higher temperatures, yielding higher eating rates (rather than increasing the number of larvae that can fit around food). Finally, there is a lot of scatter in the data at higher numbers of larvae, which may contribute to the discrepancy in N_0.

The average eating rate of one larva eating an orange is $\eta \sim 0.03 \pm 0.02$ grams per hour (based on 10 larvae data). Using our data on individual larva eating behavior from single larva experiments and values for Q from the PIV experiments, we can calculate the threshold

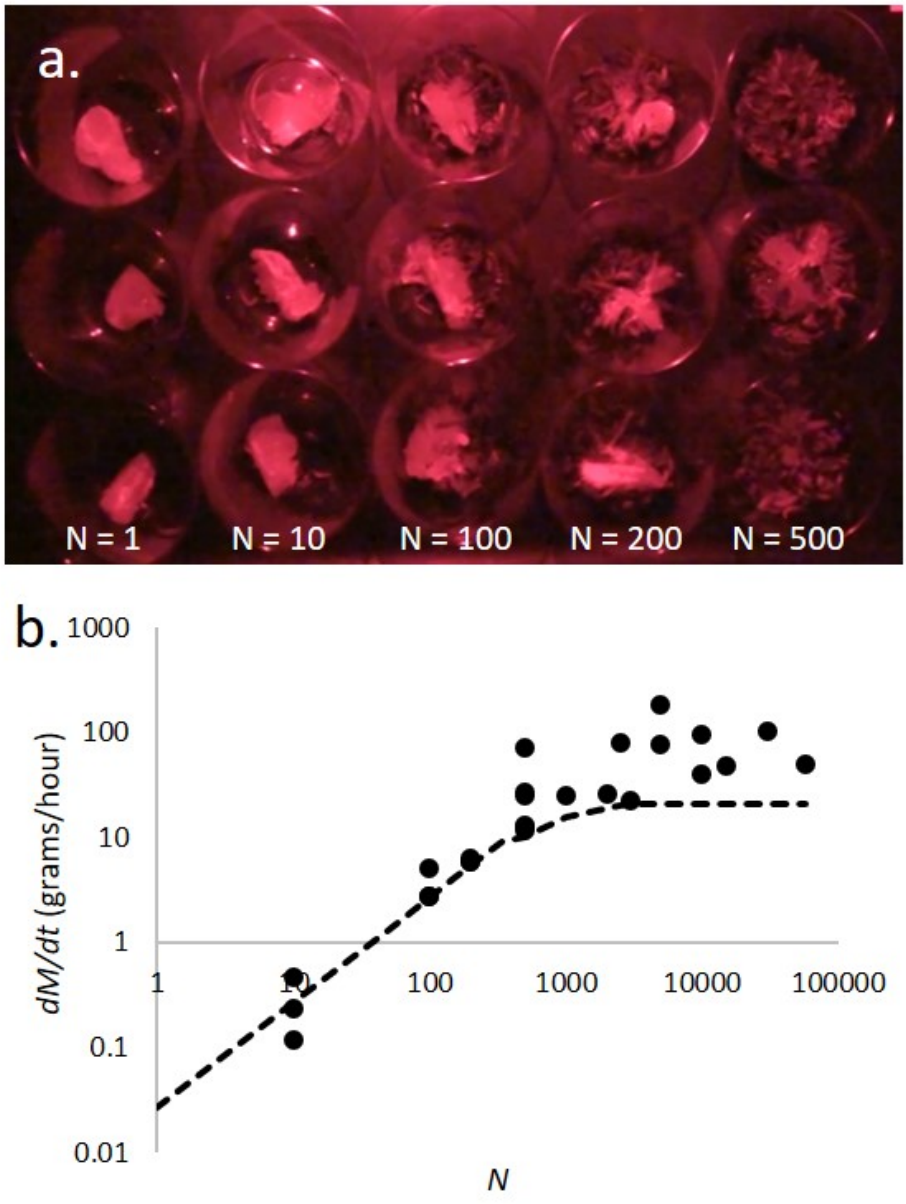

Figure 4.3.1: a. Experimental setup to measure eating rate of larvae. b. Relationship between eating rate and number of larvae. Dots are experimental data points and dashed line is the model.

when the larvae mixing does not yield any additional eating, $N' \sim 2850$ larvae (Eq. (11)). The eating rates of larvae are estimated by Equation (12) plotted alongside the experimental data as dashed lines in **Figure 4.3.1(b)** and matches the experimental trends. Thus, the "fountain" that larvae form around food increases their eating rates to a theoretical maximum, reached when there are N' larvae in the container. The eating rate model is an underestimate of the actual eating rates with many larvae, likely due to the higher temperatures that experiments with large numbers of larvae were performed at.

Larvae can consume oranges very rapidly. If a larva weighing 0.1 g eats an orange slice at a rate of $\eta \sim 0.03$ grams/hour and is not limited by surface area, it will eat 6.5 times its body weight per day. This is on the same order of magnitude as the approximately 2 body weights per day they eat in chicken feed.[1,14] Oranges, which contain more liquid than chicken feed, can be consumed by larvae more quickly.

4.4 Discussion

When larvae are raised in industry, their food is blended and then mixed with the larvae aggregation to avoid the surface area limit and allow most larvae to eat to their maximum capacity. However, food pieces cannot be perfectly distributed between all larvae. Reducing the number of larvae in a bin and increasing the surface area of food pieces can help increase how quickly larvae eat food, leaving less to rot because larvae cannot access it.

The "fountain of larvae" is not be possible for other animal species. Larvae crawl on top of one another to access food, while cattle and other land animals do not to avoid hurting one another. Fish in schools avoid touching each other, while larvae touch one another constantly, and in fact do not like to be isolated. The feeding behavior of other animals is affected by their social hierarchy,[32,33] while larvae do not have complex social dynamics. Thus, fly larvae are unique among scavengers in their group feeding abilities.

4.5 Chapter summary

In this study, we investigate how groups of black soldier fly larvae feed. The number of larvae that can feed is intrinsically limited by the surface area of food, around which only limited numbers of larvae can fit. Moreover, larvae that are eating take frequent breaks, blocking others from accessing the food. Groups of larvae overcome these two problems by generating fountains around food, where new larvae crawl in from the bottom and are

"pumped" out of the top. We present a mathematical model that predicts the rate of eating as a function of group size, taking into account the pumping action.

Now that we know that the piles of black soldier fly larvae around food allow more larvae to reach food, we are interested in finding out what is happening inside the pile. Are the larvae hurting one another in their competition for a bite of food, or are the collisions that occur inside the pile harmless? How do the larvae on the floor react to the weight of the larvae above, and how would they react to a kilogram of food suddenly dropped on top of them? How tightly can the larvae be packed for shipping? To answer these questions, we turn to compression tests and dig into the behavior of the larvae when subjected to external forces.

CHAPTER V

BLACK SOLDIER FLY LARVAE REARRANGE UNDER COMPRESSION

In this chapter, we investigate how larvae consume food so quickly in large groups. We begin by describing the natural settling behavior of larvae. We then discuss the steady-state pressure reached by live and dead larvae under compression at varying packing fractions. Then we discuss the time-dependent properties of their relaxation as a stretched exponential material. Finally we discuss implications of our work.

5.1 Results

The jostling of live larvae in a jar causes them to settle, subjecting their bodies to greater compression. **Figure 5.1.1(d)** shows larvae when they are initially placed in a 400 mL beaker at a volume fraction of $\phi = 0.55$. **Figure 5.1.1(e)** shows them having settled after 6 minutes to a volume fraction of $\phi = 0.61$. Larvae move around and rearrange during this process. Their bodies, initially horizontal, align vertically as they crawl downwards and become more closely packed. To quantify the response of the larvae to pressure, we conduct creep tests with a universal testing machine (UTM). Larvae rearrange and settle in the UTM in a visually similar manner to their settling in the beaker, as shown in the schematics in **Figure 5.1.1(b)** and **Figure 5.1.1(c)**. Dead larvae also rearrange due to applied pressure but at a slower rate than their live counterparts.

Figure 5.1.2(a) shows the time course of the pressure exerted by dead larvae (dashed lines) and live larvae (solid lines) when compressed to four different volume fractions. There is an initial spike in pressure for both dead and live larvae, and then the pressure settles to an equilibrium over time. **Figure 5.1.3(a)** and **Figure 5.1.3(b)** show the time course of pressure for dead and live larvae at a volume fraction of 0.80. The red dashed lines are a stretched exponential fit:

$$P = (P_0 - P_{SS})e^{-(\frac{t}{\tau})^{\beta}} + P_{SS}, \tag{29}$$

where the boundary conditions are set by initial pressure P_0, measured from the experiments, and the added term is the steady-state pressure P_{SS}, calculated by the average of

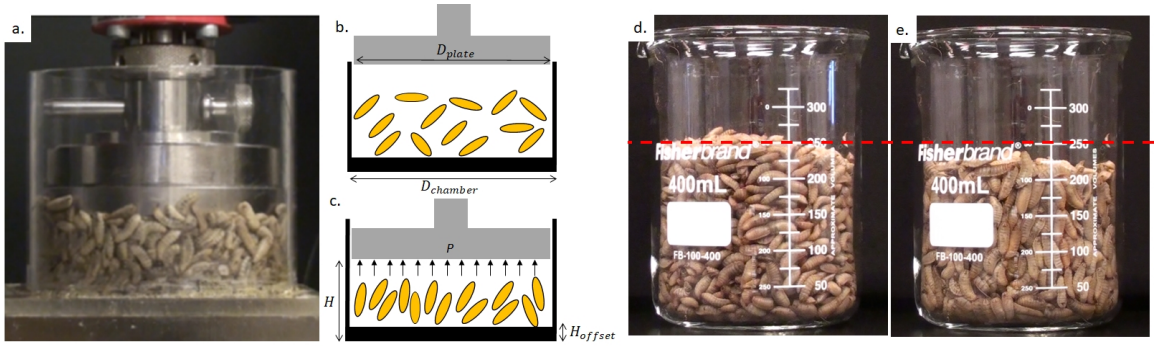

Figure 5.1.1: a. Image of live larvae being compressed to $\phi = 0.80$. b. Schematic of larvae in the UTM before compression. c. When larvae are compressed by the UTM, they rearrange and exert a pressure P on the plate. d. 2000 larvae with an average mass of 0.07 g when they are initially placed in 400 mL beaker, at volume fraction $\phi = 0.55$. e. After 6 minutes in the beaker in (d), larvae self-compress to volume fraction $\phi = 0.61$. The red dashed line in (d) and (e) across the 250 mL mark shows that larvae settle from 250 mL over time.

the last 100 seconds of the trial. We construct similar plots for volume fractions $\phi = 0.56$ to $\phi = 0.80$, but not for the lowest volume fraction $\phi = 0.56$ for the live larvae because the larvae are not fully touching the plate and a failed fit occurs due to an inconsistent pressure. The inset in **Figure 5.1.3(b)** shows the time course of pressure of live larvae at volume fraction $\phi = 0.57$, in which the pressure initially dips below steady-state. The stretched exponential does not fit the live larvae well for low volume fractions such as the one shown in the inset. Nevertheless, it provides a useful quantitative comparison between relaxation of live and dead larvae. Specifically, we will compare the variables defined in Eq. (32), including the initial pressure P_0, the relaxation time τ, and the exponent β found by least square best fit.

At the highest volume fraction of $\phi = 0.80$, live and dead larvae have comparable initial pressures ($P_0 = 6.5$ kPa for live larvae and $P_0 = 4.0$ kPa for dead larvae). These pressures are two orders of magnitude smaller than the pressures required to kill larvae, as shown in the inset of **Figure 5.1.2(a)**. In our experiments, a larva can withstand a pressure of up to 935 ± 350 kPa and be compressed by a strain of $75\% \pm 2\%$ of its initial height. This is more than 140 times greater than the maximum pressure experienced by the larvae in trials with 2000 larvae. Assuming a bulk density of compost of 500 kg per cubic meter[84], a 190 m tall pile of compost would need to be piled on a larva to kill it; the maximum pressure in our compression tests with multiple larvae is comparable to a 1.3 m pile of compost. Thus,

the pressures experienced by larvae in the UTM are likely higher than pressures they would experience in their natural environment.

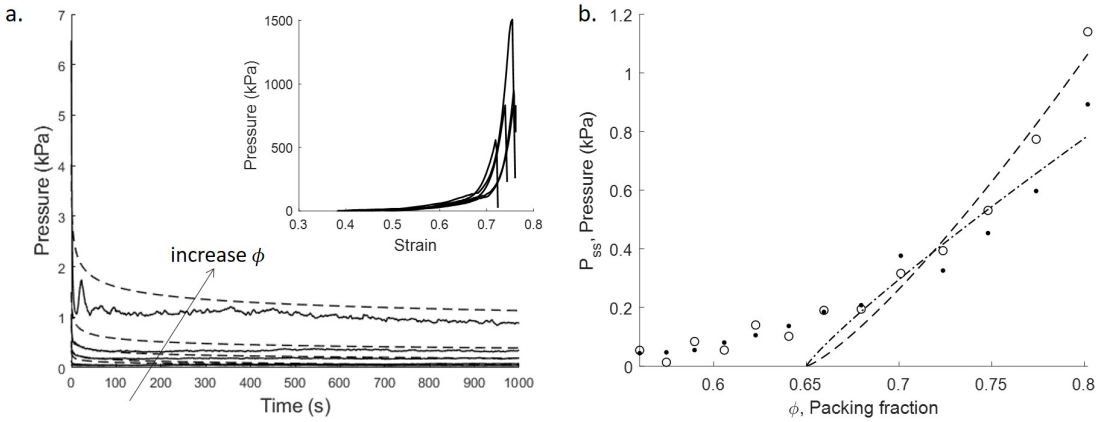

Figure 5.1.2: a. Comparison of time series of pressure of dead larvae (dashed lines) with live larvae (solid lines) at increasing volume fractions. Inset: stress-strain curve of five single larvae individually compressed to 40 N until the larva bursts. b. Steady state pressure of dead larvae (circles) and the best fit for $\phi > 0.65$ (dashed line), live larvae (points) and the best fit for $\phi > 0.65$ (dash-dot line).

The steady-state pressures P_{SS} of dead larvae (circles) and live larvae (points) at four volume fractions is shown in **Figure 5.1.2(b)**. At volume fractions above the critical volume fraction of $\phi_c = 0.65$, steady-state pressure increases rapidly, likely due to jamming and friction[85,86]. We thus fit a power law to the data for $\phi > \phi_c$ of the form

$$P_{SS} = a(\phi - \phi_c)^b. \tag{30}$$

The dashed and dashed-dotted lines are fits for dead and live larvae, respectively, and the corresponding equations are $P_{SS} = 11.4(\phi - 0.65)^{1.26}$ and $P_{SS} = 4.1(\phi - 0.65)^{0.88}$. As shown by the positive exponents, the steady-state pressure increases with volume fraction. This makes sense because the higher the volume fraction, the more the larvae are filling the container and the more elastic energy is stored during the test. The increase in pressure at higher volume fractions (and, thus, higher strains) for both live and dead larvae is as expected for a material under compression, but does not follow Hooke's law with a constant modulus E, $P = E\epsilon$, because of the spaces between the larvae. They also do not they fit an ideal gas law, which would yield a fit of $P_{SS} \sim \phi$. Nevertheless, we can say that dead larvae are "stiffer" than live larvae because at a given volume fraction, dead larvae exert a

20% higher pressure than live larvae, due to their not being able to move to dissipate their internal stress.

The relaxation time τ for live and dead larvae is shown in **Figure 5.1.3(c)** by the points and circles, respectively. The relaxation time gives the time scale at which stresses are relieved by rearrangement. In particular, live larvae relax quickly, in $\tau = 1.7 \pm 1.4$ seconds. This time scale is less than the time scale of their motion, $\tau_b = 7$ seconds, given by the ratio of their length $L = 14$ mm and crawling speed $U = 2$ mm/s. This makes sense because larvae likely need to move only a small amount in order to break the force chains stretching from the top to the bottom of the container. Dead larvae, on the other hand, take between 15 and 45 seconds to relax, ten times slower than live larvae. Their relaxation time decreases as a power law with the volume fraction, $\tau \sim \phi^{-2.8}$, as shown by the dashed line. The stretched exponential form, consistent with the behavior of other relaxing systems (e.g. binary mixtures), indicates an underlying mechanism that is characterized by a broad distribution of relaxation times rather than a single time[87]. The power-law decay with volume fraction therefore represents the evolution of this distribution with volume fraction. While we do not have a specific interpretation of the power-law behavior (as opposed to other functional forms), we note that power-law scaling of the time scale is seen in other relaxing systems[87]. Dead larvae at higher volume fractions can relax more quickly due to the greater elastic potential energy at these levels of compression.

The stretched exponential fit does not well describe the behavior of live larvae. In **Figure 5.1.3(b)** at the highest volume fraction of $\phi = 0.80$, live larvae overshoot the equilibrium pressure by 0.8 kPa at a time of 22 seconds by compressing their bodies too little. This behavior might be due to some kind of flight or fight reaction due to the applied force. On the other hand, when larvae are compressed to one of the lower volume fractions, $\phi = 0.57$, the pressure decreases below the equilibrium before ramping back up as shown in the inset of **Figure 5.1.3(b)**. This may be caused by larvae not contacting the entire pressure plate at all times. Such oscillations might be accounted for by spring-like and damper-like terms in the sensory system of the larvae, and possibly their memory span.

We verify the relaxation times of live and dead larvae by calculating the time it takes live and dead larvae to reach 50% of steady state pressure, shown in **Figure 5.1.4**. This "half-time" of live larvae is 1.2 ± 0.4 seconds; it decreases with a power law, $\phi^{-2.6}$, for dead larvae. These results are comparable to those calculated with stretched exponential fits.

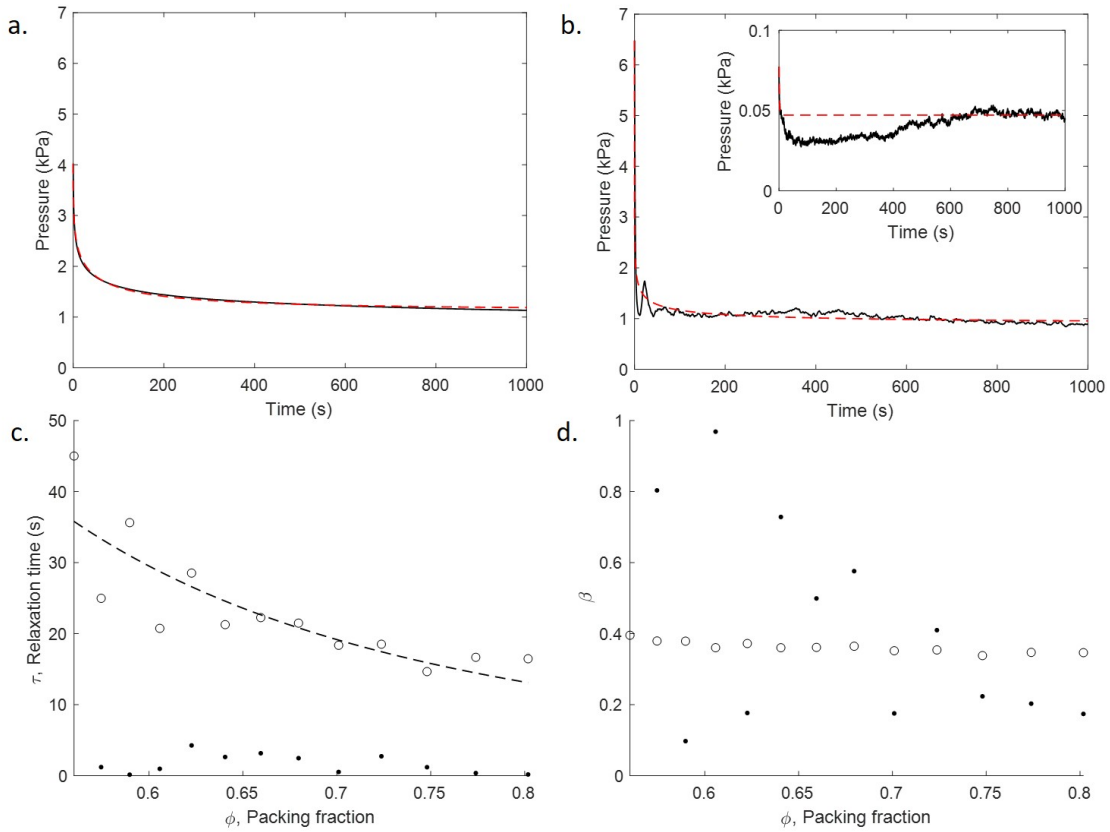

Figure 5.1.3: a-b. Time course of pressures exerted by dead larvae (a) and live larvae (b) when compressed to $\phi = 0.80$. Inset of (b): Time course of pressure of live larvae with stretched exponential fit when compressed to $\phi = 0.57$. Pressure data is a solid black line and stretched exponential fit is dashed red line. c. Relationship between relaxation time τ and volume fraction with a dashed line as the best fit to the dead larvae data. d. Relationship between exponent β and volume fraction. For c-d, dead larvae data are are shown as circles and live larvae data are shown as points.

In **Figure 5.1.3(d)**, we compare the exponent, β, defined in Eq. (32), for live and dead larvae. Most physical systems have $\beta < 1$, which acts to slow the decay of the exponential by stretching it across longer times. Studies of crumpled balls of aluminum foil are associated with a β of 0.24-0.40[43]. As shown by the open points in **Figure 5.1.3(d)**, dead larvae have a $\beta = 0.36 \pm 0.02$, whose small standard deviation shows that the fit works well across volume fractions. The similarity in exponents for crumpled paper and the collection of larvae suggest that piles of dead larvae may have some hierarchy involved, such as the force chains resulting from their bodies pressing into one another. When live larvae are fitted to a scaled exponential function, they have a more variable $\beta = 0.42 \pm 0.29$. The large range

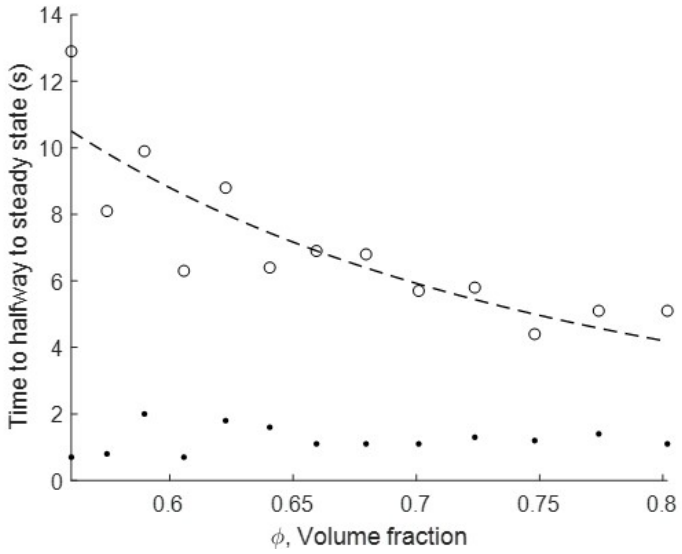

Figure 5.1.4: Time to halfway to the steady-state pressure for live larvae and dead larvae shown by points and open circles, respectively. The dashed line represents the best fit to the dead larvae data, which scales with $\phi^{-2.6}$.

of β for live larvae is likely due to the motion of the larvae, which can vary between trials.

Dead larvae are merely a granular material and can only relax the pressure on them through their material properties. Live larvae, however, are able to relax the forces on them by moving around and actively adjusting their bodies. The fluctuations above and below the equilibrium pressure show that they have mechanisms for restoring a base state despite a pressure being too high or too low. If the pressure on the larvae is too high, they move into open spaces to relieve pressure. Conversely, if the pressure is too low, larvae can push up against the plate and each other to increase the pressure. The scale of the fluctuations is 0.007 kPa, which is 38% of the pressure exerted by one larva body weight. In comparison, the dead larvae in **Figure 5.1.3(a)** show a smooth decay without fluctuations, indicating they can only dissipate the pressure but not increase it.

5.2 Discussion

Larvae are just one example of many living systems that undergo compression on a regular basis, from people to farm animals to other insects. A Tokyo subway system can pack passengers so tightly that a dedicated pusher has to squeeze them in to close the doors. When given a choice, most vertebrate animals avoid such high densities because their bodies can

be injured. Nevertheless, to reduce shipping costs we often pack animals in high densities. When transported, pigs, chickens and other farm animals are often packed tightly and keeping them alive in these conditions is a challenge faced by farmers all over the world[88,89].

Invertebrate animals are not governed by animal welfare laws, and they often experience large forces on a regular basis. Genetically modified mosquitoes for use in reducing malaria are packed densely in syringes to protect them from being thrown around during shipping[90]. An ant can survive up to hundreds of times body weight before injury[91]. If forces are applied, ant aggregations can flow to dissipate those forces, exhibiting behaviors of both fluids and solids[92,93]. Earthworms have soft bodies and are compressed as they dig, exerting forces up to 500 times their body weight. The mechanical properties of their bodies limit how well they can dig into soil[94,95]. This study provides a method for measuring the rearrangement of animals that might be applied to other types of invertebrates.

Black soldier fly larvae can experience forces due to the weight of mulch or fellow larvae on top of them. Our study shows that larvae can mitigate these forces by rearranging, even when the forces are orders of magnitude higher than would occur naturally. Moreover, the force that a single larva can survive exceeds body weight by a factor of 53000. Unlike inactive materials, their behavior under compression over time can have interesting characteristics. They exert both small oscillations, individually pushing against the pressure plate to exert low forces, and large oscillations in which they collectively increase or decrease their force before returning to equilibrium. This is reminiscent of a control system with a feedback loop, which can actively respond to external forces to reach the desired state, as opposed to a simple mass-spring-damper, which can take longer to converge.

Our study shows that larvae are very robust to packing. It should be possible to tightly pack larvae for shipping without damaging them. Currently, larvae are loosely packed with soil or other substrate in HDPE plastic containers with tight lids. Shipping costs may be lowered by omitting the substrate and packing the larvae more tightly. However, since the pressure at higher volume fraction is close to 1 kPa, it may be difficult to design a container with a lid that can be closed tightly enough to hold compressed larvae.

5.3 Chapter summary

In this study, we performed compression testing to measure the rate that black soldier fly larvae rearrange to relieve applied pressure. The pressures applied are orders of magnitude

greater than they would feel naturally, yet larvae still had the ability to rearrange to reduce this pressure. Live larvae rearranged at time scales of 2 seconds, 9 - 27 times faster than dead larvae, which settled more slowly due to applied pressure. The equilibrium pressures of both live and dead larvae are the same, indicating that live larvae do not seek pressures different from those that arise from their material properties and geometry. For dead larvae, the reduction of applied forces due to rearrangement is well described by stretched exponential functions. Live larvae are not as well described by such functions, but instead seemed to be characterized by oscillation in pressure, indicating the presence of a feedback system.

Studying the feeding fountain of fly larvae helped us understand their properties as an active fluid naturally forming a source and sink at food. Compressing larvae and measuring their creep response gave us insight into their bulk properties as an active material. For the next chapter, merely measuring the average properties of larvae does not explain their motion. We will examine how fly larvae pile up in the corners of rectangular bins, and then, without any obvious warning, switch to the other corner. To understand this, we will have to examine the bulk properties of the larva pile as well as the motion of individual larvae in the container in the next chapter.

CHAPTER VI

SYNCHRONIZING PILE FORMATION OF BLACK SOLDIER FLY LARVAE

In this chapter, we present our experiments quantifying the motion of hundreds of larvae confined to two dimensional bins using center of mass measurements and then particle image velocimetry. We show how to drive the motion of the larvae with a vertical intruder along each side wall. We then compare these experiments to a simulation in which larvae are modeled as negatively buoyant flexible rods swimming through a fluid. Both result in clustering in corners of the container, indicating that aggregation under confinement has greater generality than just in black soldier fly larvae. Finally, we discuss the implication of our results.

6.1 Results

We begin with control tests of the larvae, observing their ability to form piles without external forcing. A swarm of larvae confined to a tall flat container spontaneously forms piles and break them up, alternating between the left and right walls of the container. The time lapse images in **Figure 6.1.1(a)** show one period of motion.

To characterize the time-scale of the formation of the pile, we track the time course of the centroid of the swarm in **Figure 6.1.1(b)**. Using 8 separate swarms of larvae, we recorded N = 80 periods of this motion, and calculated a time between corners of 60 ± 32 minutes. A histogram of the time between corners is shown in **Figure 6.1.1(c)**, and is closely matched by a gamma distribution,

$$f(x) = \frac{1}{\beta^{\alpha}\Gamma(\alpha)} x^{(\alpha-1)} e^{-x/\beta} \tag{31}$$

where f is the probability density, x is the random variable (the time between corners), α is the shape parameter, β is the scale parameter, and $\Gamma = (\alpha - 1)!$ is the gamma function. The gamma distribution is often used to model the distribution of times between events, such as the distribution of rainfall or cell responses to drugs[96,97]. The scale and shape parameters of the gamma distribution for the time for larvae to switch corners are $\alpha = 4.0$

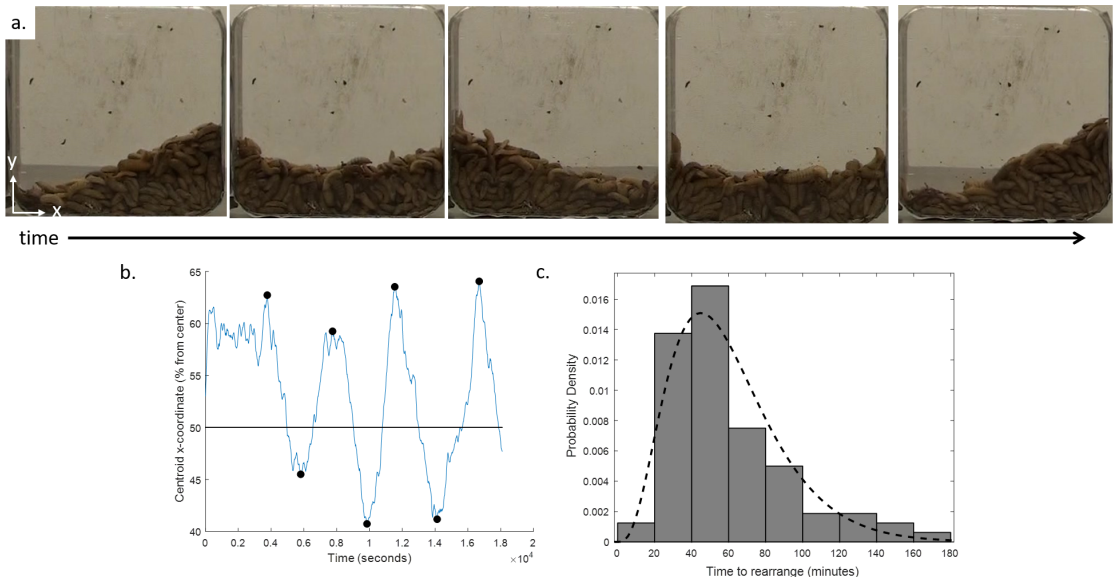

Figure 6.1.1: a. Time series of larvae rearranging between corners. b. Sample time series of centroid x-coordinate, with the times of maximum distance of center of mass from the center marked as a black point. The time series is a 100 second moving average to dampen out noise. c. Probability distribution of the time it takes larvae to go from corner to corner, where the peak frequency data is the gray bins and the gamma distribution fit is the dashed black line.

and $\beta = 14.7$. Although experiments are done on two separate days, the parameters for each day are consistent, suggesting these values are repeatable.

To better understand the events that lead to the formation of a pile, we perform particle image velocimetry. **Figure 6.1.2(a)** shows the larvae when they are fully aggregated into one corner. **Figure 6.1.2(b)** shows time-averaged velocity vectors of the larvae. during the piling process. As shown by the vectors on bottom right in the dashed region, incoming larvae travel into the corner, then along the wall before piling up. A similar motion is observed in the bottom left corner, opposite the pile.

We measure the center of mass of this experiment over time and compare it to the results from PIV to confirm that larvae begin migrating to corner before the pile begins to move. We calculate the average horizontal velocity of all the larvae. We then plot the rolling average of the horizontal velocity over 1000 seconds next to the rolling average of the position of the x-coordinate of the center of mass of the larvae over 1000 seconds in **Figure 6.1.2(c)**. These signals are very similar - the horizontal velocity appears to peak before the centroid position, indicating that the larvae start moving to a corner minutes before

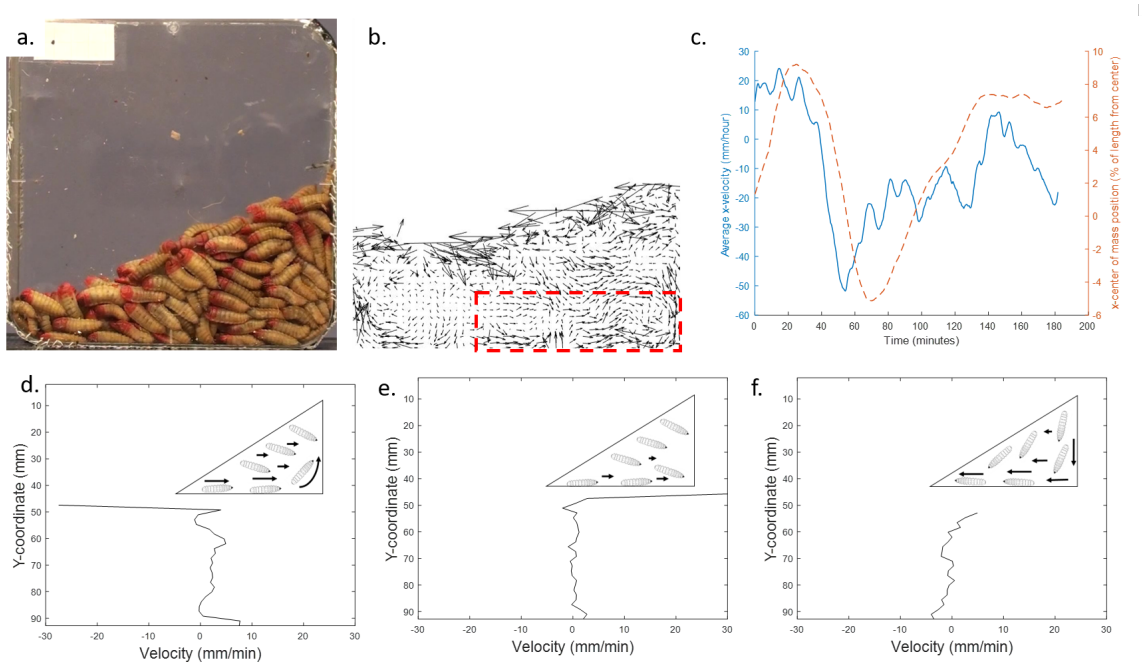

Figure 6.1.2: a. Sample frame with larvae with their rear ends colored red for tracking taken 20.5 minutes after the start of filming. b. Vectors averaged over 3 minutes showing motion around a corner, taken 8.2 minutes after the start of filming. Motion in dashed red region causes larvae to pile up. c. Comparison of x-coordinate of the centroid (dashed red line) and the average x-velocity in the container (solid blue line). Both the centroid and the x-velocity are a rolling average of 1000 seconds to dampen out noise. Larvae begin moving left 13 minutes before the center of mass shifts. d. x-velocity profile 7.5 minutes into the experiment, when larvae are moving towards the right corner. Inset: Schematic of larva motion into corner, with longer vectors corresponding to faster larvae. e. x-velocity profile 28.8 minutes into the experiment, when larvae are piled in the corner. Inset: Schematic of jammed larvae. f. x-velocity profile 49.8 minutes into the experiment when larvae are rearranging to the left corner. Inset: Schematic of larva motion as the pile breaks up. Velocity profiles in d - e are taken from the motion of the larvae in the corner in a.

the pile is fully formed. To confirm, we calculate a cross-correlation of the two signals, the peak of which occurs at 759 seconds, or 13 minutes. Thus, the horizontal velocity precedes the centroid by 13 minutes and the mean time between corners is five times the lag.

We calculate velocity profiles from PIV at vertical slices to show that piling up is mostly due to motion on the floor of the container. **Figure 6.1.2(d-f)** show profiles of the horizontal velocity averaged over the rightmost 11 mm of the container, or 12% of its width. If the experiment starts at a time of zero, these profiles are calculated at three instances: at a time of 7.5 minutes (at the start of piling), 28.8 minutes (when the pile is stable), and 49.8 minutes (when the pile is sloshing to the other side). At the start of piling, in **Figure**

6.1.2(d), the velocity profile shows the greatest speed at the bottom of the container. The speed at the bottom is 8 mm/min whereas the speed in the middle of the aggregation is 2 mm/min. The greater speed at the bottom makes sense because larvae at the bottom have a firm, flat surface on which to push and orient themselves along, compared to larvae in the middle, which are pushing off other larvae. Larvae in the middle are also jammed along their axis by the surrounding larvae, and are physically incapable of turning to move horizontally. A schematic of the initiation of the pile in the right corner with larvae moving on the floor is shown in the inset of **Figure 6.1.2(d)**.

Figure 6.1.2(e) shows that when the pile is stable, the horizontal velocity is close to zero. At this instant, the weight of the pile of larvae is so high that the larvae at the bottom can no longer keep on pushing. The inset of **Figure 6.1.2(e)** shows a schematic of larvae jammed and barely moving. When the larvae begin the next cycle in **Figure 6.1.2(f)** and its inset, they reverse direction as shown by the change in sign of the velocity. Again, larvae are the fastest close to the floor. We also observe larvae moving downwards along the side walls in the video. This motion was not captured by particle image velocimetry, likely due to the small size of the moving region along the side walls.

We thus obtain a new physical picture of the motion of the aggregation: the motion is driven by the larvae along the bottom and side walls, and the remaining larvae are pulled along with their motion. Note that many of the velocity profiles show fast motion at the top of the container due to their ability to move in any direction. However, we do not think the flows here dominate in the construction of the pile.

From particle image velocimetry, we find that horizontal motion precedes the breaking up of the pile. We test this idea using foreign intruders, screws magnetically attached to linear actuators outside the container, and driven through the pile. We drive the screw either horizontally from corner to corner or vertically from the top of the container to the bottom. We tried an 12 mm long M3 screw and a 25 mm x 13 mm x 5 mm rectangular prism magnet laid flat on the bottom of the container. If the intruder was the large magnet, it suppressed the pile breakup. This is because the screw acted as a physical obstacle preventing larvae from easily crawling past it. Dragging a small (M3 x 12 mm) screw horizontally along the bottom of the container yielded highly variable results, with the larvae either switching corners as normal or not moving from corner to corner at all. We thus turn to experiments with vertical motion of the intruder.

We wait until larvae create a pile and then drag a larva-sized screw (M3, 10 mm long) downwards along the side of the bin that they are piled in, as shown in **Figure 6.1.3(a)**. After five minutes, we drive the screw back up, but more quickly to minimize disturbance of the pile. We perform the same process on the opposite wall of the container after twenty minutes. The time course of the vertical position of the intruders are shown **Figure 6.1.3(b)**, with the right intruder shown by the solid lines and the left intruder by dashed lines. The horizontal position of the center of mass is shown in the **Figure 6.1.3(c)**. Larvae are placed in the bin at t = 0 min. At time t = 19 minutes, the first motion of the right magnet does not seem to affect the larvae, and the larvae remain in that corner for two hours. After 155 minutes, the larva pile begins to break apart and slosh from corner to corner. After this initial transient, we begin our attempt to synchronize larvae motion to the motion of the screws every twenty minutes. When the larvae are piled on the left side, we drag the left screw downwards, which breaks up the pile and allows them to move to the right.

We fit a sinusoid to the center of mass data using Matlab's Curve Fitting Tool:

$$X = A\sin(Bt + C), \tag{32}$$

where the amplitude $A = 2.4\%$, frequency $B = 0.14$, and phase $C = 1.6$. The time between corners is therefore half of the period of the motion, $\pi/B = 21.8$ minutes, which is well synchronized with the period of the perturbation. This motion is far more regular than the motion without the intruders, whose period followed a gamma distribution. Moreover, the period of the perturbed larvae matches the period of the perturbation, which is one third of the expected period without intruders. This shows that it is downward motion of larvae chasing the intruder that causes larvae piled in one corner to rearrange to the other.

The time between the left screw reaching the bottom of the pile and the larva pile breaking up is 15 minutes. We considered the pile breakup to be complete when the pile had moved to the other side of the container, and there was a local maximum in the center of mass position. Presumably, the 15 minute lag is the time that it takes for the larvae to fill in the space made by the intruder and to reorient themselves to break up the pile.

By watching videos of the intruding screw, we can speculate how it triggers the motion of the pile. The larvae are all initially jammed because they are all crawling in the direction of a wall. The intruder creates a space near the wall. This space allows the larvae to

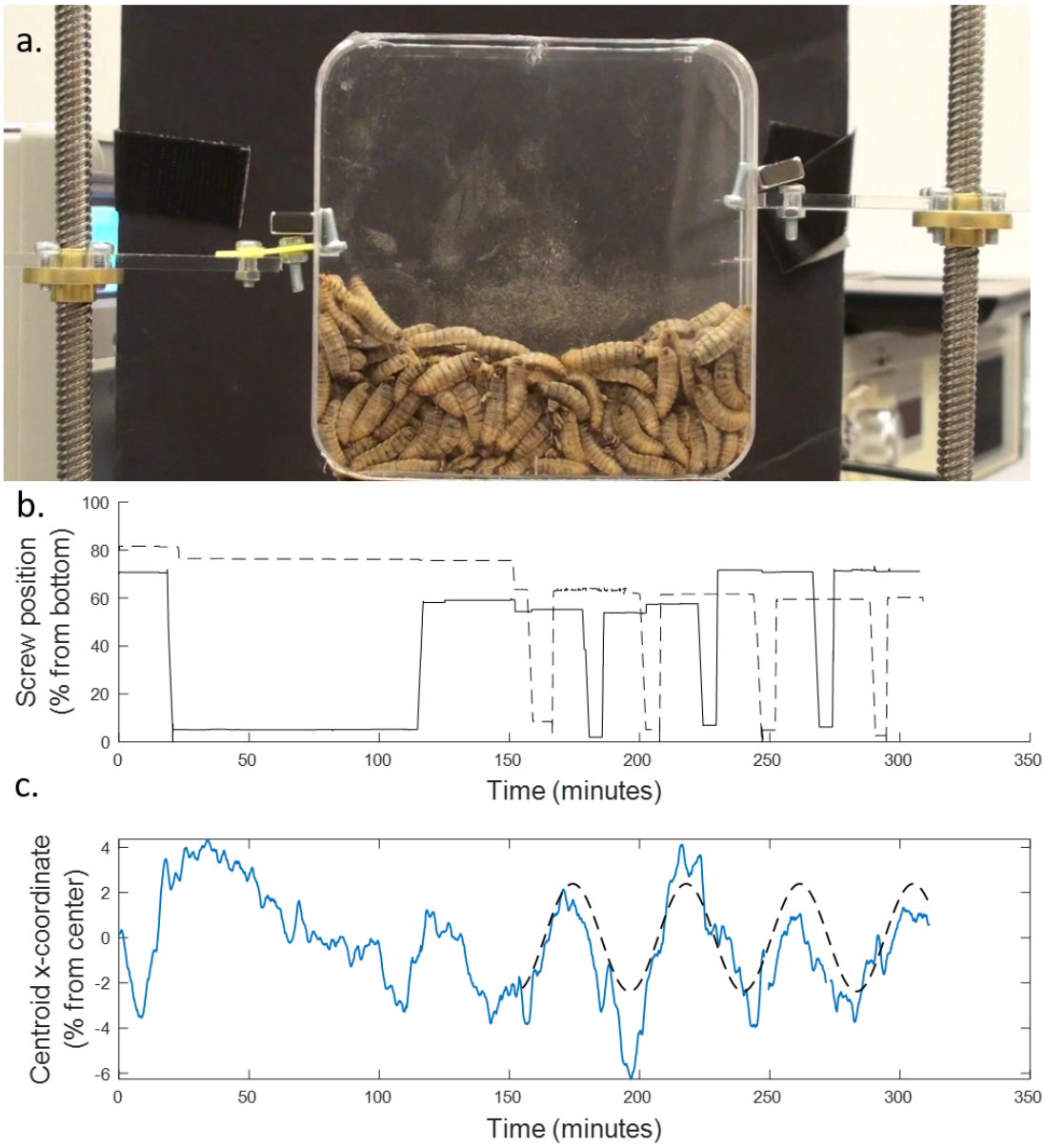

Figure 6.1.3: a. Experimental setup to drag a screw vertically through the larva pile. b. Tracks of vertical motion of magnets. Solid line is magnet on the right and dashed line is magnet on the left. c. Center of mass of larvae (solid blue line) and sine fit (dashed black line). The best fit curve starts at 155 minutes, when we begin driving the oscillation. Previous motion of the screws does not affect larva motion, likely due to transient effects in their arrangement.

reorient and face downwards. By moving downwards, and then along the bottom of the container, the larvae trigger a process that allows more larvae to follow, facilitating the complete disassembly of the pile.

We close by demonstrating that active particles can also spontaneously generate and break up piles. We simulate 50 larvae in a 2D container for $50\tau_R$, or 5 rearrangements between corners. A time series of the motion is shown in comparison to the biological larvae in **Figure 6.1.4(a)**. Although the sloshing behavior of these larvae is not as visually obvious as that of the real larvae in experiment, they do rearrange between corners. The velocity vectors of simulated larvae as they rearrange are shown in **Figure 6.1.4(b)**. In this frame, most of the larvae are moving in the same direction. **Figure 6.1.4(c)** shows the time course of the $5\tau_R$ moving averages of the position of the center of mass of these larvae and the horizontal velocity, showing similar behavior to that of the real larvae. The cross-correlation shows that the simulated larvae begin moving $3.8\tau_R$ before they rearrange. The time scale of the simulation is due to the reorientation time of the larvae, which represents their persistence to crawl forward before turning. The reorientation time of larvae was not able to measured in our experiment. Thus we cannot quantitatively compare the experiment to the simulation. However, our simulation shows that the mechanism behind the sloshing behavior of larvae is likely caused by the physics of interacting active particles rather than larval biology.

6.2 Discussion

In this study, we investigate the formation and breakup of piles of fly larvae. Piles are confined to the wall of the container, and because of the two-dimensional nature of the container, the breakup of a pile on one side is followed by formation of a pile on the opposite side. Such oscillation is a common phenomenon of swarms in confinement. Flying insects can exhibit oscillation, as shown by swarms of midges which can oscillate due to the motion of a visual cue[98]. The resulting oscillating can give insight to the viscous and elastic properties of the swarm, resulting from their aerodynamics and the communication between the midges.

While the center of the pile is jammed, we observe that the floor of the pile has greater mobility. In a previous study of larvae eating, we also observed larvae crawling towards food on the bottom of containers, getting pushed up by the incoming larvae, and then falling away from the food on the top of the pile. The cycle continues, which permits more larvae to have access to the food; when the food is gone, the aggregation disperses[48]. This previous work observed larva motion in three dimensions, which is more similar to their natural

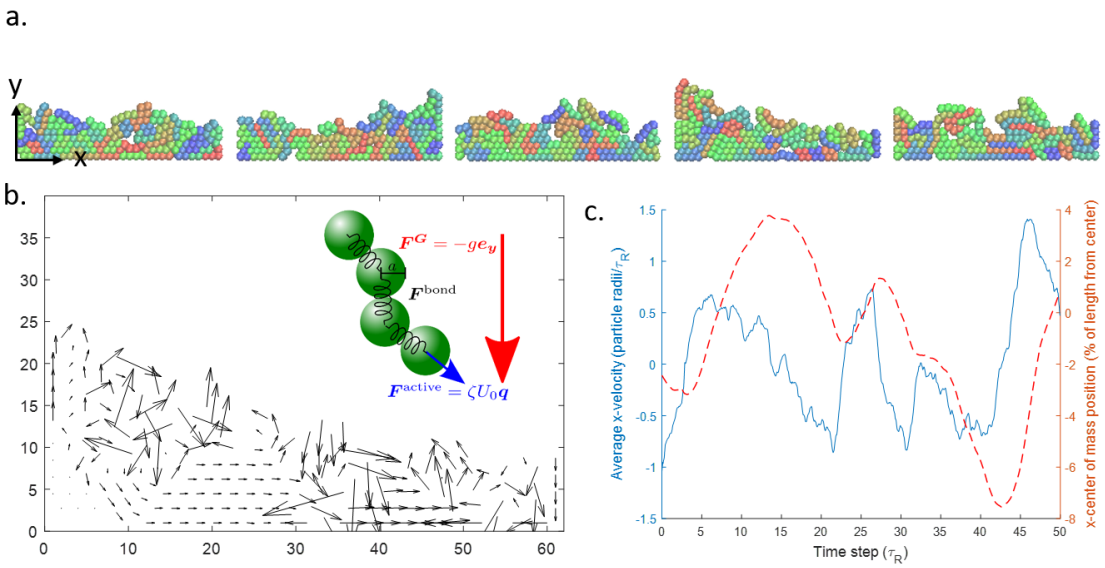

Figure 6.1.4: a. Sample frame from the simulation showing simulated larvae piling up in a corner. b. Velocity vectors of simulated larvae. Inset: A schematic of our model system. c. x-coordinate of the center of mass of the simulated larvae showing rearrangement from corner to corner (dashed red line) and average x-velocity (solid blue line) showing that the signals are similar ($5\tau_R$ moving averages).

habitat, large mounds of compost. The two-dimensional nature of the our study prevented such continuous motion. Instead, the aggregation becomes trapped along an inedible wall where there is no food to be found. When larvae are raised in rectangular plastic bins in industry, walls like those in our study may cause stationary spots in the bin of larvae. When the bin is fed, larvae far from walls can travel to the food. However, larvae near walls or corners may remain trapped as we observed in this work. This trapping near walls may inspire others to engineer larvae mixing devices to keep the larvae in bins uniformly fed.

6.3 Chapter summary

In this study, we observed the formation and breakup of black soldier fly larvae. The breakup of a pile of larvae can be driven using an external perturbation that initiates vertical motion near the wall, unjamming the larvae, and allowing them to reorient and change direction. The pile then continues to breakup with larvae leaving the pile by crawling along the bottom of the container. We also used a simulation to show that the piles form in confine active rods, indicating that the phenomenon observed is caused by physical interactions rather

than larva biology.

If larvae are piled in corners, they may not be able to reach food placed in the center of the container. A simple solution to this problem would be to raise the larva in containers with rounded floors so that there are no corners for the larvae to become trapped in. However, that would not be an efficient use of space, and would also be challenging to manufacture. Larvae can be manually mixed with their food; a more important problem to solve is that of cooling larvae. In the next chapter, we describe an aerating bed to cool larvae from their high metabolisms while eating.

CHAPTER VII

COOLING LARVAE WITH AERATION

Air conditioning an entire warehouse that larvae are raised in is an inefficient method to regulate the temperature of large masses of black soldier fly larvae in a rearing facility. In this chapter, we first examine the metabolism of fly larvae. We then present an aerating bed that cools larvae through convection. Finally, we raise 200,000 larvae in the aerating bed with potential for many more. We hope that this aerating bed can be scaled up for industrial use, allowing more larvae to be raised in the same square footage at a lower cost.

7.1 Metabolism of black soldier fly larvae

Images from the time lapse of 2,000 black soldier fly larvae eating chicken feed are shown in **Figure 7.1.1(a)** when larvae are mixed with food initially, and **Figure 7.1.1(b)** after the larvae have been eating for 78 minutes. Over the two hours of the experiment, the larvae increased in temperature by 8°C, showing that they heat up just as the blow fly larvae in literature.

We measure the oxygen consumption and CO_2 production of 50 larvae with and without food in a respirometer, shown in **Figure 7.1.1(c)**. Their CO_2 consumption is shown in **Figure 7.1.1(d)**. We use the Weir formula to estimate a metabolic rate[99]:

$$\dot{E}\left[\frac{\text{cal}}{\text{min}}\right] = -3.9\dot{V}_{O2}\left[\frac{\text{mL}}{\text{min}}\right] + 1.1\dot{V}_{CO2}\left[\frac{\text{mL}}{\text{min}}\right]. \tag{33}$$

We find when larvae are fed, their metabolism increases from 0.4 mW/larva to 0.6 mW/larva; some of this excess energy may go to heating up the larvae and producing the larval mass effect documented in blow fly larvae. We now turn to cooling larvae with aeration.

7.2 Aeration prototypes

Through testing three prototypes, scaling up from a 4 inch diameter tube to a nearly pallet-sized setup, we find that aerating larvae from underneath is an effective method for keeping their temperature manageable as they eat. Our first prototype is made out of a 4 inch outer

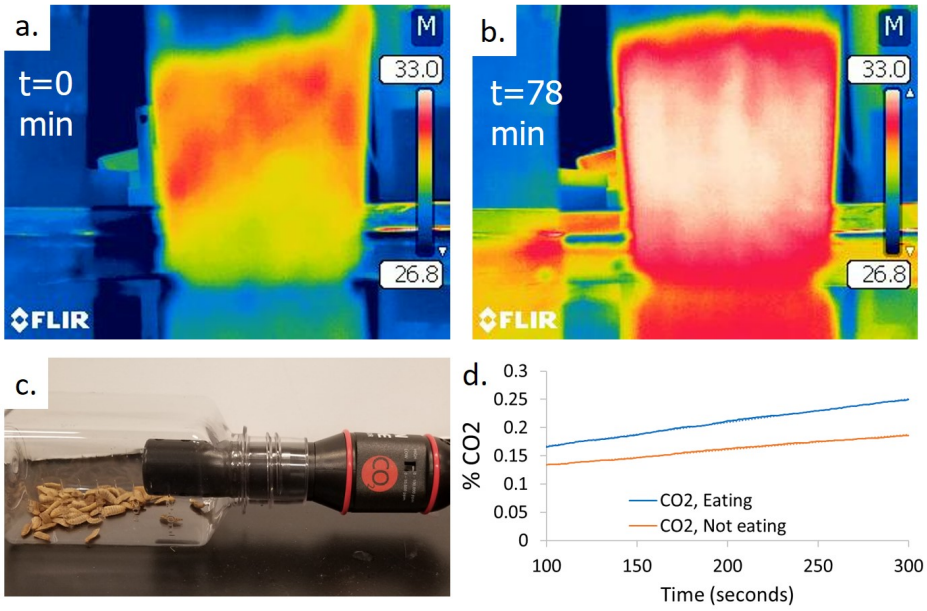

Figure 7.1.1: a-b. Thermal images of 2000 black soldier fly larvae when initially mixed with a chicken feed and water mixture (a) and 78 minutes after the start of eating (b) show that larvae heat up as they eat. c. Setup to measure metabolism of fly larvae. d. Larvae consume CO_2 faster when eating (blue) than when not eating (red).

diameter acrylic tube. This setup is shown in **Figure 7.2.1(a)** with the aerated larvae on the right and a control batch of non-aerated larvae on the left. We record the temperature over time with a FLIR thermal camera in **Figure 7.2.1(d)**. The two masses of larvae start at the same temperature, but the aerated larvae cool within five minutes while the control larvae get slightly hotter. After seven minutes, the aerated larvae have a maximum temperature of 26°C. The temperature of the aerated larvae is plotted in **Figure 7.2.1(b)**. In our estimated prediction of larva temperature, we use the lumped capacitance model to model a larva surrounded by airflow, as in **Figure 7.2.1(c)**.

We then move on to raising larvae in a 12 inch diameter bed. This setup is shown in **Figure 7.2.2**. At the suggested density of 3 lb. of mature larvae per square foot, about 5350 0.2 g larvae would fit in the bed; we have raised 20,600 in it – almost 4 times as many. The larvae do not overheat during feeding and their final mass is not affected. The larvae (in **Figure 7.2.2**) grow from 0.12 g to 0.21 g on average each over 5 days. Initially the layer of larvae and substrate was 2 inches deep; at the end the layer of larvae and substrate was 5 inches deep. Without aeration, larvae are generally only grown in 3 inch deep layers of larvae and substrate. Since the larvae reached their fully grown weight of 0.2 g without

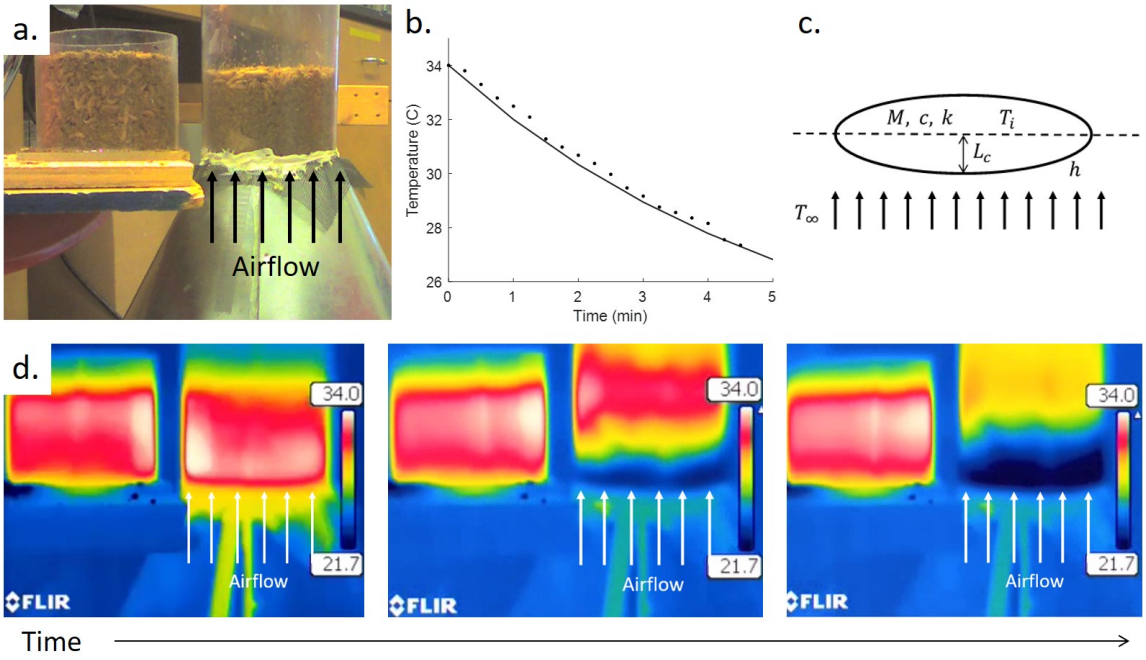

Figure 7.2.1: a. Larvae in the first prototype of the aerating bed: a 4 inch outer diameter tube with 0.125 inch thick walls. The larvae on the left are not aerated, while a fan cools larvae from underneath on the right. b. Measurement of larva cooling from the thermal video (points) and theoretical prediction (line). c. Schematic of larva cooled by aeration. d. Images from thermal video of experiment in (a). Over time, the aerated larvae on the right are cooled while the control larvae on the left become hotter.

overheating, their feeding was not disturbed by the aeration.

Experiments with this prototype were done in June 2018 in an open-air warehouse at Grubbly Farms, during hot and humid weather with highs outside reaching 33°C. The temperature inside the warehouse was hotter (but not recorded) due to the heat generated by the many larvae inside the warehouse. The air coming through the fan at this time was sufficient to cool off larvae. This setup was limited by the fan overheating, not how much air the fan could provide. It is important to choose a heat tolerant fan for the aerating bed.

With a more densely packed warehouse at higher temperatures, an additional source of cooling may be needed. If the temperatures inside a warehouse full of larvae are much hotter, the heat from the aerating bed needs to be vented to the outside, and air conditioning the air inside the warehouse will be necessary. However, air conditioning the warehouse with aerated larvae will be much cheaper than without aeration, since the cold air will reach the larvae directly and the temperature in the room will not have to be cold enough for the

larvae to be sufficiently cooled only though heat conduction.

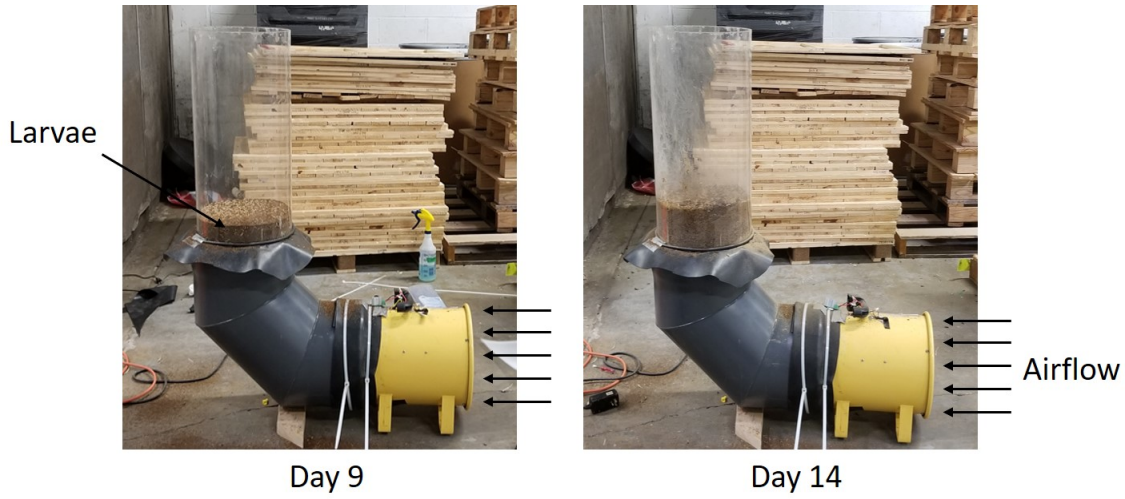

Figure 7.2.2: Prototype for testing the growth of black soldier fly larvae. 20,600 larvae are placed in the aerating bed at 9 days old, and grow to 0.21 g by 14 days old, 3.9 times the recommended density of larvae per square foot.

We now move on to scaling up our design. The current design of the system has four bins, each of which can fit tens of thousands of larvae, as in **Figure 7.2.3(a-b)**. We raise approximately 200,000 larvae in this aerating bed over 21 days. The mass of the larvae over time is shown in **Figure 7.2.3(c)**. The larvae are somewhat underfed to prevent smells of rotting food from bothering the other researchers in the Techway building. However, the larvae do pupate at the end of the trial so their development was not harmed. Further testing with this bed is necessary to determine proper feeding and aeration parameters.

One of the main challenges with this prototype is that some larvae escape through the mesh when initially placed in the bed at a weight of 0.02 g. To avoid this problem in the future, larvae should be raised in an aerating bed with a very fine stage. Very small larvae do not need to be aerated, since they do not generate enough heat for temperature to be an issue. Careful investigation needs to be done to determine the larva weight at which they begin significantly heating up.

7.3 Discussion

We are able to successfully cool larvae with aeration and raise them from newly hatched larva to fully grown adult at greater densities than possible without aeration. The future of this project requires optimizing and scaling up the bed to make it a commercially viable way

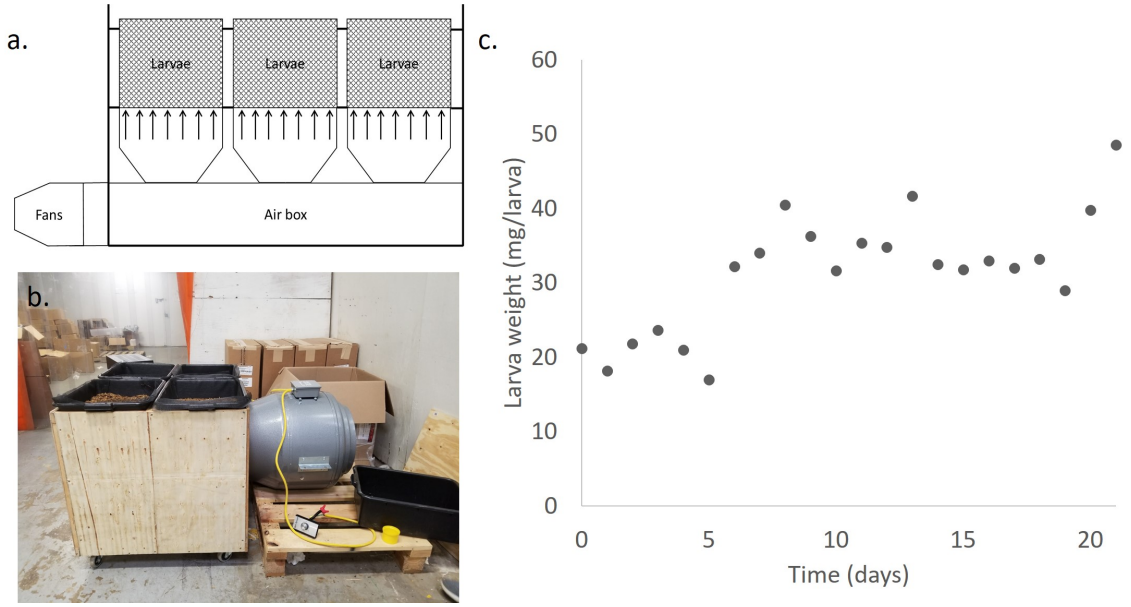

Figure 7.2.3: a. Schematic of scalable design for aerating bed. b. Photograph of current aeration setup. c. Plot of mass of 200,000 larvae as they grow in the bed.

to raise larvae. The current fan is powerful enough to aerate many times more larvae than the 200,000 in this thesis, and in thicker layers. To avoid overcooling the larvae and slowing down their growth, a feedback loop turning the fan on and off based on the temperature in the bins may be added. Scaling up the bed with additional bins either added to the sides of the bed or vertically stacked on top will allow to test the limits of this system. The excess heat should be vented into the atmosphere to avoid overloading the air conditioning building in the system.

There may be an additional benefit to using the aerating bed for growing larvae. Pulsing the fan when the larvae are fed may mix the larvae with their food without manually touching them, reducing the labor necessary to raise a batch of larvae. We have observed in previous chapters that larvae tend to cluster in corners of containers. It appears that when air is added, larvae tend to cluster around air pockets as well as in the corners, which may reduce their chances of piling up and escaping from the bed. This aerating bed has potential to revolutionize the black soldier fly industry if it is expanded and adapted for growing out a full warehouse full of larvae.

7.4 Chapter summary

In this chapter, we showed that black soldier fly larvae generate heat just like other species of maggots. We cool them from this excess heat in minutes by aerating them from underneath. With aeration, we grew nearly four times as many larvae in the same space as without aeration. The largest prototype can contain 200,000 larvae with potential for many more. This invention has potential to significantly improve the black soldier fly larva industry.

The work presented in this thesis has obvious applications to the black soldier fly industry, from understanding how fly larvae feed in large groups to technology to raise larvae in. For the final chapter of this thesis, we turn to a different application of our work: swarm robotics.

CHAPTER VIII

SPINNING DURING FEEDING

Unlike fly larvae, which can crawl on top of one another to reach food, many animals that try to feed in groups, such as puppies trying to eat from a circular bowl, are trapped in a flat plane. In this chapter, we look at how feeding in 2D forces animals to move in circles. We proceed by presenting our analysis of Youtube videos of puppy motion, continue in with a bristlebot model of puppy feeding, and develop an agent-based model in the Georgia Tech Robotarium.

8.1 Puppy pinwheels

We begin our investigations of spinning around bowls with an overview of videos of "puppy pinwheels" found on Youtube. We observe from two to thirteen puppies gathering around food bowls and spinning in circles. Once the puppies begin spinning, they travel at an average angular velocity ω, as in **Figure 8.1.1(a)**. We count the number of revolutions per minute of a puppy in each video to get a sense of how the number of dogs affects their motion in **Figure 8.1.1(b)**. Overall, the angular speed of puppies w decreases with greater number of puppies N: $\omega = -6.8N + 90.3$ deg/sec, $R^2 = 0.18$. This is likely because a large number of puppies provides more chances for the dogs to become jammed, and decreases their speed. However, there is a lot of noise in the data. The dogs in the videos are of different ages and breeds, ranging from very young terrier puppies to fully grown huskies. Thus, we do not know what aspects of their motion are caused by the characteristics of the individual dogs and which aspects are a collective dynamics phenomenon. To simplify this problem, we turn to robot models.

8.2 Robotarium model

To develop an agent-based model of puppy motion, we set up an experiment in the Georgia Tech Robotarium in Spring 2019. To simulate attraction to food, all twelve robots in the experiment are asked to set their target to the center of the experimental area. A circular border simulates the round edge of the food bowl. The robots spin around this "bowl" at

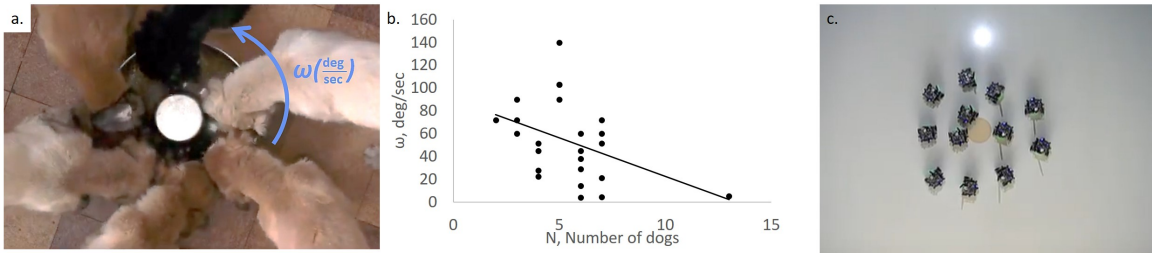

Figure 8.1.1: a. Puppies gathered around a food bowl spin around a dish with an angular velocity ω. Original video can be found at www.youtube.com/watch?v=UnGJV_jmh-k. b. Measurements of puppy speeds in degrees per second vs. number of puppies (points) and linear best fit (solid line). When there are more dogs around a bowl, they tend to spin slower. c. Twelve robots in the Georgia Tech Robotarium spin around an orange patch of "food".

1.4 degrees per second, slower than any of the puppies. We have observed them spinning either clockwise or counterclockwise, indicating no bias in the robot motion. A snapshot of the Robotarium setup, with robots clustered around a circular patch of food, is shown in **Figure 8.1.1(c)**. However, soon after the end of the Spring 2019 semester, an update to either the code of the robots, the flooring used in the Robotarium, or both, changed the behavior of the robots. Instead of the robots spinning around the food, they became trapped at the center and wriggled in place.

To reduce the spinning motion to a simple a model as possible, self propelled rods around an attractive point, we turn to Bristlebots in a bowl.

8.3 Bristlebot model

Bristlebots are small robots powered by a vibrating motor. When turned on, they travel forwards with a roughly constant velocity. We aim to investigate two aspects of puppy pinwheels with these robots: the effect of adding more puppies, and the effect of increasing attraction to food. To simulate attraction to food, we 3D print bowls at different angles: a shallow bowl with its edges at an angle of 160 degrees, a medium bowl with the side at 145 degrees, and a steep bowl with its edges at 130 degrees, as in **Figure 2.5.1**. A round inset is glued to the center of the bowl to simulate the edge of the food. We film from one to nineteen robots spinning in the bowl, with three trials per number of robots in each bowl, and track the motion of a robot to estimate the rotational velocity ω in the bowl. Bristlebots in a bowl are shown in **Figure 8.3.1(a)** and a sample plot of angular

velocity vs. number of robots in the 145-degree bowl is shown in **Figure 8.3.1(b)**. As with the puppies in **Figure 8.1.1**, the angular velocity decreases with the number of robots, indicating that the robots are jammed.

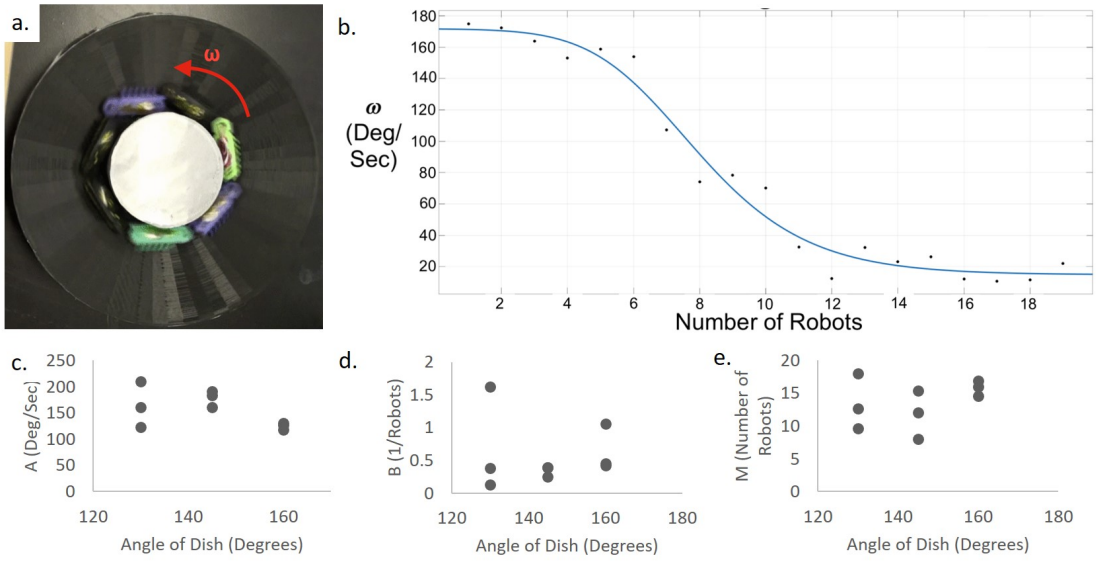

Figure 8.3.1: a. Bristlebots in the 145-degree bowl spin around the center inset. This experiment was repeated three times at each angle. b. Angular velocity of Bristlebots in the 145-degree bowl (points) with a sigmoid best fit (solid blue line). c - e. Sigmoid fit parameters: c. A, top speed of robots; d. B, the slope of their jamming; e. M, the number of robots at which the robots slow down.

A sigmoid function is found to be a good fit for ω as a function of number of robots N. This function is found to represent many distributions, from plant growth in botany to approximations in neural networks[100,101]:

$$\omega = \frac{A}{1 + e^{B(N-M)}}. \tag{34}$$

The parameter A represents the top speed of robots in the bowl, B characterizes the slope of the curve, and M represents the inflection point of the angular velocity. The top speed of the robots is $A = 156 \pm 34$ deg/sec; it may decrease with number of robots. The jamming speed of robots, $B = 0.6 \pm 0.5$ 1/robots. The inflection point in the curve occurs at $M = 13.7 \pm 3.4$ robots, which is close to where we observe the 145-robot curve to flatten out. These S-shaped curves are indicative of three regimes: with few robots around the center, they are able to spin around the bowl around their top speed. As more robots are added to the bowl than can fit around the center, they spin slower and slower. Finally,

when the robots are jammed and barely moving, they move very slowly.

8.4 Discussion

Although this work began with an interest in how animals other than fly larvae feed, it has implications for robotics. Animals collectively feeding from a single source may be used to inspire swarm robots gathering material from a single point – for example, removing debris from a disaster site, mining material from a hole dug in the ground, or charging from a single charging station. Understanding how animals such as puppies move when limited by the space around the food, such as pinwheeling puppies that are confined to 2D or larvae crawling on top of each other, can help understand how to best program autonomous robots for these scenarios.

Why the Robotarium robots suddenly changed their behavior and stopped spinning with the same programming remains unsolved. It is likely due to either a change in the flooring material, which may have affected their motion, or in their object avoidance programming, which may have affected how they interact with one another. This is worth exploring in future work, as it may provide insight into what animals may spin around food bowls and which animals may remain jammed and unmoving. This can then be used for programming robot swarms where motion may or may not be desirable.

8.5 Chapter summary

In this chapter we present work on spinning during feeding a flat plate. We find that "puppy pinwheels", in which dogs spin around food bowls when feeding in large numbers, are caused by the mechanics of the motion of active particles. We are able to replicate this motion with an agent-based model in the Robotarium and with simple mechanical Bristlebots. This work has implication for the motion of rolling robots attempting to reach a limited resource, such as removing debris from a disaster site.

Experiments with fly larvae were done in many different containers and on many different time scales. In the next chapter, we summarize larva behavior on time scales from seconds to hours to understand their behavior around food and near walls.

CHAPTER IX

SCALING OF LARVA MOTION

In this chapter we discuss the implications of the sizes and time scales of the experiments and how this affects larva motion. We normalize our dimensions, such as L by characteristic parameters denoted as L^*. Normalized variables are denoted as $\bar{L}$.

In our experiments, a larva is approximately $L^* = 13.7$ mm long. It is 4.3 mm ($0.3L^*$) wide and 3.2 mm ($0.2L^*$) tall. A free larva crawls at $V^* = 2$ mm/s on glass, or 8.6 body lengths per minute. On uneven surfaces, such as the top of other larvae, its speed may be impeded. Larvae also slow down when jammed in very large aggregations.

In this chapter we begin by defining dimensionless parameters for larvae. Since larvae can be seen as an active fluid, we attempt to find some dimensionless parameters for them. The most useful is the volume fraction, volume of larvae divided by volume of the space they take up which we calculate in Equation 3 to be $0.56 \leq \phi \leq 0.80$. Larvae self-pack to a volume fraction of about $\phi = 0.62$, and getting them to be more tightly packed requires external compression. They pack more tightly than other insects. Fire ants in a raft, for example, have a volume fraction of 0.21 [91]. Bee clusters can be more tightly packed than those of ants, with a simulated maximum volume fraction of 0.8, but this can cause thermoregulation problems for the bees [102].

We also calculate a Reynolds number and Froude number for confined larvae. The Reynolds number, ratio of inertial viscous forces, is [83]

$$\mathrm{Re} = \frac{\rho u L^*}{\mu}. \tag{35}$$

We base our calculation of Reynolds number on the larva length L^*, density of many larvae $\rho \sim 0.62$ g/mL (estimated from the density of a single larva, $\phi\rho_{larva} = 0.62 \times 1$ g/mL), velocity $u = 8$ mm/min measured on the bottom of the confined aggregation. The viscosity is estimated by dropping a sphere with an $d_{sphere} = 8.8$ mm diameter and $\rho_{sphere} = 7.7$ g/mL density through an aggregation of larvae in a 95 mm x 95 mm x 18 mm vertically oriented bin (same as used in Chapter 6), as in **Figure 9.0.1(a)**. We track the sphere starting after an initial 10 second transient, and it falls through the container

at $u_{sphere} = 2.7$ mm/min (comparable to the speed of larvae). Notably, as the experiment goes on the ball does not fall smoothly, and instead travels throughout the container as the larvae exert forces on it from all sides. The viscosity can be calculated with a Stokes drag estimate[92],

$$\mu = \frac{(\rho_{sphere} - \rho_{larva}) g d_{sphere}^2}{4 u_{sphere}} \sim 30350 \text{ Pa s}. \tag{36}$$

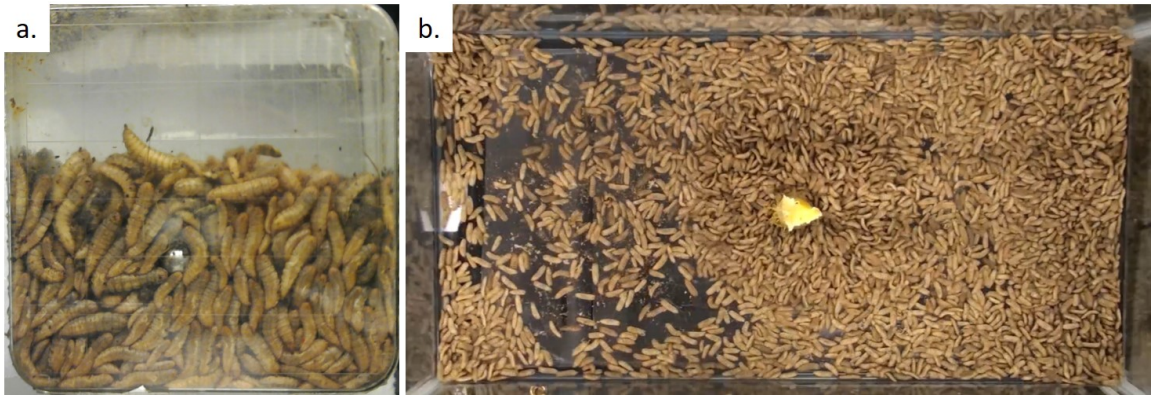

Figure 9.0.1: a. Dropping a sphere through larvae to measure their viscosity. b. Zoomed out view of 5,000 larvae in an aquarium eating an orange slice, showing piles near the orange and near the walls.

This viscosity is close to that calculated for fire ants, 35800 Pa s[92], and 3050 times the viscosity of molasses (up to 10 Pa s)[103]. We calculate the Reynolds number in a jammed pile of larvae to be $\text{Re} = 3.7 \times 10^{-8}$. The Reynolds number is very low, since the larvae move through the pile very slowly, making their inertia very low, and are very densely packed, making them highly viscous.

The Froude number, or the ratio of inertial to gravitational forces is[83]

$$\text{Fr} = \frac{u}{\sqrt{g L^*}}. \tag{37}$$

The Froude number is $\text{Fr} = 3.6 \times 10^{-4}$. The low Froude number suggests that gravitational forces are very important in a larva pile, and their inertia is very low. Larvae are a unique active matter system where gravity is significant, resulting in phenomena such as sloshing between corners.

We now discuss the details of the individual experiments. We present the dimensions of the containers L and the larva speeds V in our experiments normalized by the body length and the speed of the larva respectively: $\bar{L} = L/L^*$ and $\bar{V} = V/V^*$. We normalize

the times t reported in the experiments by the length and velocity as well: $\bar{t} = t/t^*$, where $t^* = L^*/V^* = 6.9$ s.

The feeding behavior studies (Chapter 4) were done in 10 gallon aquariums measuring $37L^*$ long by $19L^*$ wide by $22L^*$ tall (508 mm long x 254 mm wide x 309 mm tall) using 500 to 10000 larvae. Using large aquariums to measure larva motion was necessary to highlight the mixing region that formed around a piece of food attached in the center. Larvae piled up around the orange slice to a height of 25 mm ($2L^*$), which was measured separately from the experiments used in PIV. The mixing region is defined as the area around the orange slice where the bulk speed on the top layer is greater than a threshold of 0.125 mm/s ($0.06V^*$), which selects the area where there is an outflow of larvae. The bulk speed outside of the mixing region is slower, 0.05 mm/s ($0.03V^*$); outside the mixing region, there is no average motion towards or away from the food. The average bulk velocity in the mixing region as measured by PIV on the top layer of the experiment with 5000 larvae was 0.35 ± 0.05 mm/s, or $\bar{V}_{mix} = 0.18 \pm 0.03V^*$, 6 times slower than a free larva. This is likely because the larvae impede each other when they move and because larvae are moving in all directions on the top layer, but we only report the time-averaged velocity.

The feeding time for a single larva was 5 ± 8 minutes, or $\bar{t}_{feed} = 44 \pm 80t^*$. It eats for 44% of the time it is around food. This was measured for 10 larvae freely individually feeding in petri dishes. The large standard deviation arises from the wide range of eating times, and a larva cannot have a negative eating time. On average, feeding takes a long time compared to the motion of a larva since an individual larva's mouth is small, about 0.5 mm ($0.04L^*$) long and the larva needs to spend time eating small food pieces to reach its goal of eating twice its body weight (or 0.2 g) per day. When larvae are in large groups, their competition may result in them not getting the full five minutes to feed.

The diameter of the mixing region varied with number of larvae; for the 5000 larvae experiment it was 170 mm, or $\bar{d}_{mix} = 12.4L^*$. A larva thus needs about $d_{mix}/(2V_{mix}) = 4$ minutes to cross the radius of the mixing region and reach food, nearly the same as the time it takes a larva to feed. At this number of larvae, the surface area of the food is surrounded by eating larvae and increasing the speed of larvae within the mixing region cannot allow more larvae to feed.

We also calculated the spatial average of the vorticity and divergence for the time-averaged vectors of larvae on the top and bottom layer within the mixing region. The

average vorticity was 0.001 1/s, or 0.005 $1/t^*$. This value is very low, and represents the existence of shear within the container of larvae (although not necessarily spinning of the fountain). A nonzero vorticity suggests that a particle placed in the fluid would spin, and we do observe that the food rotates back and forth as the larvae eat it.[83] The average divergence magnitude was 0.0016 1/s, or 0.01 $1/t^*$. The divergence was positive on the top layer and negative on the bottom layer. Divergence represents how much the fluid expands (for a positive divergence) or contracts (for a negative divergence). If the divergence was zero, the mass of larvae on the top or bottom layer would be constant. Instead, we observe a positive divergence (increasing mass, or a source) on the top layer and negative divergence (decreasing mass, or a sink) on the bottom layer.[104] The outflow of larvae was also measured by summing up the velocity vectors flowing out (Equation 1). The average divergence and vorticity numbers are very small, likely because the speed of larvae in the mixing region is very small and the time scale for this flow is longer than t^*. They are only presented as further evidence of a source of flow on the top layer and sink of flow on the bottom layer. The characteristics of this flow are worth investigating in detail in future studies with tracks of individual larvae in the mixing region to calculate streamlines of larvae.

The large mixing region does not just maximize eating rate; it also entrains more larvae from far away and draws them close to the food. Larvae far away from the food are not aware of its presence, but a large mixing region brings larvae close to food from far away. This allows more larvae to feed even if not all larvae get to eat their fill. It also keeps larvae that have eaten their fill close enough to the food that they can return once they want to eat again. Nevertheless, there are still some larvae trapped in corners away from the food in this experiment that likely never get to eat.

Confining 2000 larvae to a 95 mm inner diameter cylinder ($\bar{d} = 6.9L^*$) allowed us to investigate the larvae as an active material in Chapter 5. Larvae react to external forces very quickly: their time constant is $\tau = 1.7$ s, or $\bar{\tau} = 0.3t^*$. The characteristic time for larva motion and the relaxation time under compression are comparable: relaxing forces on their bodies requires them to move a distance less than a full body length. However, larvae in this container have little space to move. Although their speed was not measured, since the curved walls of the container and scuff marks make it difficult to get an accurate measurement, it is likely as slow as in the other experiments with large numbers of larvae. Larvae around a piece of food are always moving around and pushing against one another,

just like in the compression chamber. The constant wriggling of larvae within the mixing region likely allows them to quickly respond to being pushed by other larvae and either stay near the food or be carried away from it by the current of larvae.

The piling experiments in Chapter 6 were done in bins that measured $6.9L^*$ (95 mm) tall and long, and $1.3L^*$ (18 mm) wide, oriented vertically. Confining 300 larvae to these bins allowed us to isolate their switching from corner to corner, and measure it on a reasonable time scale. Within this bin, larvae took 60 ± 32 minutes, or $525 \pm 280t^*$ to switch from corner to corner. The lag between the x-velocity of the larva and the centroid x-coordinate was 13 minutes ($114t^*$), 22% of the time to switch corners. Once the larvae become unjammed it takes them much less time to move than the time they spent jammed. The time scale of the motion of the 300 larvae is $300t^* = 34$ minutes, half of the 60 minutes taken between corners. All of the larvae need to move for the center of mass to shift. When the larvae are jammed, each larva needs more time to move a full body length and rearrange.

The speed of larvae on the floor of the vertical bins as they move is slow, 8 mm/min or $0.07V^*$, and comparable to the speed of the larvae in the mixing region. At this speed, it should take larvae 12 minutes, or $104t^*$ to travel from corner to corner, close to the measured 13 minute lag between velocity and position. Therefore the lag likely arises from the travel time of larvae from corner to corner, and in a larger container larvae would take a longer time to switch from corner to corner. When we drive the motion of larvae with vertical intruders, we move them once every 20 minutes ($175t^*$); the lag between the motion of a magnet and the position of the centroid of the pile is 15 minutes ($131t^*$). We would most likely not be able to drive the larvae any faster, as this is close to the 12 minutes it takes for larvae to travel from corner to corner.

We repeated observations of piling in corners with larvae in a larger container, 228 mm long x 127 mm tall x 19 mm wide ($16.6L^* \times 9.3L^* \times 1.4L^*$). The mass of larvae was not recorded but we can estimate their number based on the mass of a larva, 0.1 g, and their packing density, 0.62 g/mL. When we place 1300 larvae in this container, they fully rearrange five times within 22 hours (for 4.4 hours between corners), but the piles often break up in small pieces rather than fully rearranging from corner to corner. Although a 2.4 times longer bin was used, it is notable that 4.3 times as many larvae in these experiments took 4.4 times longer to rearrange. Breakup time of the pile appears to increase with bin size and number of larvae. However, when we place 2700 larvae or more in the container, their

piling is suppressed. The reason for this is unknown but is likely because there is no longer enough space on the floor at this depth, and larvae are constantly jammed. Investigating how larger piles of larvae behave in future experiments is warranted to understand how these behaviors arise.

We observed piling in container corners in our experiments of measuring the outflow of larva fountains while feeding in rectangular aquariums, but not switching from corner to conner, as in **Figure 9.0.1(b)**. We do not observe sloshing from corner to corner in feeding experiments because the container is too large: the minimum distance from corner to corner of the aquarium is $18L^*$, larger than $6.9L^*$ in the piling experiments. If the relationship between container size and travel time is linear, the lag between centroid position and center of mass would be at least 31 minutes ($278t^*$). Additionally, there are more larvae in feeding experiments, which also appears to slow down their switching time. If these experiments lasted longer, we might see larva piles changing from corner to corner; we only observed larvae feeding from 30 minutes to an hour. How many larvae are in the corner piles in the feeding experiments is unknown, since we do not have a side view of these experiments to estimate their volume.

Notably, the radius of the mixing region of larvae near food (Chapter 4), and the length of container in which we measure piling in corners (Chapter 6) are both near 100 mm ($\sim 7L^*$) so the measured velocity profile where we observed piling and sloshing between the corners is likely to be similar to larva motion within the "fountain": faster motion on the bottom of the container, slowing down in the center, and fast motion on the top. The speed of larvae on the bottom of piles the vertical bins ($0.07V^*$) and on the top layer of the mixing region ($0.18V^*$) are comparable as well. Larva piles near food dissipate when the food is gone, while piles in corners near walls dissipate on their own, since there is no motivation for larvae to stay near a wall besides being jammed near it.

Attempts to confine larvae to bins flatter than one larva length resulted in all of the larvae being jammed, suggesting that a larva's motion is inherently three-dimensional. The body segments of fly larvae rise and fall by 5% to 10 % of their height as crawl on a flat surface, and confining them so they cannot do that can make them get stuck[105]. More careful investigations of the limit of the container size in which larvae can switch from corner to corner are warranted. This can explain whether this is caused by too many larvae attempting to squeeze themselves into a small space or with a single larva needing a full

length's worth of space around it to turn at all.

In this thesis, we use a variety of containers in our experiments to investigate different aspects of larva motion, from petri dishes to aquariums. Larvae move more slowly when they are trapped in large groups and need to all rearrange before group motion can occur. However, this trapping allows large groups of larvae to eat faster by bringing them in towards food. This is driven by competition between all the larvae, not by the larvae intentionally working together. The behavior of larvae takes place on time scales from seconds to respond to forces, to hours to move when they are jammed. The short, nearly imperceptible motions of larvae as they push on one another result, over long periods of time, in larvae being able to form piles to feed, and to break their jamming when piled against walls. A company raising black soldier fly larvae in rectangular bins may want to make sure the larvae are mixed either when they are fed, or once per hour to prevent pile formation from interfering with eating behavior.

CHAPTER X

CONCLUSIONS

Black soldier fly larvae are an important decomposer of food waste and a source of proteins and fats in chicken feed. To realize the true potential of this insect by decomposing tons of food waste per day with them, we must first understand the biology and physics of their behavior. In this thesis, we investigated the behavior of black soldier fly larvae from the individual to groups of thousands.

Investigating eating rates of larvae led us to discover that the larvae form a "fountain" around food: they crawl towards food on the bottom of the container, pile up as they eat, and then fall away on the top layer. Since each larva only eats for five minutes at a time, for 44% of the time it is around food, this allows hungry larvae to replace full larvae that are taking up space around food.

Our investigations of one thousand larvae under mass compression creep tests showed that, by wriggling, larvae are able to relax the pressure on their bodies in seconds – ten times faster than dead larvae at corresponding levels of compression. The time course of pressure for dead larvae is best fit by a stretched exponential, suggesting that their bodies form a hierarchical material. This has implications for compressing larvae during shipping, and also for how active materials may behave if manufactured in large quantities.

Our investigations of larvae piling in corners show that larvae switch corners of vertical containers once per hour, but can be driven with vertical intruders along the container's side walls to switch within twenty minutes. This study considers larvae as an active granular material – it is the interactions of the larva bodies, not any intent on their part, that causes them to pile along walls.

The aerating bed we built for fly larvae can easily cool larvae from the heat generated by their metabolism. We can raise nearly 4 times as many larvae in the aerating bed as the suggested 3 lbs per square foot without aeration. With optimization, future iterations of the bed will be able to raise even more larvae in greater densities, both saving black soldier fly startups money in energy costs, and being able to raise more larvae in the same space. Excess heat from this bed may be harvested for other use.

Our robotic model of puppy feeding is merely a start to the investigations of collective feeding behaviors of other animals. We found that, when animals or robots are confined to two dimensions, they spontaneously begin spinning while eating - but if too many animals are present, they become jammed. Characterizing this motion can help engineers make decisions for how to program individual robots.

Calculating dimensionless parameters for larvae in large groups shows that their motion has strong viscous and gravitational forces, and has very low inertial forces. Larva motion is slow in large aggregations. The trapping of larvae decreases their speed but brings more larvae in towards food, allowing them to eat.

CHAPTER XI

APPENDICES

11.1 Aeration parameters

Table 3: Parameters used to calculate air flow through bed of larvae and sand.

Friction factor, f	0.018
Loss coefficient K	0.08
Length of tube, L	12 in
Tube diameter, D	3.75 in
Layer depth, L_{bed}	2.5 in
Air viscosity, μ	1.77×10^{-5} kg/m/s
Void space, ϵ	0.4
Flow rate, Q	2905 CFM
Fan power, P	3/8 HP
Sand diameter, d_{part}	0.2 mm
Air density, ρ_{air}	1.12 kg/m^3
Air speed through bed, V	**0.0745 m/s**

Table 4: Parameters used to cooling of larvae.

Mass of larva, M	0.1 g
Larva heat capacity, c	3.34 J/g/K
Air heat capacity, c_p	1006.5 J/kg/K
Initial temperature, T_i	34 °C
Air temperature, T_∞	22 °C
Air speed through bed, V	0.0745 m/s
Larva height, H	3 mm
Larva width, W	4 mm
Larva length, L	14 mm
Larva thermal conductivity, k	0.4 W/m/K
Air thermal conductivity, k_{air}	0.026 W/m/K
Convective heat transfer coefficient, h	**8.2 W/m²/K**
Reynolds number of flow past larva, Re	20
Prandtl number, Pr	0.04
Nusselt number, Nu	1.27
Biot number, Bi	**0.03**

11.2 List of puppy videos

Table 5: List of videos used in analysis of puppy pinwheels.

Link	# of dogs	deg/sec
https://www.youtube.com/watch?v=vDa0z0gEvI4	6	28.8
https://www.youtube.com/watch?v=0JmeZXBaUFo	7	60.0
https://www.youtube.com/watch?v=8NoTmaRk0jo	7	4.5
https://www.youtube.com/watch?v=g4USPuAZaTE	5	140.0
https://www.youtube.com/watch?v=4W0EocAOf-A	6	14.4
https://www.youtube.com/watch?v=DI2e_KcEpno	6	45.0
https://www.youtube.com/watch?v=JbtXsx1rpXA	2	72.0
https://www.youtube.com/watch?v=1skpkQec8dk	3	90.0
https://www.youtube.com/watch?v=UnGJV_jmh-k	5	102.9
https://www.youtube.com/watch?v=3jywP-BaRPk	7	21.2
https://www.youtube.com/watch?v=_xHTPeL3M64	5	102.9
https://www.youtube.com/watch?v=AoAkJXFde_o	7	51.4
https://www.youtube.com/watch?v=RVLUsyRVSVM	6	3.8
https://www.youtube.com/watch?v=Hk-mVHzOIFg	4	22.5
https://www.youtube.com/watch?v=pUhuqA2gLA0	3	72.0
https://www.youtube.com/watch?v=A5f-9CpW7z4	6	37.9
https://www.youtube.com/watch?v=cEQ4Cj4fYrk	5	90.0
https://www.youtube.com/watch?v=YOim8k1pClY	6	60.0
https://www.youtube.com/watch?v=te4W96G9rzk	4	45.0
https://www.youtube.com/watch?v=LYdgTScYbmA	4	51.4
https://www.youtube.com/watch?v=6LImcLkik9o	7	72.0
https://www.youtube.com/watch?v=GA_0mNpams8	4	27.7
https://www.youtube.com/watch?v=G7oqOOBLsiQ	3	60.0
https://youtu.be/DvrTEDDnB3s	13	5.1

Bibliography

[1] Diener, S., Zurbrugg, C. & Tockner, K. Conversion of organic material by black soldier fly larvae: establishing optimal feeding rates. *Waste Manag Res* **27**, 603–10 (2009).

[2] Gustavsson, J., Cederberg, C., Sonesson, U., Van Otterdijk, R. & Meybeck, A. *Global Food Losses and Food Waste: Extent Causes and Prevention* (Rome, Food and Agriculture Organization (FAO) of the United Nations, 2011).

[3] Hall, K. D., Guo, J., Dore, M. & Chow, C. C. The progressive increase of food waste in america and its environmental impact. *PloS one* **4**, e7940 (2009).

[4] Diener, S. *et al.* Black soldier fly larvae for organic waste treatmentprospects and constraints. *Proceedings of the WasteSafe* **2**, 13–15 (2011).

[5] Sanchez, P. A. & Swaminathan, M. S. Cutting world hunger in half. *Science* **307**, 357–359 (2005).

[6] Hunter, M. C., Smith, R. G., Schipanski, M. E., Atwood, L. W. & Mortensen, D. A. Agriculture in 2050: recalibrating targets for sustainable intensification. *Bioscience* **67**, 386–391 (2017).

[7] Saer, A., Lansing, S., Davitt, N. H. & Graves, R. E. Life cycle assessment of a food waste composting system: environmental impact hotspots. *Journal of Cleaner Production* **52**, 234–244 (2013).

[8] Hale, O. Dried hermetia illucens larvae (diptera: Stratiomyidae) as a feed additive for poultry. *Ga Entomol Soc J* (1973).

[9] Newton, G., Booram, C., Barker, R. & Hale, O. Dried hermetia illucens larvae meal as a supplement for swine. *Journal of Animal Science* **44**, 395–400 (1977).

[10] Sheppard, C. House fly and lesser fly control utilizing the black soldier fly in manure management systems for caged laying hens. *Environmental entomology* **12**, 1439–1442 (1983).

[11] Sheppard, D. C., Newton, G. L., Thompson, S. A. & Savage, S. A value added manure management system using the black soldier fly. *Bioresource technology* **50**, 275–279 (1994).

[12] Liu, Q., Tomberlin, J. K., Brady, J. A., Sanford, M. R. & Yu, Z. Black soldier fly (diptera: Stratiomyidae) larvae reduce escherichia coli in dairy manure. *Environmental entomology* **37**, 1525–1530 (2008).

[13] Sheppard, D. C., Tomberlin, J. K., Joyce, J. A., Kiser, B. C. & Sumner, S. M. Rearing methods for the black soldier fly (diptera: Stratiomyidae). *Journal of Medical Entomology* **39**, 695–698 (2002).

[14] Makkar, H. P., Tran, G., Heuz, V. & Ankers, P. State-of-the-art on use of insects as animal feed. *Animal Feed Science and Technology* **197**, 1–33 (2014).

[15] St-Hilaire, S. *et al.* Fish offal recycling by the black soldier fly produces a foodstuff high in omega-3 fatty acids. *Journal of the World Aquaculture Society* **38**, 309–313 (2007).

[16] Kim, W.-T. *et al.* The larval age and mouth morphology of the black soldier fly, hermetia illucens (diptera: Stratiomyidae). *International Journal of Industrial Entomology* **21**, 185–187 (2010).

[17] Myers, H. M., Tomberlin, J. K., Lambert, B. D. & Kattes, D. Development of black soldier fly (diptera: Stratiomyidae) larvae fed dairy manure. *Environmental entomology* **37**, 11–15 (2014).

[18] Tomberlin, J. K., Sheppard, D. C. & Joyce, J. A. Selected life-history traits of black soldier flies (diptera: Stratiomyidae) reared on three artificial diets. *Annals of the Entomological Society of America* **95**, 379–386 (2002).

[19] Berdahl, A., Torney, C. J., Ioannou, C. C., Faria, J. J. & Couzin, I. D. Emergent sensing of complex environments by mobile animal groups. *Science* **339**, 574–576 (2013).

[20] Hager, F. A. & Kirchner, W. H. Directional vibration sensing in the termite macrotermes natalensis. *Journal of Experimental Biology* **217**, 2526–2530 (2014).

[21] Reid, C. R. *et al.* Army ants dynamically adjust living bridges in response to a cost–benefit trade-off. *Proceedings of the National Academy of Sciences* **112**, 15113–15118 (2015).

[22] Trepat, X. *et al.* Physical forces during collective cell migration. *Nature physics* **5**, 426 (2009).

[23] Şahin, E. Swarm robotics: From sources of inspiration to domains of application. In *International workshop on swarm robotics*, 10–20 (Springer, 2004).

[24] Pickem, D. *et al.* The robotarium: A remotely accessible swarm robotics research testbed. In *2017 IEEE International Conference on Robotics and Automation (ICRA)*, 1699–1706 (IEEE, 2017).

[25] Rubenstein, M., Ahler, C., Hoff, N., Cabrera, A. & Nagpal, R. Kilobot: A low cost robot with scalable operations designed for collective behaviors. *Robotics and Autonomous Systems* **62**, 966–975 (2014).

[26] Rubenstein, M. *et al.* Collective transport of complex objects by simple robots: theory and experiments. In *Proceedings of the 2013 international conference on Autonomous agents and multi-agent systems*, 47–54 (International Foundation for Autonomous Agents and Multiagent Systems, 2013).

[27] Rubenstein, M., Cornejo, A. & Nagpal, R. Programmable self-assembly in a thousand-robot swarm. *Science* **345**, 795–799 (2014).

[28] Mayya, S., Pierpaoli, P., Nair, G. & Egerstedt, M. Collisions as information sources in densely packed multi-robot systems under mean-field approximations. In *Robotics: Science and Systems* (2017).

[29] Schmickl, T. *et al.* Get in touch: cooperative decision making based on robot-to-robot collisions. *Autonomous Agents and Multi-Agent Systems* **18**, 133–155 (2009).

[30] Sumpter, D. J. The principles of collective animal behaviour. *Philosophical Transactions of the Royal Society of London B: Biological Sciences* **361**, 5–22 (2006).

[31] Hefti, E., Trechsel, U., Rfenacht, H. & Fleisch, H. Use of dermestid beetles for cleaning bones. *Calcified Tissue International* **31**, 45–47 (1980).

[32] Nielsen, B. L., Lawrence, A. B. & Whittemore, C. T. Effect of group size on feeding behaviour, social behaviour, and performance of growing pigs using single-space feeders. *Livestock Production Science* **44**, 73–85 (1995).

[33] Grant, R. & Albright, J. Effect of animal grouping on feeding behavior and intake of dairy cattle. *Journal of dairy science* **84**, E156–E163 (2001).

[34] Evangelista, D. J., Ray, D. D., Raja, S. K. & Hedrick, T. L. Three-dimensional trajectories and network analyses of group behaviour within chimney swift flocks during approaches to the roost. *Proc. R. Soc. B* **284**, 20162602 (2017).

[35] Attanasi, A. *et al.* Information transfer and behavioural inertia in starling flocks. *Nature physics* **10**, 691 (2014).

[36] Dunkel, J. *et al.* Fluid dynamics of bacterial turbulence. *Physical review letters* **110**, 228102 (2013).

[37] Sanchez, T., Chen, D. T., DeCamp, S. J., Heymann, M. & Dogic, Z. Spontaneous motion in hierarchically assembled active matter. *Nature* **491**, 431 (2012).

[38] Christensen, R. *Theory of viscoelasticity: an introduction* (Elsevier, 2012).

[39] Gottesman, O., Andrejevic, J., Rycroft, C. H. & Rubinstein, S. M. A state variable for crumpled thin sheets. *Communications Physics* **1**, 70 (2018).

[40] Lakes, R. Materials with structural hierarchy. *Nature* **361**, 511 (1993).

[41] Fratzl, P. & Weinkamer, R. Natures hierarchical materials. *Progress in materials Science* **52**, 1263–1334 (2007).

[42] Michel, J. A. & Yunker, P. J. Structural hierarchy confers error tolerance in biological materials. *Proceedings of the National Academy of Sciences* **116**, 2875–2880 (2019).

[43] Albuquerque, R. & Gomes, M. Stress relaxation in crumpled surfaces. *Physica A: Statistical Mechanics and its Applications* **310**, 377–383 (2002).

[44] Phillips, J. Stretched exponential relaxation in molecular and electronic glasses. *Reports on Progress in Physics* **59**, 1133 (1996).

[45] Sasaki, N., Nakayama, Y., Yoshikawa, M. & Enyo, A. Stress relaxation function of bone and bone collagen. *Journal of biomechanics* **26**, 1369–1376 (1993).

[46] Phonekeo, S., Mlot, N., Monaenkova, D., Hu, D. L. & Tovey, C. Fire ants perpetually rebuild sinking towers. *Royal Society open science* **4**, 170475 (2017).

[47] Peleg, O., Peters, J. M., Salcedo, M. K. & Mahadevan, L. Collective mechanical adaptation of honeybee swarms. *Nature Physics* 1 (2018).

[48] Shishkov, O., Hu, M., Johnson, C. & Hu, D. L. Black soldier fly larvae feed by forming a fountain around food. *Journal of the Royal Society Interface* **16**, 20180735 (2019).

[49] Shishkov, O., Trebuchon, J., Yunker, P. J., Franklin, S. & Hu, D. L. Black soldier fly larvae rearrange under compression. *Integrative and comparative biology* (2019).

[50] Jaeger, H., Liu, C.-h. & Nagel, S. R. Relaxation at the angle of repose. *Physical Review Letters* **62**, 40 (1989).

[51] Daerr, A. & Douady, S. Two types of avalanche behaviour in granular media. *Nature* **399**, 241–243 (1999).

[52] Nagel, S. R. Klopsteg memorial lecture (august, 1998): Physics at the breakfast tableor waking up to physics. *American Journal of Physics* **67**, 17–25 (1999).

[53] Faraday, M. Xvii. on a peculiar class of acoustical figures; and on certain forms assumed by groups of particles upon vibrating elastic surfaces. *Philosophical transactions of the Royal Society of London* 299–340 (1831).

[54] Milburn, R. *et al.* Faraday tilting of water-immersed granular beds. *Physical Review E* **71**, 011308 (2005).

[55] Burtally, N., King, P., Swift, M. R. & Leaper, M. Dynamical behaviour of fine granular glass/bronze mixtures under vertical vibration. *Granular Matter* **5**, 57–66 (2003).

[56] Naylor, M., Swift, M. R. & King, P. Air-driven brazil nut effect. *Physical Review E* **68**, 012301 (2003).

[57] Tomberlin, J. K., Adler, P. H. & Myers, H. M. Development of the black soldier fly (diptera: Stratiomyidae) in relation to temperature. *Environmental entomology* **38**, 930–934 (2009).

[58] Harnden, L. M. & Tomberlin, J. K. Effects of temperature and diet on black soldier fly, hermetia illucens (l.)(diptera: Stratiomyidae), development. *Forensic science international* **266**, 109–116 (2016).

[59] Diener, S., Solano, N. M. S., Gutiérrez, F. R., Zurbrügg, C. & Tockner, K. Biological treatment of municipal organic waste using black soldier fly larvae. *Waste and Biomass Valorization* **2**, 357–363 (2011).

[60] Richards, C. S., Price, B. W. & Villet, M. H. Thermal ecophysiology of seven carrion-feeding blowflies in southern africa. *Entomologia Experimentalis et Applicata* **131**, 11–19 (2009).

[61] Charabidze, D., Bourel, B. & Gosset, D. Larval-mass effect: characterisation of heat emission by necrophageous blowflies (diptera: Calliphoridae) larval aggregates. *Forensic science international* **211**, 61–66 (2011).

[62] Heaton, V., Moffatt, C. & Simmons, T. Quantifying the temperature of maggot masses and its relationship to decomposition. *Journal of forensic sciences* **59**, 676–682 (2014).

[63] Kotzé, Z., Villet, M. H. & Weldon, C. W. Heat accumulation and development rate of massed maggots of the sheep blowfly, lucilia cuprina (diptera: Calliphoridae). *Journal of insect physiology* **95**, 98–104 (2016).

[64] Abduh, M. Y., Nadia, M. H., Manurung, R., Putra, R. E. *et al.* Factors affecting the bioconversion of philippine tung seed by black soldier fly larvae for the production of protein and oil-rich biomass. *Journal of Asia-Pacific Entomology* **21**, 836–842 (2018).

[65] Paz, A. S. P., Carrejo, N. S. & Rodríguez, C. H. G. Effects of larval density and feeding rates on the bioconversion of vegetable waste using black soldier fly larvae hermetia illucens (l.),(diptera: Stratiomyidae). *Waste and Biomass Valorization* **6**, 1059–1065 (2015).

[66] Donev, A. *et al.* Improving the density of jammed disordered packings using ellipsoids. *Science* **303**, 990–993 (2004).

[67] Depickère, S., Fresneau, D. & Deneubourg, J.-L. The influence of red light on the aggregation of two castes of the ant, lasius niger. *Journal of Insect Physiology* **50**, 629–635 (2004).

[68] Thielicke, W. & Stamhuis, E. Pivlab–towards user-friendly, affordable and accurate digital particle image velocimetry in MATLAB. *Journal of Open Research Software* **2**, 30 (2014).

[69] Thielicke, W. *The Flapping Flight of Birds - Analysis and Application.* PhD thesis, Rijksuniversiteit Groningen (2014).

[70] Schneider, C. A., Rasband, W. S. & Eliceiri, K. W. Nih image to imagej: 25 years of image analysis. *Nature methods* **9**, 671 (2012).

[71] Thielicke, W. & Stamhuis, E. Pivlab–towards user-friendly, affordable and accurate digital particle image velocimetry in matlab. *Journal of Open Research Software* **2** (2014).

[72] Delaney, G., Weaire, D., Hutzler, S. & Murphy, S. Random packing of elliptical disks. *Philosophical Magazine Letters* **85**, 89–96 (2005).

[73] Bechinger, C. *et al.* Active particles in complex and crowded environments. *Rev. Mod. Phys.* **88**, 045006 (2016).

[74] Takatori, S. C. & Brady, J. F. Forces, stresses and the (thermo?) dynamics of active matter. *Curr. Opin. Colloid Interface Sci.* **21**, 24–33 (2016).

[75] Heyes, D. & Melrose, J. Brownian dynamics simulations of model hard-sphere suspensions. *J. Non-Newtonian Fluid Mech.* **46**, 1–28 (1993).

[76] Foss, D. R. & Brady, J. F. Brownian dynamics simulation of hard-sphere colloidal dispersions. *J. Rheol.* **44**, 629–651 (2000).

[77] Moran, M. J., Shapiro, H. N., Munson, B. R., DeWitt, D. P. & Thermodynamics, F. M. Introduction to thermal systems engineering. *Thermodynamics, Fluid Mechanics, and Heat Transfer* (2003).

[78] Heinrich, B. *The hot-blooded insects: strategies and mechanisms of thermoregulation* (Springer Science & Business Media, 2013).

[79] Valvano, J. W., Cochran, J. & Diller, K. R. Thermal conductivity and diffusivity of biomaterials measured with self-heated thermistors. *International Journal of Thermophysics* **6**, 301–311 (1985).

[80] Xu, D. *et al.* The ellipsoidal area ratio: an alternative anisotropy index for diffusion tensor imaging. *Magnetic resonance imaging* **27**, 311–323 (2009).

[81] Churchill, S. & Bernstein, M. A correlating equation for forced convection from gases and liquids to a circular cylinder in crossflow (1977).

[82] Ergun, S. Fluid flow through packed columns. *Chem. Eng. Prog.* **48**, 89–94 (1952).

[83] Pritchard, P. J. & Mitchell, J. W. *Fox and McDonald's introduction to fluid mechanics* (John Wiley & Sons, 2016).

[84] Schaub-Szabo, S. & Leonard, J. Characterizing the bulk density of compost. *Compost Science & Utilization* **7**, 15–24 (1999).

[85] Ohern, C. S., Silbert, L. E., Liu, A. J. & Nagel, S. R. Jamming at zero temperature and zero applied stress: The epitome of disorder. *Physical Review E* **68**, 011306 (2003).

[86] Majmudar, T., Sperl, M., Luding, S. & Behringer, R. P. Jamming transition in granular systems. *Physical review letters* **98**, 058001 (2007).

[87] Piazza, R. *et al.* Stretched-exponential relaxation of birefringence in a critical binary mixture. *Physical Review B* **38**, 7223 (1988).

[88] Lambooy, E., Garssen, G., Walstra, P., Mateman, G. & Merkus, G. Transport of pigs by car for two days; some aspects of watering and loading density. *Livestock Production Science* **13**, 289–299 (1985).

[89] Mitchell, M. & Kettlewell, P. Physiological stress and welfare of broiler chickens in transit: solutions not problems! *Poultry science* **77**, 1803–1814 (1998).

[90] Chung, H.-N. *et al.* Toward implementation of mosquito sterile insect technique: The effect of storage conditions on survival of male aedes aegypti mosquitoes (diptera: Culicidae) during transport. *Journal of Insect Science* **18**, 2 (2018).

[91] Mlot, N. J., Tovey, C. A. & Hu, D. L. Fire ants self-assemble into waterproof rafts to survive floods. *Proceedings of the National Academy of Sciences* **108**, 7669–7673 (2011).

[92] Tennenbaum, M., Liu, Z., Hu, D. & Fernandez-Nieves, A. Mechanics of fire ant aggregations. *Nature Materials* **15**, 54 (2015).

[93] Phonekeo, S., Dave, T., Kern, M., Franklin, S. V. & Hu, D. L. Ant aggregations self-heal to compensate for the ringelmann effect. *Soft Matter* **12**, 4214–4220 (2016).

[94] Quillin, K. Ontogenetic scaling of burrowing forces in the earthworm lumbricus terrestris. *Journal of Experimental Biology* **203**, 2757–2770 (2000).

[95] Ruiz, S. A. & Or, D. Biomechanical limits to soil penetration by earthworms: direct measurements of hydroskeletal pressures and peristaltic motions. *Journal of The Royal Society Interface* **15**, 20180127 (2018).

[96] Thom, H. C. A note on the gamma distribution. *Monthly Weather Review* **86**, 117–122 (1958).

[97] Sun, Y.-N. & Jusko, W. J. Transit compartments versus gamma distribution function to model signal transduction processes in pharmacodynamics. *Journal of pharmaceutical sciences* **87**, 732–737 (1998).

[98] van der Vaart, K., Sinhuber, M., Reynolds, A. M. & Ouellette, N. T. Mechanical spectroscopy of insect swarms. *Science advances* **5**, eaaw9305 (2019).

[99] Weir, J. d. V. New methods for calculating metabolic rate with special reference to protein metabolism. *The Journal of physiology* **109**, 1–9 (1949).

[100] Yin, X., Goudriaan, J., Lantinga, E. A., Vos, J. & Spiertz, H. J. A flexible sigmoid function of determinate growth. *Annals of botany* **91**, 361–371 (2003).

[101] Tommiska, M. Efficient digital implementation of the sigmoid function for reprogrammable logic. *IEE Proceedings-Computers and Digital Techniques* **150**, 403–411 (2003).

[102] Ocko, S. A. & Mahadevan, L. Collective thermoregulation in bee clusters. *Journal of The Royal Society Interface* **11**, 20131033 (2014).

[103] Kaur, S., Kaler, R. *et al.* Effect of starch on the rheology of molasses. *Journal of Food Engineering* **55**, 319–322 (2002).

[104] Marsden, J. E. & Tromba, A. *Vector calculus* (Macmillan, 2003).

[105] Berrigan, D. & Pepin, D. J. How maggots move: allometry and kinematics of crawling in larval diptera. *Journal of Insect Physiology* **41**, 329–337 (1995).

Scholarly Achievements

Journal Publications

1. Shishkov, O., Hu, D. L. Synchronizing pile formation of black soldier fly larvae. Accepted at the European Physical Journal.

2. Shishkov, O., Trebuchon, J., Yunker, P., Franklin, S., Hu, D. L. (2019) Black soldier fly larvae rearrange under compression. Integrative and Comparative Biology.

3. Shishkov, O., Hu, M., Johnson C., Hu, D. L. (2019) Black soldier fly larvae feed by forming a fountain around food. Journal of the Royal Society Interface.

4. Shishkov, O., Hu, M., Johnson C., Zhang, B., Hu, D. L. (2018) Black Soldier Fly larvae consume food by actively mixing. In the 7th International Symposium on Aero-aqua Bio-Mechanisms, Tokyo.

Patents

Shishkov, O., Hu, D. L. (2018). SYSTEMS AND METHODS FOR COOLING A PLURALITY OF CONTAINERIZED ANIMALS. International Application No.: PCT/US2019/016945, Priority Serial No.: 62/627,355. February 7, 2019

Conference Presentations

1. Shishkov, O., Hu, D. L. Feeding, Squishing, and Cooling Fly Larvae. (Invited) Guest lecture at Cutting Edge Technologies class. January 23, 2020.

2. Shishkov, O., Hu, D. L. Aerating black soldier fly larvae for cooling. Poster presented at the 2019 Entomological Society Annual Meeting. St. Louis, MO., November 18, 2019

3. Shishkov, O., Trebuchon, J., Yunker, P., Franklin, S., Hu, D. L. Black soldier fly rearrange under compression. Poster presented at the Granular and Particulate Networks International Workshop 2019. Dresden, Germany, July 8, 2019.

4. Shishkov, O., MacAlino, M., Franklin, S., Hu, D. L, Fly larvae rearrange under compression. American Physical Society March Meeting 2019, Boston, MA, March 5, 2019.

5. Shishkov, O., Hu, M., Johnson, C., Hu, D. L., Fly Larvae Feed by Forming a Flowing Fountain. 2019 AAAS, Annual Meeting Washington, DC, February 16, 2019.

6. Shishkov, O., Hu, M., Johnson, C., Hu, D. L Feeding Fly Larvae Form a Fountain. Poster presented at the Society for Integrative and Comparative Biology, Tampa, FL. January 4, 2019 (Invited).

7. Shishkov, O., Hu, M., Hu, D. L. Fly Larvae Feed by Forming a Flowing Fountain. APS DFD 2018 Annual Meeting, Atlanta, GA, November 19, 2018.

8. Shishkov, O., Fuentes-Cabrera, M., Hu, D. L. Active mixing in aggregations of black soldier fly larvae. Poster presented at the 2018 CNMS User Meeting, Oak Ridge National Laboratory, August 13, 2018.

9. Shishkov, O., Hu, D. L Competition of feeding fly larvae causes active mixing. iPoLS 2018 Annual Meeting, Rice University, June 24, 2018.

10. Shishkov, O., Hu, D. L Collective motion of fly larvae during feeding. 11th Annual Meeting on Soft Materials, Emory University, May 23, 2018.

11. Shishkov, O., Hu, D. L Collective forces of black soldier fly larvae. American Physical Society March Meeting, Los Angeles, CA , March 8, 2018.

12. Shishkov, O., Hu, D. L. Fly larvae mix to increase eating rates. 2017 AIChE Annual Meeting, Minneapolis, MN., November 1, 2017.

13. Shishkov, O., Hu, D. L. Fly Larvae Mix to Increase Eating Rates. Society of Engineering Science 54th Technical Meeting. Boston, MA, July 26-28, 2017.

14. Shishkov, O., Hu, D. L. Fly larvae mix to increase eating rates. 2017 Active Materials Project Summer School. Georgetown University, Washington, DC, June 11, 2017.

15. Shishkov, O., Hu, D. L. Active mixing of black soldier fly larvae during feeding. The 10th Southeast Meeting on Soft Materials. Atlanta, GA, Friday, May 12, 2017.

16. Shishkov, O., Hu, D. L. Self-mixing of fly larvae during feeding. The Geilo School 2017: Physics Inspired by Living Matter. Geilo, Norway, March 20-30, 2017.

17. Shishkov, O., Johnson, C., Hu, D. L. Self-mixing of fly larvae during feeding. American Physical Society March Meeting. New Orleans, LA, March 13-17, 2017.

18. Shishkov, O., Johnson, C., Zhang, B., Hu, D. L., Self-mixing of fly larvae during feeding. Division of Fluid Dynamics annual meeting. Portland, Oregon, November 20-22, 2016.

19. Shishkov, O., Johnson, C., Hu, D. L. Active mixing increases feeding rate of black soldier fly larvae. Active and Smart Matter: A New Frontier for Science and Engineering. Syracuse University, Syracuse, NY, June 20-23, 2016.

20. Shishkov, O, Hu, D. L. Active mixing of black soldier fly larvae, Soft Matter & Lunch

Event. Georgia Institute of Technology, Atlanta, GA, April 2016.

Awards

1. Shishkov, O., Hu, D. L.. One of two Outstanding Poster Awards at the Geilo School 2017 for "Self-mixing of fly larvae during feeding." The Geilo School 2017: Physics Inspired by Living Matter. March 2017. Geilo, Norway.

2. Winner of 2019 Steven Vogel Award for Best Student Poster within the Division of Comparative Biomechanics for "Feeding Fly Larvae Form a Fountain" at the Society for Integrative and Comparative Biology, January 5, 2019.

3. iBiology Young Scholars Seminar Series Finalist. May 2019.

4. 3 Minute Thesis Finalist. "Feeding, Squishing, and Cooling Maggots". November 14, 2019.

5. 2016 Junior Scientist Travel Award to Active and Smart Matter: A New Frontier for Science and Engineering, June 20-23, 2016

Funding

1. Hu, D. L. NSF career award (PHY-1255127)

2. Georgia Research Alliance award for "Rearing black soldier fly larvae in a fluidized bed." January 2017 - June 2019

3. US Army Research Office Mechanical Sciences Division, Complex Dynamics and Systems Program, under contract no. W911NF-19-1-0086.

4. US Army Research Office under MURI award #W911NF-19-1-02339